



UNIVERSITÀ
DEGLI STUDI
FIRENZE

**DOTTORATO DI RICERCA
INTERNATIONAL DOCTORATE IN STRUCTURAL BIOLOGY**

CICLO XXXI

COORDINATOR Prof. Claudio Luchinat

Characterization of the human immune response after vaccination with Bexsero through structural and functional studies of human Fabs from a longitudinal memory B-cell repertoire

Settore Scientifico Disciplinare CHIM/03

PhD student

Dott. Federica Bianchi

Tutor

Dott. Domenico Maione(GSK), Prof. Lucia Banci(CERM)

Coordinator

Prof. Claudio Luchinat

Novembre 2015 - 2018

***This thesis has been approved by the University of Florence,
the University of Frankfurt and the Utrecht University***



INDEX

1. INTRODUCTION	3
2. MATERIAL AND METHOD	5
3. RESULTS	10
3.1 110 recombinant huFabs were successfully produced in <i>E. coli</i> for high through put screening	10
3.2 Select 13 Abs can bind the three variants of fHbp by Gyros analysis	11
3.3 Expression of recombinant mAbs in mammalian cells allowed to obtain pure IgGs in high yield	12
3.4 Selected mAbs have high affinity for the three fHbp main variants	12
3.5 mAbs recognize native fHbp on live bacteria	14
3.6 α -fHbp mAbs compete with fHbp for human factor H binding	16
3.7 Cross-protective anti-fHbp human mAbs	17
3.8 Low resolution epitope mapping suggested mAbs have different recognition profile	18
3.9 Crystallization data collection	20
3.10 Overall crystal structure of huFab 4B3 in complex with fHbp v1	21
3.11 Molecular insight of the cross-reactivity of mAb 4B3	26
3.12 Nature of mAb 4B3 and human Factor H competition for fHbp v1 binding	28
3.13 Overall crystal structure of Fab 1E6 in complex with fHbp v3	30
3.14 High conservation of the epitope indicate broadly coverage of mAb 1E6	34
3.15 Cross-reactive anti-fHbp antibodies exhibit vary binding model	36
4. DISCUSSION	38
5. RESULTS OBTAINED VS RESULTS EXPECTED	41

1. INTRODUCTION

Neisseria meningitidis is a leading cause of meningitis and sepsis worldwide [1]. Before the introduction of intensive use of antibiotic 70–85% of meningococcal disease cases were fatal [2]. Meningococcal disease is also associated with marked sequelae including limb loss, hearing loss, cognitive dysfunction, visual impairment, educational difficulties, developmental delays, motor nerve deficits, seizure disorders, and behavioral problems. Of the 12 known meningococcal capsular groups, five are associated with the majority of disease A, B, C, Y and W. Meningococcal capsular polysaccharide vaccines inducing serogroup-specific protective antibodies are available against serogroups A, C, Y, and W [3] [4] but, the capsular polysaccharide of serogroup B is structurally similar to certain abundant human glycoproteins like NCAM therefore is not a suitable immune target due to the risk of autoimmune damage through molecular mimicry [5], [6].

The first broad-spectrum recombinant protein vaccine against serogroup B meningococcus (MenB), called Bexsero (or 4CMenB) has been approved by the EMA in 2013 for prevention of MenB disease in all age groups, and by the US FDA in January 2015 for use in adolescents and young adults. One of the three main antigens of Bexsero is the factor H binding protein (fHbp) a 28-kDa surface exposed lipoprotein that specifically binds the human factor H.

The human factor H (hfH), one of the most abundant complement components in human blood (with plasma concentrations ranging from 200 to 800 $\mu\text{g/ml}$ [7]) is a conserved glycoprotein that inhibits the human complement and it is associated to the ability of the immune system to discriminate between *self* and *non-self-elements* [8, 9]. It is composed by 20 individually folded complement control protein (CCP) domains linked head to tail by a short linker. The C-terminal CCPs 19 and 20 can bind sialylated glycans of the host cells and “mark them as self” [10, 11]. The interaction with the sialic acid enhances and accelerates the decay activities of hfH on the mammalian plasma membrane and prevents the inappropriate complement activity against host tissues [8, 12]. However, many pathogenic organisms such as *Neisseria meningitidis* [13] *Haemophilus influenzae* [14], *Bordetella pertussis* [15], *Pseudomonas aeruginosa* [16], *Streptococcus pneumoniae* [17], *Candida albicans* [18], *Borrelia burgdorferi* [18], *B. hermsii* [18] have evolved several strategies to recruit host factor H (fH) to escape the attack of complement response allowing their proliferation in the host.

Neisseria meningitidis covers itself with the human factor H mimicking the host “*self*”, evading the complement activation and surviving in human blood [13].

To date, more than 1000 natural amino acid sequences of fHbp have been identified and are accessible in the public database at <http://pubmlst.org/neisseria/fHbp>. They can be classified in three variants which are immunologically distinct. Within the fHbp variant groups the sequence identity is usually above 87%, while between variant groups the sequence identity can be as low as 62%. [19] [20]. The structures of the fHbp were solved at atomic resolution by NMR [21] and X-ray crystallography [22] and despite sharing poor amino acid identity, the 3D structure of the fHbp variants is well conserved and consists of two domains. While the C-terminal domain adopts a canonical β -barrel conformation, the N-terminus of the v1 and v3 shows an unusual taco-shaped β -barrel fold characterized by higher intrinsic flexibility. Differential scanning calorimetry profiles showed independent unfolding of the two barrels. The C-terminal barrel melts at temperatures above 80°C in all three variants, in contrast, the N-terminal barrel

exhibits highly variable melting at 69.5 °C in v1, 60.6 °C in v3 and at 36.6 °C in v2 fHbp. This intrinsic instability and susceptibility to the protease cleavage could explain why the structure characterization of the N-terminal of v2 was unsuccessful so far [23]. The variability in the amino acid composition between the fHbp variants results in relevant chemical and physical differences that regulate the molecular and dynamic properties of fHbp. In particular, all fHbp variants bind to the human factor H with high affinity with K_d in the nanomolar range, but large differences in the stability of the complexes were observed [24]. According to these data, the crystal structures human factor H (hfH)(domain 6 and 7) bound to fHbp v1 and to fHbp v3 confirmed that hfH binding to fHbp variants is mediated by a distinct set of residues [23].

Preclinical studies demonstrated that fHbp elicits a robust bactericidal antibody response in mice, rabbit and human, but presumably due the high antigenic variability, the vast majority of them displayed variant- group specificity [25] [26] [27] [28] [29] [30] [31] [32], only in few instances anti-fHbp antibody were able to recognize different variants of fHbp [33] [34] [35] [36].

Some murine α -fHbp monoclonal antibodies (mAbs) previously described inhibited the binding of hfH to fHbp suggesting that the antibody's epitopes overlapped with the hfH binding region[27] [26] but, so far none human mAbs able to compete with human hfH binding has been identified[37], [36]. *Neisseria meningitidis* 's fHbp specifically binds the human factor H but not the factor H of other species [38] therefore in precedent publications some researchers has been supposed that upon human vaccination, the fHbp present in the vaccine bound the human factor H concealing the hfH:fHbp binding area, which become not accessible to human immune response [39] [40]. In this work, investigating a panel of over 100 human α -fHbp human Fab (huFab) isolated from adults immunized with Bexsero, we identified a sub-set of 13 Fabs able to recognize the three variants of fHbp. We characterized their antigen binding selectivity and affinity, and their ability to inhibit binding of hfH to live meningococci; the most interesting were chosen for structural analyses of the fHbp/huFab complexes. Further, a subset of cross-reactive huFabs was cloned and expressed as full-length mAbs (IgG1) to investigate their cross-protective ability against MenB strains expressing fHbp variants not present in 4CMenB.

2. MATERIAL AND METHODS

2.1 Human samples

Human samples were collected from three adults immunized with 4CMenB vaccine, in clinical trial conducted in Krakow, Poland, approved by the Bioethics Committee of the District Medical Doctors' Chamber in Krakow and conducted in accordance with the Declaration of Helsinki. The use of samples was performed upon written informed consent obtained from participants before the study-specific procedures.

2.2 Recombinant huFabs production in *E.coli*

Heavy and light chain variable regions of single plasmablasts, isolated from peripheral blood, were amplified and cloned into pET22 vector (Novagen) as bicistronic expression cassettes encoding for huFab antibody fragments. Anti-fHbp huFabs were expressed as recombinant proteins with a C-terminal hexahistidine (His6) tag in *E.coli* ROSETTA 2 (DE3). Cultures were grown in Enpresso B (biosilta) or HTMC medium (auto-induced medium developed in house) and protein expression was induced by IPTG 1mM for 24h at 25 °C. Cell lysis has been performed by using different techniques; chemical lysis, osmotic shock and sonication. The recombinant antibodies were purified by immobilized metal ion chromatography using Ni-NTA agarose resin (Qiagen) according to the manufacturer's instruction. Recombinant huFabs were quantified by BCA and their purity was assessed by SDS-PAGE after Coomassie staining in reducing and non-reducing conditions.

2.3 fHbp variants expression in *E.coli*

Factor H binding protein was expressed as recombinant protein with a C-terminal hexahistidine (His6) tag in *E.coli* BL21 DE3 transformed by heat shock standard protocol. Cultures were grown in HTMC medium and protein expression was induced by IPTG 1mM for 24h at 25 °C. fHbp expressing *E. coli* cells were lysed by cell lytic express (Sigma-Aldrich) as manufacture's instruction and centrifuged at 9000 rpm for 30 min. The soluble fraction was then filtered by 0.22-microliter filter (Millipore) to remove cell debris and loaded on a Ni²⁺ Sepharose 6 Fast Flow column (GE Healthcare) pre-equilibrated by a binding buffer composed 100mM Tris, 300 mM NaCl and 10mM imidazole. To obtain pure samples, after loaded the soluble fraction, two washing steps were performed using buffer containing low concentrations (10 and 20 mM) of imidazole. Finally the elution of the his-tagged fHbp was obtained with a buffer containing 100mM Tris, 300 mM NaCl and 300mM imidazole. Protein concentration was determined by nanodrop spectrophotometer (Thermo Scientific) and its purity was assessed by SDS-page on a 4-12% Bis-Tris Gel after Problue Safe Stain (Giotto Biotech). When necessary, a second purification step of ion-exchange chromatography was performed to remove all the impurities using a pre-packed HiLoad 26/60 column Superdex 75 prep grade (GE) following manufacturer's instructions.

2.4 Recombinant mAbs production in mammalian cells

The genes of the variable region (V) of the heavy (H) and light (L) chains of human monoclonal antibodies, codon optimized for mammalian expression, were synthesized by Geneart (Life Technologies) with the 5' and 3' extremities containing the Eco31I site. After resuspension in 50 µl nuclease-free water, the synthetic DNA strings were digested with the Eco31I restriction enzyme, purified and ligated into pRS5a expression vectors containing the Eco31I cloning site upstream of human IgG1 and Igκ/λ generic constant region sequences. For Fabs production, the vector containing the complete HC has a cleavable C-terminal Strep-tag II.

All cloning steps were performed in *E. coli* strain DH5a using standard ligation and transformation protocol. In the pRS5a antibody expression vectors, the transcription is under the CMV promoter in frame with a human leader sequence for secretion derived by human immunoglobulin (Novartis-NIBR). Expression of the recombinant antibodies (IgGs or Fabs) was achieved by transient transfection of Expi293 cells (Life Technologies) in suspension using Expi293 Expression Medium, according to the manufacturer's protocol. Equal amounts (15 µg each per 30 ml of transfection volume) of vector DNA codifying the heavy and light chains were used to transfect Expi293 cells. The cells were incubated at 37°C in a humidified atmosphere of 8% CO₂ in air on an orbital shaker rotating at 125 rev min⁻¹. The cell-culture supernatants were harvested 3 days and 6 days post-transfection, clarified by centrifugation for 30 min at 4000 rev min⁻¹ and concentrated using centrifugal concentration devices with a 10 kDa molecular-weight cutoff membrane (Millipore). The recombinant full IgGs were purified by affinity chromatography using a protein G Sepharose 4 fast flow (GE Healthcare) according to the manufacture's protocol. After the elution, the buffer of purified mAbs was exchanged in PBS using PD-10 (GE Healthcare) desalting column. IgGs concentration was quantified using absorbance at 280 nm by NanoDrop spectrophotometer (Thermo Fisher) and their purity was assessed by SDS-PAGE gel after Coomassie staining (Problue Safe Stain GiottoBiotech) in reducing and non-reducing conditions. Fabs were purified from the cell-culture supernatant by Strep-affinity chromatography, which was performed using a StrepTrap HP column (GE Healthcare) in 100 mM Tris, 150 mM NaCl, 1 mM EDTA pH 7.5, exploiting the highly selective double Strep-tag II at the C-terminus of the Fab heavy chain. The Strep-tag was removed using recombinant Tobacco etch virus (TEV) protease, which was prepared and purified in-house as described previously [42]. The Fabs were further purified by preparative size-exclusion chromatography on Superdex 200 resin in a 10/300 column (GE Healthcare) in buffer consisting of 20 mM Tris, 150 mM NaCl pH 8.

2.7 Immunoassay by Gyrolab®

All recombinant purified huFabs were analyzed by Gyrolab at the concentration of 10 µg/ml. As capture reagent biotinylated fHbp v1, fHbp v2, fHbp v3 and NadA were used at 100 µg/ml. As detection reagent Goat Anti-Human IgG, Fab fragment specific-Alexa 647 (Jackson 115-606-072) was used at 25 nM. All Fabs were analyzed using Gyrolab Bioaffy 200 CDs and the standard Gyrolab three-step method (capture-analyte-detection).

2.8 Surface Plasmon Resonance

Surface Plasmon Resonance (SPR) was used to measure and compare the binding affinities of the tested monoclonal antibodies with the three variants of fHbp recombinant proteins. All SPR experiments were performed in running buffer (10mM Hepes, 150mM NaCl, 3mM EDTA pH 7.4) supplemented with 0,05% (vol/vol) P20 surfactant using Biacore T200 (GE Healthcare) at 25 °C. 9000-10000 response units (RU) of an anti-human Fab binder were immobilized on CM5 sensor chip serie S, using the Fab antibody Capture kit (GE Healthcare). To determinate the k_d and kinetics parameters, schematically, the experiments were designed into four main steps:

- 800-1200 RU of mAbs at 20ug/ul were immobilized by Fabs binder on the surface of the chip in running buffer. An anti-Fab binder coated flow cell without mAbs immobilized was applied as blank reference.
- A blank injection of buffer alone was subtracted from each curve, and reference sensorgrams were subtracted from experimental sensorgrams to yield curves representing specific binding. For the determination of K_d and kinetic parameters, a titration series of five consecutive injections of increasing analyte concentration at a flow rate 30-40 μ L/min. The concentrations of fHbp were adapted to each mAbs, ranging from 0.39-6.25 nM to 3.1-50 nM, to measured maximum 200 RU of fHbp on immobilized mAbs.
- Finally the chip's surface was regenerated using a buffer containing 10 mM glycine pH 2.1 (180 seconds, flow rate 10ul/min). All mAbs were tested in duplicate.

SPR data were analyzed using the Biacore T200 Evaluation software (GE Healthcare). Each sensogram was fitted with the 1:1 Langmuir binding model, including a term to account for potential mass transfer, to obtain the individual k_{on} and k_{off} kinetic constants; the individual values were then combined to derive the single averaged K_d values reported.

2.9 Bacterial strains and culture conditions

N. meningitidis strains MC58 and M11295 were used as reference strains for fHbp v1, M08-240104 (UK104) was used as reference strain for fHbp v2, M01-0240320 (UK320) and M1239 were used as reference strains for fHbp v3. Bacteria were grown on chocolate agar (Biomerieux 43101) at 37°C, 5% CO₂ overnight. For liquid cultures, colonies from overnight growth were used to inoculate 7 ml cultures (in MH broth supplemented with 0.25% glucose) to an optical density at 600 nm (OD₆₀₀) of 0.05. The culture was incubated for approximately 1.5 to 2.5 h at 37°C with shaking until early log (OD₆₀₀ of 0.25) or mid-log phase (OD₆₀₀ of 0.5).

2.10 Native fHbp recognition by mAbs

The ability of different mAbs to bind antigen exposed on the surface of *N. meningitidis* bacteria was determined using a FACS (fluorescence-activated cell sorting) flow cytometer. Bacteria, expressing different variants of fHbp, grown until mid-log phase (OD₆₀₀ of ~0.5) were incubated with monoclonal antibodies at the final concentration of 10ug/ml. Antibody binding was detected using an Anti-Human IgG (Fab specific)-FITC conjugated produced in goat (Sigma) or an Anti-Human IgG-FITC conjugated produced in goat (Jackson Immuno Research) at a 1:100 dilution. Bacteria plus PBS-1%BSA and secondary antibody were used as negative control.

2.11 Serum bactericidal activity assay (SBA)

Serum bactericidal activity against *N. meningitidis* strains was evaluated as reported elsewhere [43]. Bacteria grown until early log phase (OD₆₀₀ of ~0.25) were diluted in Dulbecco's Phosphate Buffered Saline (DPBS- SIGMA D8662) containing 1% bovine serum albumin (BSA) and 0.1% glucose at the working dilution of 10⁴-10⁵ and incubated with serial two fold dilutions of test monoclonal antibodies starting from a concentration of 125 µg/ml. Serum bactericidal titers were defined as the monoclonal antibody dilution resulting in 50% decrease in CFU per milliliter after a 60-min incubation of bacteria with the reaction mixture compared to the control CFU per milliliter at time zero. Pooled baby rabbit sera from Cedarlane or human serum, obtained from volunteer donors under informed consent, have been used as a complement source for rSBA (rabbit SBA) or hSBA (human SBA) respectively.

2.13 Inhibition of binding of human factor H

The ability of the recombinant anti-fHbp mAbs to inhibit binding of human factor H (hfH) to live bacteria was measured by flow cytometry. Bacterial cells grown until mid-log phase (OD₆₀₀ of ~0.5) were incubated with α-fHbp mAbs (50 µg/ml for M1239 and UK104, 10 µg/ml for MC58 in PBS-1%BSA buffer) for 30 min at room temperature, followed by the addition of purified hfH (10 µg/ml for M1239 and UK104, 50 µg/ml for MC58), which was incubated for an additional 30 min at room temperature in a final reaction volume of 100 µl. hfH binding was detected with a anti-hfH goat polyclonal antiserum (Calbiochem 341276) diluted 1:100 and incubated for 30 min at room temperature, followed by an additional incubation of 30 min with a donkey anti-goat IgG–fluorescein isothiocyanate (FITC) conjugate antibody (Jackson ImmunoResearch 705.095.003) diluted 1:100 in PBS-1%BSA buffer.

2.14 Epitope mapping of α-fHbp mAbs by Protein microarray

To identify the mapping region, human mAbs were tested on protein microarrays containing recombinant full length fHbp proteins as well as overlapping fragments of heterogeneous length (40aa to 602aa) spanning the entire protein sequences of fHbp variant 1.1, variant 2.16 and variant 3.28,[36].

Nonspecific binding was minimized by pre-incubating protein microarray slides with a blocking solution (BlockIt, ArrayIt) for 1 hour. mAbs were diluted 1:2000 in BlockIt and overlaid on the protein arrays for 1h at room temperature. Alexa Fluor®647-conjugated anti-Human IgG secondary antibody (Jackson ImmunoResearch) was added for 1h at room temperature in the dark, before proceeding with slide scanning. Fluorescence signals were detected by using a PowerScanner confocal laser scanner (Tecan Trading AG, Switzerland) and the 16-bit images were generated with PowerScanner software variant 1.2 at 10 µm/pixel resolution and processed using ImaGene 9.0 software (Biodiscovery Inc, CA). Elaboration and analysis of image raw Fluorescence Intensity (FI) data was performed using in-house developed software and R scripts. Signals were considered as positive when their MFI value was higher than 15,000, corresponding to the MFI of protein spots after detection with anti-AlexaFluor®647 polyclonal antibody (Jackson ImmunoResearch) alone, plus 10 standard deviation values.

2.15 Protein crystallization and diffraction data collection and processing

To induce the formation of fHbp:huFab complex, 7,5 mg of fHbp and 5 mg of huFab were incubated overnight at 4 °C and further purified by size exclusion chromatography to remove the protein in excess, using a pre-packed HiLoad 26/60 column Superdex 75 prep grade (GE) following manufacture's protocol. huFab:fHbp complexes concentrated at 25 mg/ml in 50mM tris-HCl were screened using pre-packed 96 deep-well blocks commercialized by Molecular dimension using Crystal Gryphon robot (Art Robbins Instruments). In each crystallization screening experiment, 96 different crystallization conditions were tested thanks the robotic 96-channel that filled the screen wells with 70 ul of crystallization buffers followed by the 1-channel dispenser that quickly aspirates and dispenses 200 nl of huFabs complex in the each wells. In total each complex, were tested at least 500 different crystallizations buffers.

2.16 Structure solving and refinement

Crystals diffraction was tested at the beamline ID29 of the European Synchrotron Radiation Facility (ESRF) and several full datasets were collected at 100K, at wavelength $\lambda = 0.983 \text{ \AA}$, on a Pilatus 6M detector. Diffraction datasets were indexed and integrated using iMOSFLM and reduced using Aimless, via the CCP4 suite[44]. The structure of the complex was solved by molecular replacement with Phaser [45] using as model templates for fHbp the protein data bank (PDB) code 2YPV, for the variable region of the light and heavy chain of Fab 4B3 the PDB code 5I17 and for Fab1E6 the PDB code 3Z14. Initial molecular replacement solutions were subjected to subsequent cycles of manual building in Coot with Phenix.refine57 [46]. The buried surface areas, atomic interactions/contacts and the root mean square displacements were calculated with PISA and Superpose, respectively.

3. RESULTS

3.1 110 recombinant human Fabs were successfully produced in *E. coli* for rapid screening

To investigate the α -fHbp repertoire of three adults immunized with Bexsero, the heavy and the light chain immunoglobulin variable region genes (VH and VL genes, respectively) were isolated from peripheral blood mononuclear cells and cloned into a huFab's expression constructs as previously describe be Beernink and co-workers [37]. This longitudinal analysis allowed obtaining more than 100 α -fHbp huFabs, which derived from different, and unrelated memory B cell, which had distinct immunoglobulin gene rearrangement therefore each huFab expresses distinct paratope.

The first objective of my PhD studies was the setup of a protocol suitable to obtain the recombinant 110 α -fHbp huFabs in *E. coli* in a small scale for a rapid and efficient screening. To achieve this purpose the expression protocol was optimized by testing two different expression media and lysis conditions. A pilot experiment was performed on 24 huFabs, which were grown either in Enpresso B (Biosilta) medium followed by whole cell lysis obtained by cell lytic express (chemical and enzymatic lysis), either in HTMC medium (complex-auto-induction medium) followed by osmotic shock lysis to collect only the periplasmic fraction. Whole cell lysis allowed to collect all proteins present in cytoplasm instead, shock osmotic method was used to collect only periplasmic proteins. Protein profile of the total, soluble and purified fraction was analyzed by SDS-PAGE as shown in figure 1. Thick protein bands were observed at the expected molecular weight of 25 kDa in insoluble, soluble and purified cytoplasmic fractions but not in soluble periplasmic samples therefore the rest of the library of huFabs were produced using the first protocol (Enpresso B /cell lytic). All affinity-purified huFabs were quantified and, on average, from 8 ml of bacterial culture 0.1 mg of huFabs could be obtained.

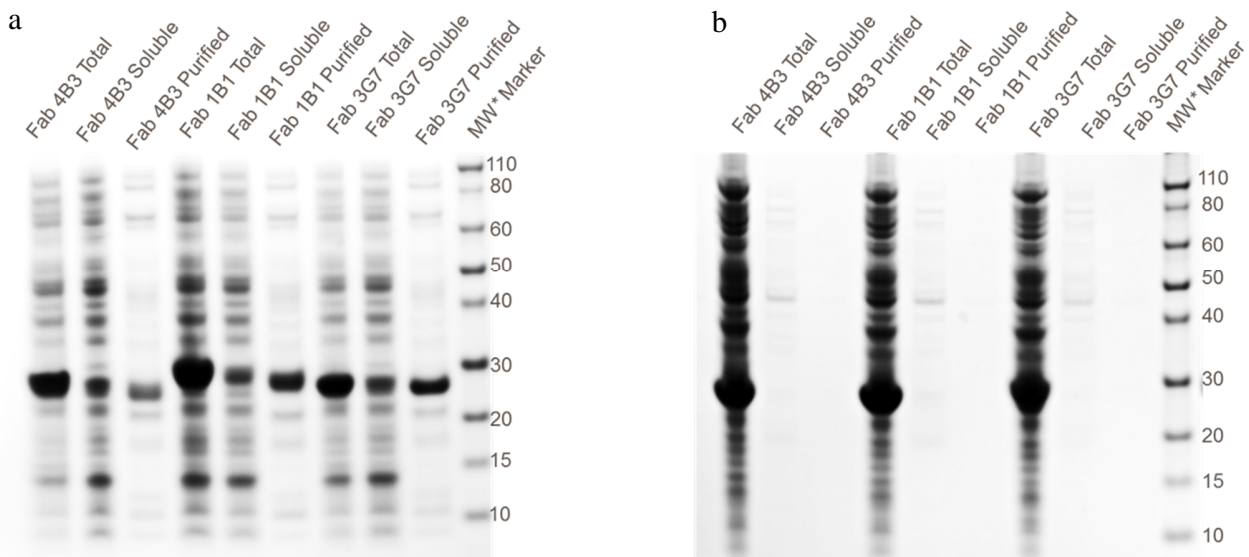


Figure 1. Comparison between the two expression methods tested for Fab production. SDS-Page analysis for the comparison of the two expression/lysis systems for three of the 24 huFabs produced in the pilot experiment. Samples are run in reducing condition followed by Coomassie staining of the fraction from whole cell lysis by cell lytic express (a) and from periplasmic samples obtained by shock osmotic (b). MW: molecular weight.

3.2 13 cross-reactive monoclonal antibodies have been selected by Gyros analysis

After miniaturized IMAC purification, all huFabs were analyzed at Gyros®, a nanoliter-scale immunoassay system, which is a highly sensitive technology allowing the determination of binding specificity even for samples with sub-optimal quality. As shown in figure 2, the majority of the huFabs tested recognized the fHbp v1 because it is the variant present in the vaccine used for immunization. On the other hands, despite only the fHbp v1 is included in 4CMenB vaccine, thirteen huFabs resulted to be cross-reactive between the three main variants of fHbp. One huFab, called 1B, resulted specific for the fHbp v2 being very interesting as none human anti-fHbp V2 specific antibody has been identified so far, therefore was also selected for further characterization.

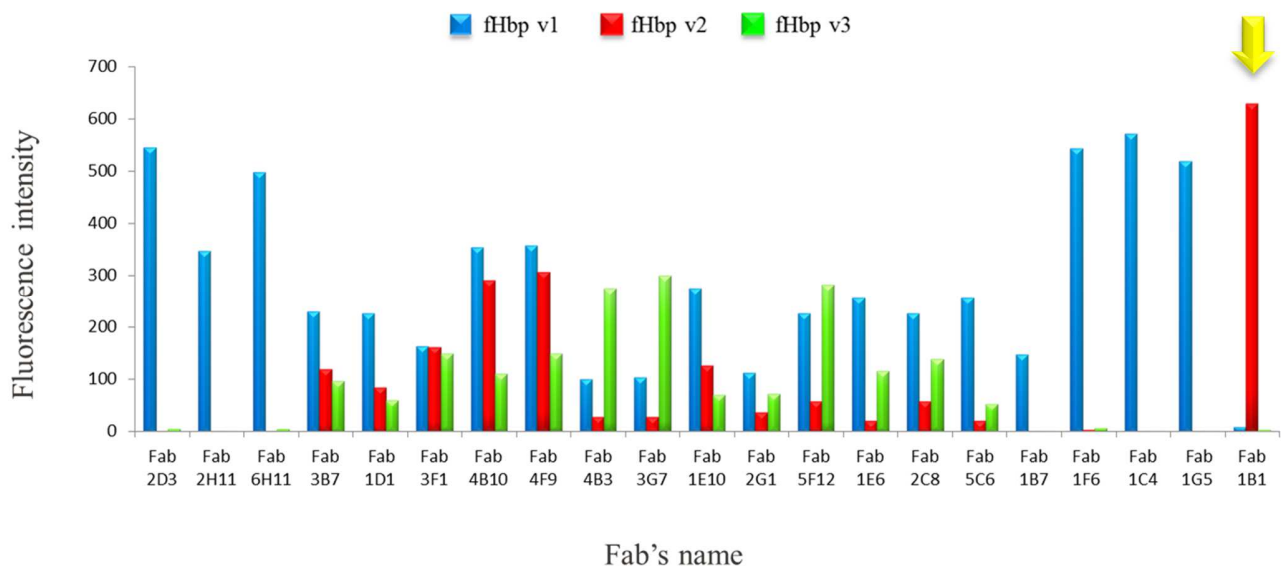


Figure 2. Histogram of binding specificity of 21 huFabs, including all the 13 cross-reactive identified by Gyros immuno-binding assay. The bars blue, red and green refers to the binding to fHbp v1, v2 and v3 respectively. The yellow arrow point to the interesting case of the Fab 1B1 seemed specific only for v2. The rest of huFabs tested are not shown.

3.3 Expression of recombinant mAbs in mammalian cells allowed obtaining pure IgGs with high yield

E. coli has been a popular mean for production of recombinant proteins. It is a well-established host that offers short culturing time, easy genetic manipulation and low cost media. However, it also has many disadvantages. For example, the rapidity of bacterial protein expression often results in unfolded/misfolded proteins, especially for heterologous proteins that require longer times and/or molecular chaperones to fold correctly. In addition, the highly reductive environment of the bacterial cytosol and the inability of *E. coli* to perform several eukaryotic post-translational modifications results in the insoluble expression of proteins [47]. Due to the low yield and the high impurity of the huFabs produced *in E. coli*, prokaryotic expression resulted to be not a suitable method for further functional and structural study. However new advances in monoclonal antibodies (mAbs) technology allow to produce high amounts of mAb in mammalian cells. Two plasmids were constructed which separately encodes for

light chain (VL) and heavy chain (VH) for each mAbs. To perform a deeper functional characterization of these antibodies, we produced them in mammalian cells as full recombinant IgG isotype 1 as IgGs 1 are the most abundant immunoglobulin subclass in human sera [48]. Expression of recombinant mAbs in mammalian cells allowed obtaining antibodies with high purity and high yield as from 60 ml of transfection we could recovery 4-7 mg of pure proteins immediately after the first step of purification as shown in figure 3.

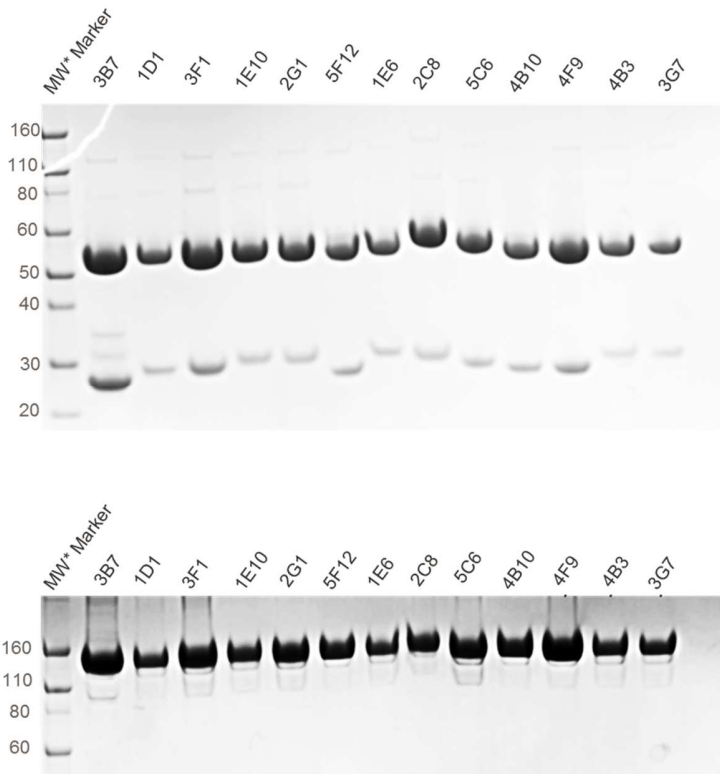


Figure 3. Purity and quality check of the recombinant cross-reactive mAbs. SDS-PAGE gel of thirteen cross-reactive mAbs sample run in in reducing (a) and non-reducing conditions (b) followed by Coomassie staining

The selected 13 recombinant cross-reactive antibodies and the mAb 1B1, were used for further functional analysis and characterized for antigen binding affinities, complement-mediated bactericidal activity and their ability to compete with fHbp for the binding of human fH (hfH).

3.4 Selected mAbs have high affinity for the three fHbp main variants

Surface plasmon resonance (SPR) was used to investigate the interaction between mAbs and the purified recombinant fHbp variants, in terms of binding affinity and association/dissociation kinetics. As shown in table 1 the analysis revealed that all mAbs have moderate/high affinity for the three variants of fHbp with K_d ranking from $10E-9$ M to $10E-11$ M. Overall kinetics constants measured indicate mAbs bind the fHbp forming stable complexes. Except for the case of mAb 1E6 which shows rapid association to fHbp v1 followed by a fast dissociation, suggesting the formation of a “short life” 1E6: fHbp v1 complex, Interesting the mAb 1B1, that at to the first screening appeared to be specific for v2, is able to bind with high affinity the v1 and the v3.

Tables 1. Summary of SPR analysis

mAbs	fHbp v1		
	Ka (M ⁻¹ s ⁻¹)	Kd (s ⁻¹)	Kd (M)
3B7	1,71E+6 ± 0,02	4,42E-3 ± 0,03	2,6E-9 ± 0,06
1D1	1,81E+6 ± 0,67	1,54E-3 ± 0,04	8,93E-10 ± 1,03
3F1	8,85E+5 ± 0,49	9,17E-4 ± 0,15	1,04E-9 ± 0,05
1B1	6,90E+5 ± 0,06	5,14E-4 ± 0,03	7,44E-10 ± 0,02
1E10	4,27 E+5 ± 0,26	6,57E-4 ± 0,19	1,54 E-9 ± 0,05
2G1	4,51E+6 ± 0,48	5,0E-3 ± 0,01	1,08E-10 ± 0,08
5F12	8,54E+5 ± 0,13	8,46E-4 ± 0,07	1,01E-9 ± 0,02
1E6	5,25E+7 ± 0,15	1,4E-2 ± 0,01	2,65E-10 ± 0,15
2C8	1,16E+6 ± 0,13	3,88E-4 ± 0,37	3,4E-10 ± 0,68
5C6	4,2E+5 ± 0,02	4,54E-4 ± 0,09	1,08E-9 ± 0,02
4B10	7,7E+6 ± 0,9	2,5E-3 ± 0,2	2,96E-10 ± 0,08
4F9	3,29E+7 ± 0,19	2,51E-3 ± 0,03	7,7 E-11 ± 1,2
4B3	6,61E+5 ± 0,02	2,17E-4 ± 0,15	3,28E-10 ± 0,25
3G7	9,03E+5 ±	3,11E-4 ± 0,25	3,44E-10 ± 0,32

mAbs	fHbp v2		
	Ka (M ⁻¹ s ⁻¹)	Kd (s ⁻¹)	Kd (M)
3B7	1,32E+6 ± 0,10	7,13E-6 ± 0,01	5,51E-10 ± 0,49
1D1	4,5E+5 ± 3,0	2,64E-3 ± 0,04	2,61E-9 ± 0,37
3F1	3,82E+5 ± 0,79	4,78E-3 ± 0,03	1,13E-8 ± 0,06
1B1	7,15E+5 ± 0,48	1,19E-4 ± 0,003	1,68E-10 ± 0,11
1E10	6,3E+5 ± 2,9	7,9E-4 ± 1,6	1,4E-9 ± 0,4
2G1	2,7E+5 ± 0,6	4,5E-4 ± 0,4	1,7E-9 ± 0,2
5F12	6,9E+5 ± 1,3	1,88E-3 ± 0,02	2,75E-9 ± 0,15
1E6	1,2E+5 ± 0,15	4,3E-4 ± 1,3	3,6E-11 ± 0,7
2C8	1,31E+7 ± 0,02	6,89E-4 ± 0,09	5,25E-11 ± 0,03
5C6	2,04E+5 ± 0,05	3,45E-4 ± 0,08	1,7E-9 ± 0,01
4B10	1,57E+7 ± 0,07	7,06E-4 ± 0,09	4,51E-11 ± 0,25
4F9	1,16E+6 ± 0,01	3,30E-5 ± 0,01	2,85E-11 ± 0,02
4B3	2,73E+6 ± 0,34	7,98E-5 ± 0,20	2,9E-11 ± 0,35
3G7	7,41E+5 ± 0,52	3,89E-5 ± 0,11	5,26 E-11 ± 0,22

mAbs	fHbp v3		
	Ka (M ⁻¹ s ⁻¹)	Kd (s ⁻¹)	Kd (M)
3B7	3,82 E+5 ± 0,85	8,3E-4 ±0,7	2,2E-9 ± 0,3
1D1	3,71E+5 ± 0,03	6,42E-4 ± 0,03	1,72E-9 ± 0,01
3F1	3,4 E+5 ± 0,8	6,3E-4 ± 3,2	1,80E-9 ± 0,01
1B1	5,98E+5 ± 0,01	3,14 E-4 ± 0,05	5,25E-10 ± 0,09
1E10	3,9E+5 ± 0,1	4,95E-4 ± 0,09	1,27E-9 ± 0,02
2G1	3,32E+5 ± 0,01	5,84E-4 ± 0,01	1,75E-9 ± 0,01
5F12	3,50E+5 ± 0,01	6,13E-3 ± 0,02	1,75E-9 ± 0,01
1E6	5,7E+5 ± 1,8	1,3E-3 ± 0,3	2,7E-9 ±1,3
2C8	4,3E+5 ± 0,1	2,0E-4 ± 0,6	4,6E-10 ± 1,6
5C6	3,50E+5 ± 0,01	7,10E-4 ± 0,07	2,03E-9 ± 0,02
4B10	2,84E+5 ± 0,06	4,73E-4 ± 0,01	1,67E-9 ± 0,03
4F9	3,8 E+5 ± 0,5	9,5E-4 ± 4,3	2,4E-10 ± 0,9
4B3	3,15E+5 ± 0,06	2,00E-4 ±0,01	6,33E-10 ± 0,13
3G7	2,58E+5 ± 0,01	1,76E-4 ± 0,35	6,8E-10 ± 1,4

Binding affinity and association/dissociation kinetics were measured at Biacore T200 (GE Healthcare). According to the manufacturer's instruction, consultable to web site:

https://www.biacore.com/lifesciences/help/kinetics_and_affinity/index.html, we define:

- high affinity $K_d \geq 10E-10$ (M), moderate affinity $K_d = 10E-9$ (M) and low affinity $K_d > 10E-8$ (M)
- fast association $K_a \geq 10E+5$ (M⁻¹ s⁻¹), moderate $K_a = 10E+4$ (M⁻¹ s⁻¹) and slow $K_a \leq 10E+3$ (M⁻¹ s⁻¹)
- fast dissociation $K_d \geq 10E-2$ (s⁻¹), moderate dissociation $K_d = 10E-3$ (s⁻¹), slow dissociation $K_d \leq 10E-4$ (s⁻¹)

3.5 mAbs recognize native fHbp on live bacteria

Meningococcal fHbp is a surface-exposed 28 kDa globular lipoprotein bound to the outer membrane by an N-terminal lipid anchor. Therefore, flow cytometry represents a remarkably versatile tool to detect the α -fHbp mAbs binding directly to the surface of the bacteria. FACS analysis confirmed that all 14 human α -fHbp recombinant IgGs bind naive fHbp to the surface of live MenB strains MC58, M08-0240104 and UK320, currying respectively the fHbp v1, v2 and v3, excepted mAbs 5C6, negative on v3. In figure 4 we can also observed that all mAbs shown different order of fluorescent signals intensity; 10 fold stronger on the meningococcal strain expressing v2, while slightly lower differences of binding were found on v1 and v3. The amount of fHbp presents on bacterial surface varies between meningococcal strains and it has been previously described that the strain M08-0240104 carries an fHbp surface density higher than the other strains [49] could explaining the higher florescent intensity measured.

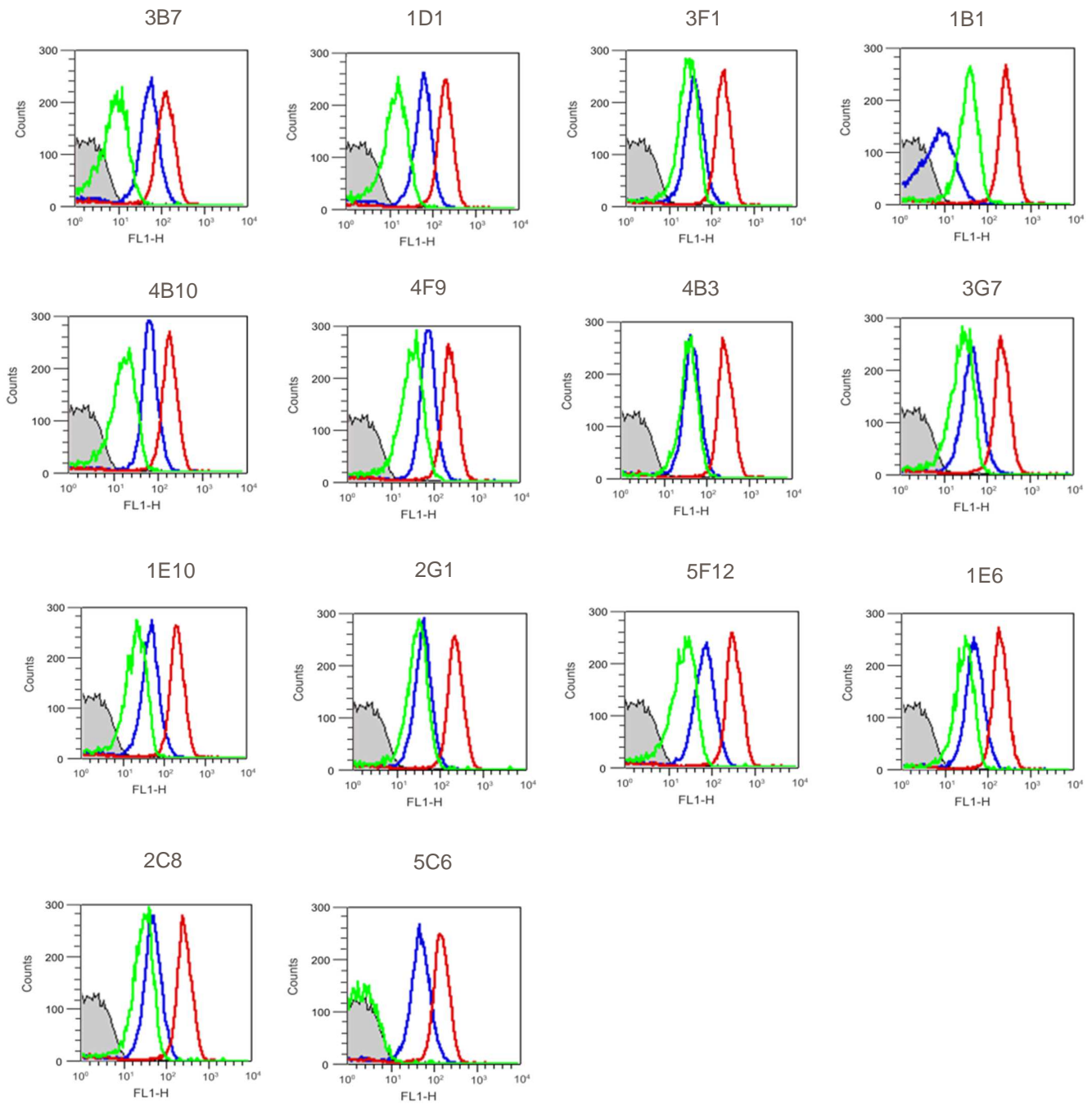


Figure 4. Binding of mAbs to live meningococci as measured by flow cytometry. In blue the H44/76 expressing v1, in red the M08-0240104 expressing v2 and in green the M01-0240320 exposing the v3. Gray-filled area represents negative control bacteria incubated with PBS and secondary antibodies FITC-conjugated antibodies.

3.6 α -fHbp mAbs compete with fHbp for human factor H binding

The meningococcal fHbp binds human fH with high affinity [24]. So far, none human anti fHbp mAb has been described to be able to compete with human hfH binding to fHbp, probably due to the small amount of human monoclonal antibodies tested. The 14 human recombinant mAbs were also tested for their ability to inhibit hfH binding to native fHbp by FACS analysis. Remarkably, we found that four of these mAbs are able to compete with fHbp for human hfH binding. As shown in figure 5, signal reduction of hfH binding (green line) was observed for mAb 4F9, 4B3 and 3G7 compared with the hfH binding detected alone in PBS on strains MC58, UK104, UK320 expressing fHbp v1, v2 and v3 respectively. The mAb 1B1, instead, competes with hfH binding in strains expressing fHbp v2 and v3, but not v1.

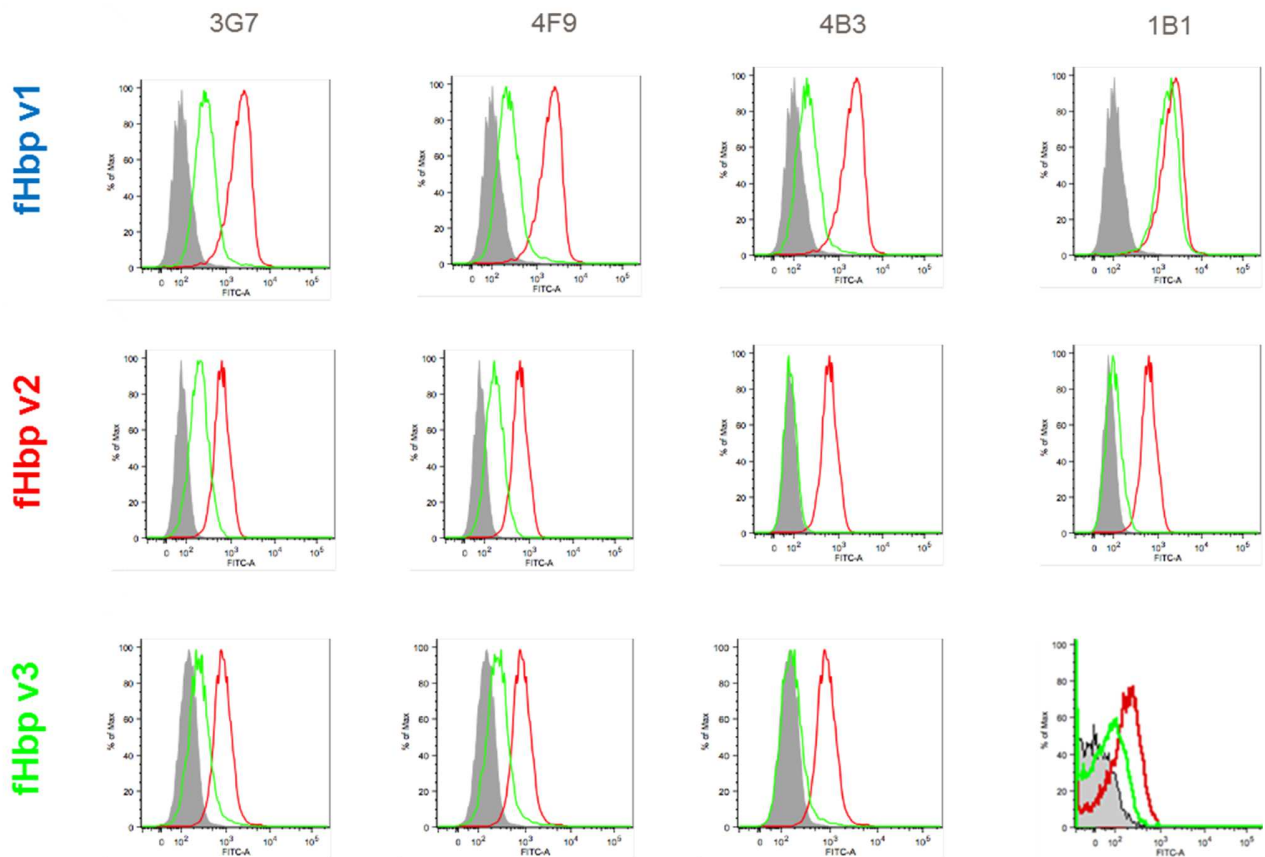


Figure 5. Flow cytometry analysis of hfH binding inhibition. Gray-filled area represents negative control bacteria incubated with PBS and secondary antibodies FITC-conjugated. Histograms showing effect of 4 HumAbs anti-fHbp on binding of human fH to live meningococci strains. Red line, binding of hfH alone (10 μ g/ml); green line, binding of hfH when bacteria were pre-incubated with 50 μ g/ml of HumAbs anti-fHbp. In the last histogram of panel B, inhibition of hfH binding by murine anti-fHbp polyclonal serum (1:100). Gray-filled histogram represents negative control bacteria incubated with PBS and secondary antibodies FITC-conjugated.

3.7 Cross-protective anti-fHbp human mAbs

The bactericidal activity of the human mAbs was tested against MenB strains expressing distinct fHbp v1, v2 and v3 and using baby rabbit serum as source of exogenous complement. Rabbit serum bactericidal assay (rSBA) is a standardized and validate method to evaluate the immune response to *Neisseria Meningitidis* [50] and it is widely use to estimate protection of the vaccine [51] [52].

The analysis revealed that eight mAbs were bactericidal against strains carrying fHbp v1 and six against strains carrying fHbp v3, meanwhile all anti-fHbp antibodies were bactericidal against the strain carrying fHbp v2 (Figure 6a). After repeating the experiment using the human serum, only four mAbs resulted to be able to activate the complement cascade and induced bacterial killing against MenB strains carrying the three variants of fHbp (Figure 6.b). As expected, titers obtained with human complement source are lower compared to those obtained with rabbit complement.

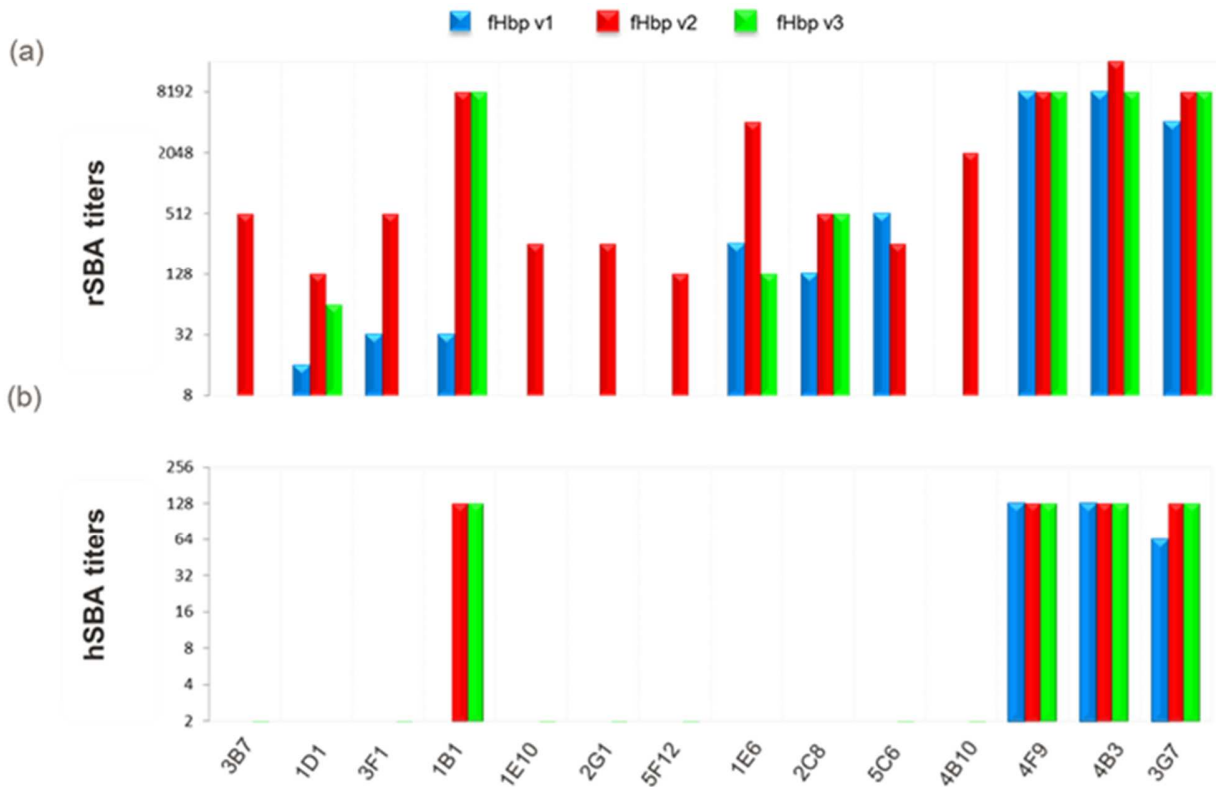


Figure 6. Bactericidal killing assay (SBA). Histograms of bactericidal titers (a) using rabbit (rSBA) and (b) human serum (hSBA) as source of complement against meningococcal strains expressing v1, v2 and v3 colored in blue, red and green respectively.

3.8 Protein chip epitope mapping suggested mAbs have different recognition profile

To map and identify the binding epitope regions, each mAbs was tested by a protein microarray, containing the full lengths and different overlapping recombinant fragments covering the entire length of the fHbp v1, v2 and v3 [36].

Protein chip experiments (Table 2) suggested that all mAbs recognize conformational epitopes present on the entire full-length sequence of fHbp variants, with two exceptions: the mAb 1B1 did not bind to the fHbp v3 and the mAb 5C6 did not recognize the fHbp v2 and v3. Four mAbs (1B1, 4F9, 4B3, 3G7) recognized, in addition to the full-length fHbp proteins, a fragment corresponding to the C-terminal β -barrel (residues 319–434) suggesting that the epitope is localized in that region of fHbp. Finally the mAb 5F12, is the unique antibody able to bind the fragment corresponding the N-terminus (residues 1-259 of fHbp variants) fig7.

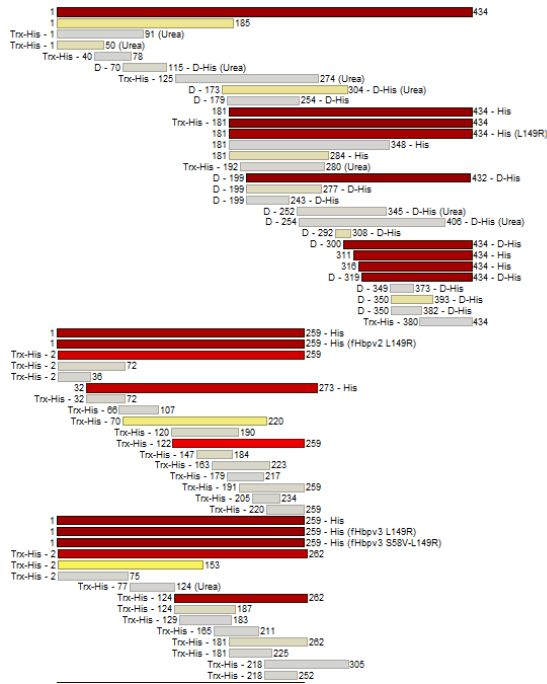
mAbs	fHbp v1			fHbp v2			fHbp v3		
	full length	β -Barrel	N-terminus	full length	β -Barrel	N-terminus	Full Length	β -Barrel	N-terminus
3B7	X			X			X		
1D1	X			X			X		
3F1	X			X			X		
1B1	X	X		X	X				
4B10	X			X			X		
1E10	X			X			X		
2G1	X			X			X		
5F12	X		X	X		X	X		X
1E6	X			X			X		
2C8	X			X			X		
5C6	X								
4F9	X	X		X	X		X	X	
4B3	X	X		X	X		X	X	
3G7	X	X		X	X		X	X	

Table 2. Protein chip epitope mapping results

Epitope localization and cross-reactivity with different fHbp variants assessed by protein microarrays
Symbol X is used to indicate which region of fHbp are recognized by tested mAbs, instead the empty boxes indicate no binding.

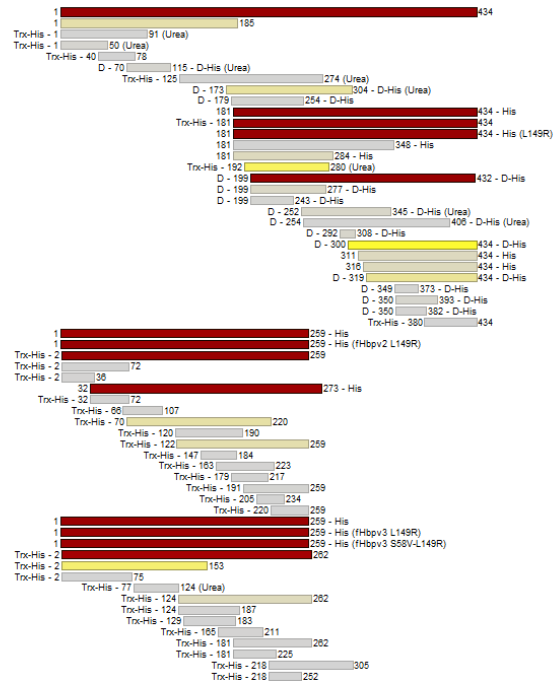
a

mAb4B3



b

mAb1E6



c

mAb5F12

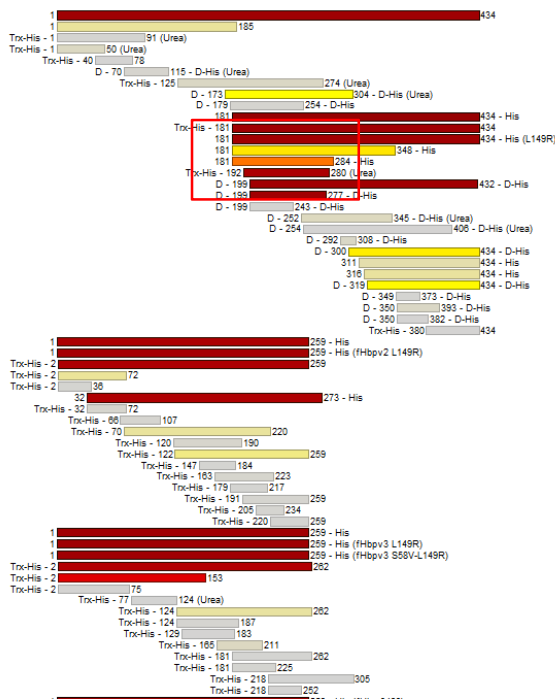


Fig.7 protein chip epitope profile of the cross-reactive mAbs. In the figure are reported the profiles of three representative mAbs:

- a) mAb4B3 which recognizes the full length and the C-terminal β -barrel in all fHbp variants.
- b) mAb1E6 mAbs that binds only the full length in all fHbp variants.
- c) mAb5F12 that is able to bind N-terminal domain in all fHbp variants.

Bars which represents fragments at different length, are colored in yellow (low) to brown (high), according to the binding fluorescent signal intensity .

3.9 Crystallization conditions identification and optimization.

Based on the functional and biochemical data obtained, six antibodies have been selected for expression as high quality Fabs in mammalian cells and co-crystallization studies. The antibodies 3G7, 4B3 and 4F9 have shown cross-protection in human SBA for all fHbp variants, the highest affinity for all fHbp variants and they are able to compete with human fH for fHbp binding. However, they all recognize the β -barrel of the fHbp in all 3 variants, and they share 99,8% of sequence similarity of the variable regions. We decided to select the mAb 4B3 for crystallization trials as it is more easy to produce (higher yield) respect to the other two mAbs. The antibody 5F12 has been selected as it recognizes, in the protein chip experiments, N-terminal domain of fHbp in all 3 variants, differently from what have been observed for all the other human mAbs anti-fHbp antibodies tested so far (which recognized the full length protein and the C-terminal β -barrel domain or only the full length fHbp [36]). Three of the mAbs (1D1, 1E6, 2C8) were selected for being cross-protective in rSBA having different variable region sequences. Finally, the antibody 1B1 was mostly selected for its ability to compete with human fH for fHbp binding and for being protective in hSBA.

The structure determination of protein complexes by X-ray crystallography is strictly dependent on obtaining a crystal suitable for data collection. The conditions for complex crystallization have to be determined empirically and are specific to each protein complex. To perform crystallization screening, the protein/antibody complex must be pure and at high concentration. Therefore, after overnight incubation, complexes huFab:fHbp were purified by size exclusion chromatography to remove the un-complexed protein. In total 10 complexes were successfully purified and tested at least in 480 different crystallization conditions(see table 3).

Table 3: Summary of the crystallization screening.

	complex	crystallization conditions	n. crystals	Diffraction
1	huFab 4B3:fHbp v1	864	70	2.4 Å
2	huFab 4B3:fHbp v2	480	-	-
3	huFab 4B3:fHbp v3	480	25	-
4	huFab 5F12:fHbp v2	480	10	2.1 Å
5	huFab 5F12:fHbp v1	480	-	-
6	huFab 1E6:fHbp v3	576	15	2.7 Å
7	huFab 1D1:fHbp v1	576	-	-
8	huFab 1D1:fHbp v2	576	10	-
9	huFab 2C8:fHbp v1	576	-	-
10	huFab 1B1:fHbp v2	576	3	2.3 Å

In the table are shown the complexes obtained and tested. For each complex is reported the number of crystallization conditions tested, many crystals were collected and diffraction data collected at the Synchrotron in Grenoble.

3.10 Overall crystal structure of huFab 4B3 in complex with fHbp v1

The human Mab 4B3 is one of the most interesting monoclonal antibodies emerged from the screening, being cross-reactive, cross-protective with human complement and able to compete with human fH binding to fHbps. For these reasons it was selected for co-crystallization experiments. Despite the complex huFab4B3:fHbp v1 was tested in more than 800 crystallization conditions, crystals were obtained only in one condition (buffer containing 0.1M HEPES with 20% w/v jeff ED-2001 as precipitant at pH 6.5). The 3D structure of the complex was solved by molecular replacement and the resulting electron density map allowed unambiguous model building. X-ray data collection, processing and refinement statistics are show in the **table 4** below.

resolution range (Å)	41.55 - 3.399 (2.485 - -2.399)
Space group	P1 21 1
Unit cell dimensions	
<i>a, b, c</i> (Å)	47.34 90.4 97.94
<i>α, β, γ</i> (°)	90 98.81 90
Total reflections	103526 (11534)
Unique reflections	29999 (3201)
Completeness (%)	92,95 (99.88)
Mean <i>I</i> / <i>σ</i> (<i>I</i>)	17.61 (2.49)
Wilson <i>B</i> -factor	50.42
Rmerge	0.05551 (0.5353)
Rmeas	0.06573 (0.6304)
CC1/2	0.997 (0.822)
R-work	0.2122 (0.2802)
R-free	0.2715 (0.706)
Number of atoms	
Macromolecules	5053
Protein residues	666
RMS bonds (Å)	0.004
RMS angles (°)	0.65
Ramachandran favored (%)	96.64
Ramachandran allowed (%)	3.06
Ramachandran outliers (%)	0.31
Rotamer outliers (%)	0.18
Average <i>B</i> -factor	56.19
Macromolecules	556.25
Solvent	50.97

Considered separately, the fHbp and Fab structures show no major differences from those structures reported previously. [21] [30] [22] [23]. The huFab 4B3 has a canonical β -sandwich immunoglobulin fold with the heavy chain folding into VH and CH (variable and constant heavy) domains, and the light chain folding into VL and CL (variable light and constant light) domains (figure 8). The elbow angle, defined as the subtended angle by the two pseudo twofold axes relating VH to VL and CH to CL, of the Fab 4B3 is 161 °C [53].

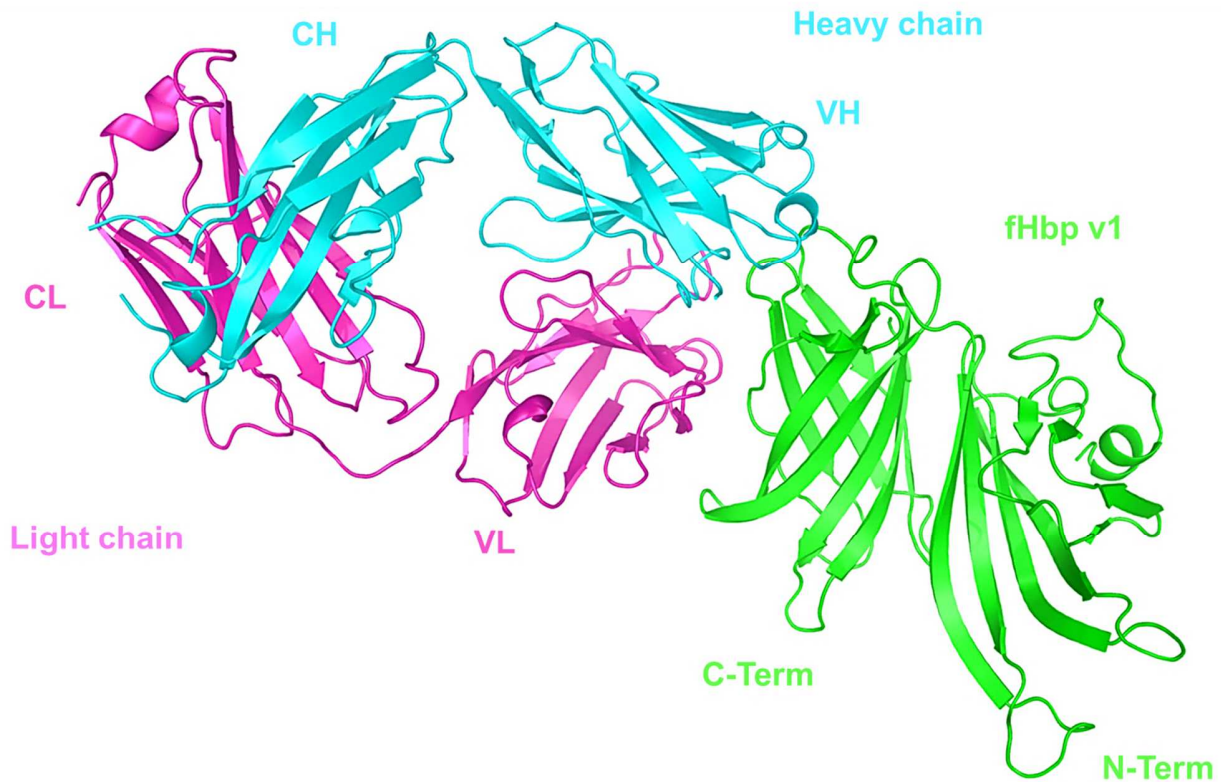


Figure 8. Crystal structure of huFab4B3 in complex with the fHbp v1. The structure of huFab 4B3 and fHbp v1 are represented as cartoons, with the heavy chain, the light chain and the fHbp v1 colored in cyan, light pink and green respectively.

The antigen-binding site of an antibody is localized on six-hypervariable loop or CDR (Complementarity-determining regions) mapped as L1: Q27-F33, L2:G51-D58, L3: Q90-T98, H1: G26-Y33; H2: I52-K58; H3: C96-W106. Overall, although there is great variation in the aminoacidic sequence and length of the CDRs, it has been shown that five of them (with CDR-H3 being the only exception) possess a small set of main-chain conformations termed canonical structures [54], based on the length and key residues of loops. HuFab 4B3's CDRs L2, L3, H1 and H2 assumed the canonical structure of Chothia class 1,1,1,3 respectively instead, the CDR-L1 shows no canonical conformation of the same loop length known [55]. All six CDR loops of Fab 4B3 are projected to the C-terminal β -barrel of fHbp v1, whereas the N-terminal region is not involved in the interaction (Figure 8). Interestingly, the surface of the fHbp at the interface between the antibody appeared irregular with protuberances and with a well

define depressed area which accommodated the serine 31 (from H1) and the asparagine 53 (from H2) Figure 9(a). Moreover, we identified an isolated small cavity, which lodged the phenylalanine 33 of light chain (L1) Figure 9(b).

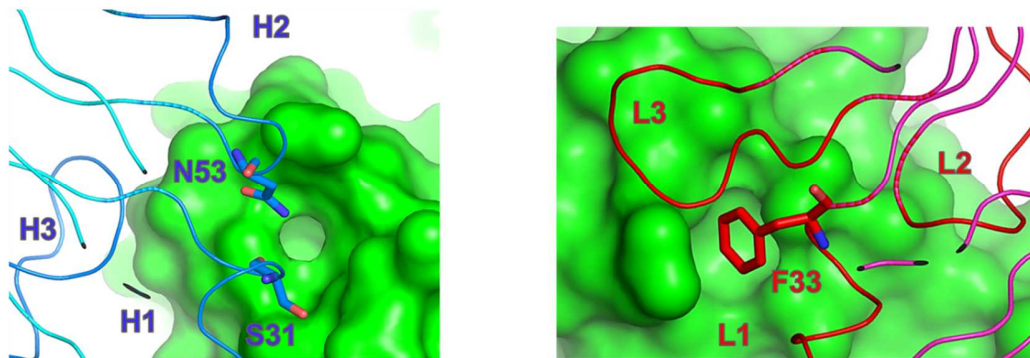


Figure 9. Crystal structure of CDRs of huFab 4B3 in complex with the fHbp v1. The structure of huFab 4B3 and fHbp v1 are represented as cartoons, with the variable heavy chain, the light chain and the fHbp v1 colored in cyan, light pink and green respectively. The CDRs of the variable region of the heavy chain named H1, H2, H3 are aligned in dark blue, the CDRs of the variable portion of the light chain, L1, L2, L3 are colored in red.

Shape complementarity is an important feature of the interfaces of biological assemblies of protein-protein complexes. Although it does not represent a physical interaction, it is highly correlated with certain interaction energies, such as van der Waals and non-polar desolvation [51]. The paratope form cleft and grooves assuming a shape that fit with epitope (Figure 10).

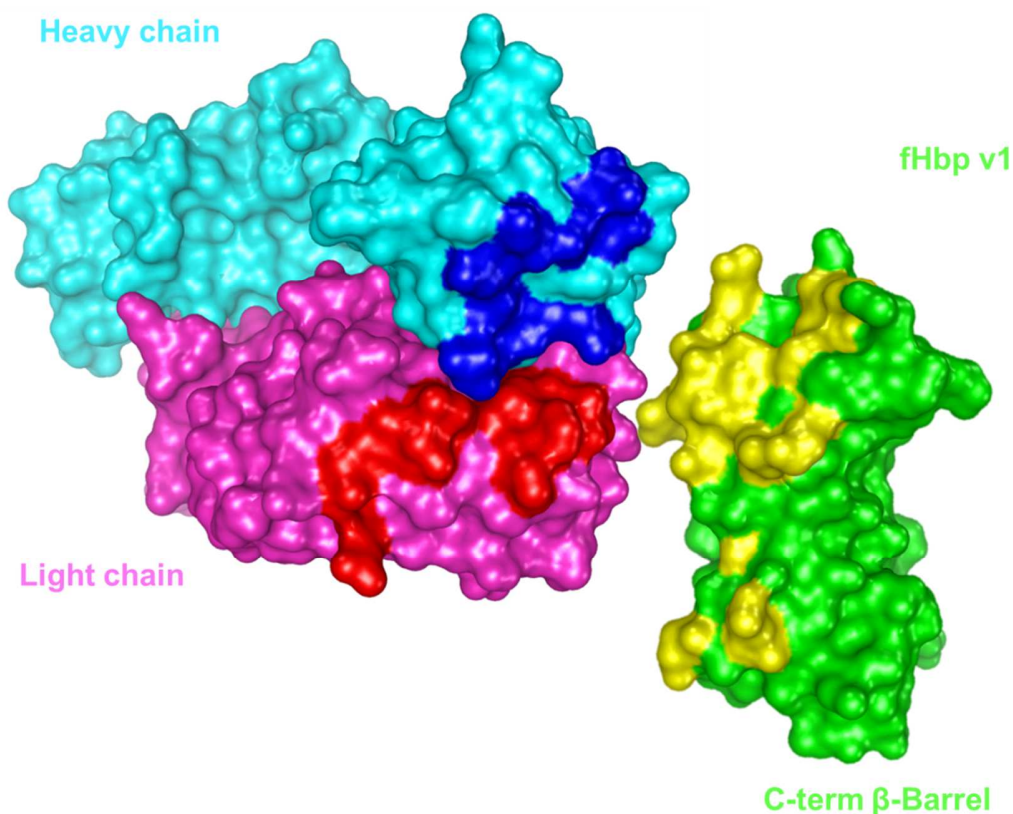


Figure 10. Buried complementary surfaces interactions. Representation of the complementary shape of the paratope of the huFab4B3 alighted in blue on heavy chain and in red on light chain surfaces. The surface of the epitope is colored in yellow on the C-term β -barrel of the fHbp v1.

The interaction of the huFab 4B3 with fHbp v1 buries a total area of 828 \AA^2 , which is in the typical range of the interaction surface between antibodies and protein antigens [56] [57]. The buried surfaces of the heavy chain and of light chain are similar (Figure 11(a)), with a major contribution from the heavy chain respect to the light chain (455.8 \AA^2 vs 372.2 \AA^2 respectively). The surface modeling of the contacts area provided additional information on the conformation of the epitope. The interactions occurring in the binding of huFab 4B3 define a discontinuous conformational epitope on the fHbp v1 surface, in which an extensive contact area is targeted by the light and the heavy chain simultaneously and a smaller contact area is determined by the L2 of the light chain (Figure 11 (a)).

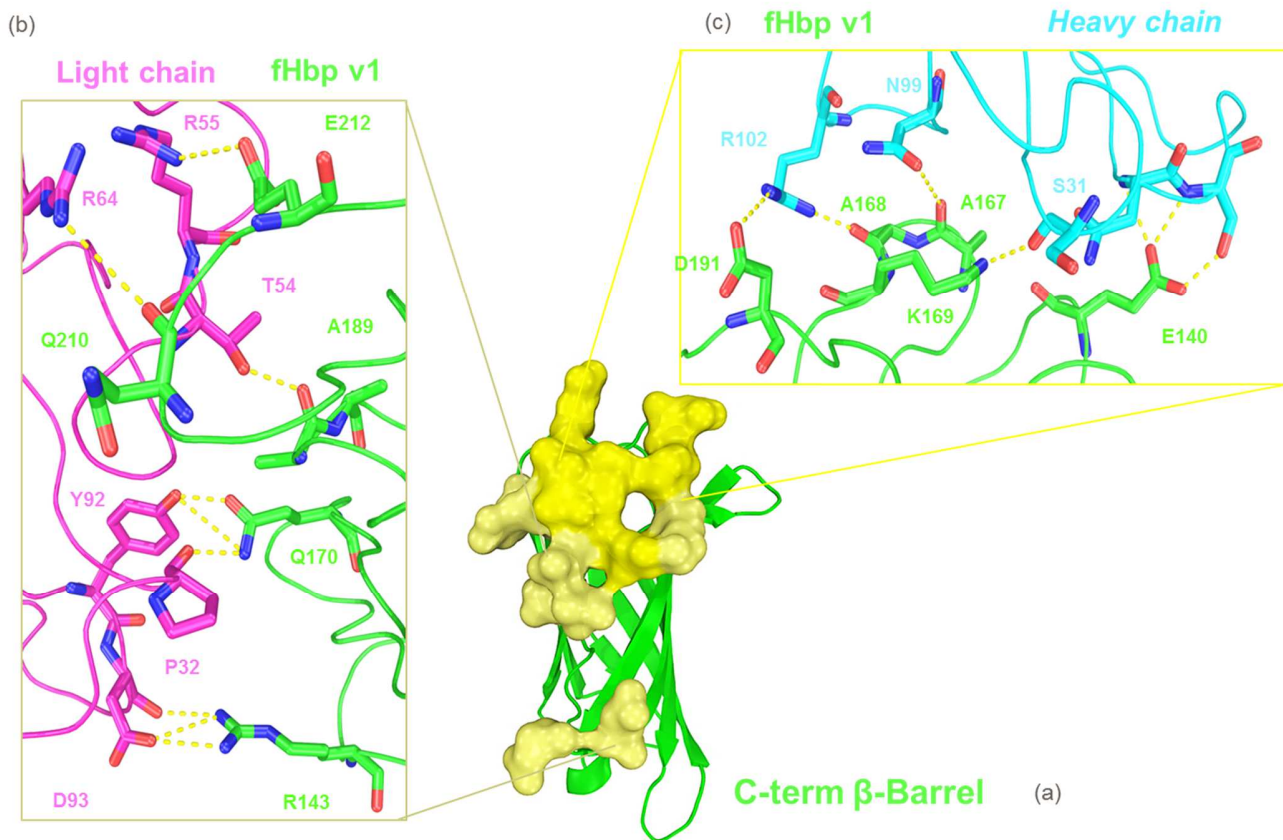


Figure 11. Intermolecular interactions in the Fab 4B3/fHbp-binding interface (a) Surface representation of the epitope on fHbp v1, colored in wheat is highlighted the contact surface of fHbp with the light chain while in yellow with the heavy chain. In the boxes is reported a closer view of key residues (shown as sticks) of the interaction between the C-terminal domain of fHbp (in green) and the light chain (in pink panel (a)) and the heavy chain (in cyan panel (c)). In both panels yellow dashed lines indicate intermolecular Hydrogen-bonds or salt bridges $<4 \text{ \AA}$.

Atomic resolution of the binding site enabled very accurate determination of key residues involved in the interaction. In total fifteen residues of fHbp engage very strong interactions as salt bridge or hydrogen bonds (Figure 11 panel (b) and (c)), with eight residues of the heavy chain and with seven of the light chain fully listed in Table 5. Interestingly, a supplementary contribution to strength the interaction comes from the arginine 64 of the light chain that is not included in any CDRs loops but it engages an hydrogen bond with the glutamine 210 of fHbp.

Table 5. Molecular interactions between key residues constituent the Fab4B3:fHbp v1 epitope

fHbp v1	huFab 4B3	CDR	Bond type
F135	S31, Y32	H1	Hydrogen bound, VdW
D136	S31	H1	Hydrogen bound
E140	N52, N53,S54	H2	Salt bridge, salt bridge, hydrogen bound
R143	D93	L3	Salt bridge
D165	F33	L1	VdW
A167	N99, Y33	H3, H1	Hydrogen bond , VdW
A168	R102	H3	Salt bridge
K169	S31	H1	Salt bridge
Q170	Y92, P32, R102	L3, L1, H3	Hydrogen bond, VdW, VdW
N172	P32	L1	VdW
A189	T54	L2	Hydrogen bond
D191	R102, Y50	H3, L2	Salt bridge, hydrogen bond
K193	T57	L2	Hydrogen bond
Q210	R64	-	Salt bridge
E212	R55	L2	Salt bridge

* VdW: Van Der Waals

3.11. Molecular insights of the cross-reactivity of mAbs 4B3

High-resolution epitope mapping allowed investigating deeper on the molecular basis of the mAb 4B3 ability to recognized different variants of fHbp observed in the functional characterization of this important antibody. To understand the main features that confer cross-reactivity ability to mAbs 4B3 we calculated the degree of conservation of the key residues of the epitope upon fHbp repertoire accessible in *Neisseria Meningitidis* multilocus sequence typing (MLST) databases. The main findings are reported in table 6 and in Figure 12. Upon 1119 allele of fHbp isolated from all meningococcal serogroup and depositate in MLST database we identified a cluster of residues, F135, D165, Q170, K193, E212 conserved more than 99% moreover the residues K169 was present in all isolated tested. Considering other two residues A167 and A168 present in more of the 75% of the instances, we observed a well-conserved and extensive core of the epitope colored in red and dark pink in Fig 10, instead the residue E212 represented an isolated key spot. Three residues, D136, A189, Q210 are present in 50-60% of fHbp variants known. Moreover the aspartic acid 191 (D191), even if being present at 20%, in the

40% of the cases is substituted by a glutamic acid likely maintaining the same characteristics and functions. The remaining key residues identified as important for mAb 4B3 binding localized around the core, show a substantial variability among the fHbp variants (table 6).

Table 6: Degree of conservation of the key residues involve in fHbp v1 and mAb 4B3

	%G	%A	%L	%M	%F	%W	%K	%Q	%E	%S	%P	%V	%I	%C	%Y	%H	%R	%N	%D	%T	%K
F135			0.27		99.64										0.09						
D136	1.70	0.09																43.1	55.1		
E140	0.09	0.09					32.3		24.4										0.09		43.1
R143				13.9			42.9		17.1									25.9			
D165	0.26																	0.09	99.64		
A167	0.09	80.8										0.45									18.7
A168		76.8					15.5		0.5			3.6						3.1			0.36
K169																					100
Q170								99.9										0.1			
N172									0.09					0.09	22.97	73.55			3.31		
A189		53.44							26.63	0.09	3.40										16.44
D191									43.43						35.57			0.63	20.38		
K193							99.29		0.63									0.09			
Q210	15.28							56.3	28.2							0.2					
E212							0.09		99.91												

The table shows the degree of conservation of the key residues of the mAb 4B3 epitope between fHbp sequences repertoire accessible in the *Neisseria Meningitidis* multilocus sequence typing (MLST) database at the website to <https://pubmlst.org/neisseria> which includes 1119 alleles of fHbp.

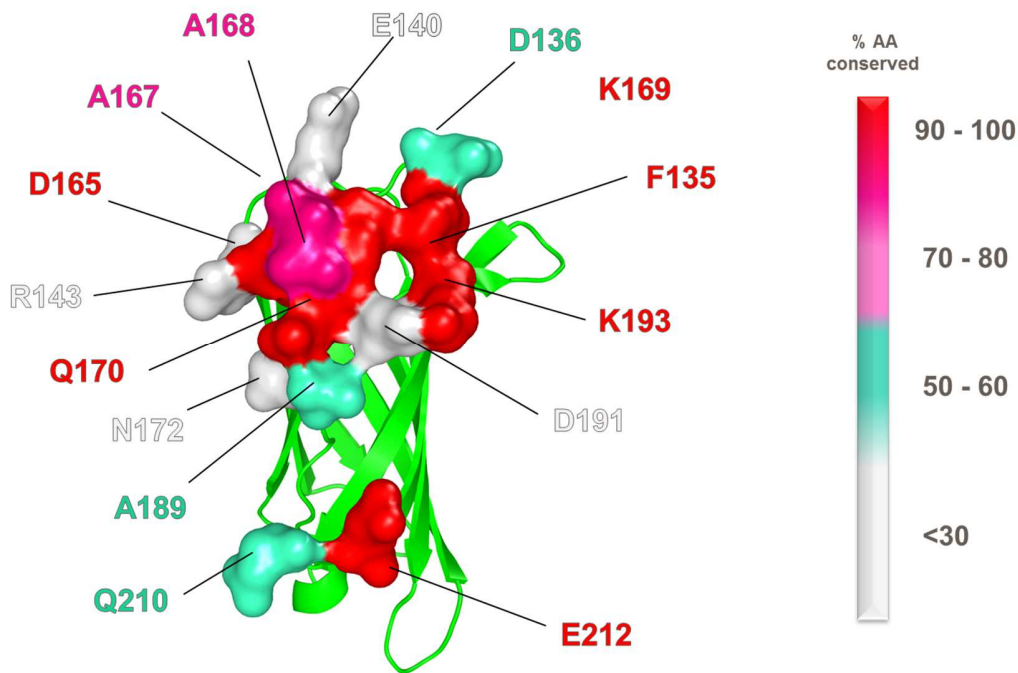


Figure 12. The 4B3 epitope and its allelic diversity in the fHbp global gene repertoire. The figure shows the C-terminal β-barrel of fHbp v1 and the surface of the epitope of the huFab 4B3. Each residue is colored based on its conservation among the fHbp gene repertoire, which included 1119 allelic sequences.

3.12 Nature of Ab 4B3 and human Factor H competition for fHbp v1 binding

The ability of the mAb 4B3 to reduce the human factor H binding on live bacteria assessed by flow cytometry suggests a competition for the binding region on fHbp. To better understand the molecular basis which take part in this complicated interactions, we superimposed the crystallographic structure of the huFab 4B3 with the structure of the short complement regulator domains 6 and 7 of the human factor H, available in the PDB [23], bound simultaneously to the fHbp v1.

Interestingly, surface modeling of the structure in exam revealed that the surface of the light chain of the huFab 4B3 slightly overlaps with the surface of the domain 6 of the human factor H (indicated in the blue box in Figure 13) suggesting that steric clashes occurs when these two proteins try to bind the fHbp at the same time. A deeper inspection shown in Figure 14, comparing the buried surface of fHbp confirmed that the binding site of the fHbp v1:huFab4B3 and fHbp v1:hfH partially overlapped in correspondence of three common key residues engaged in both complexes, the, K193, E212, D191. The first two residues are well conserved in almost all fHbp sequences known 99,3 % and 99,9% respectively instead the residues D191 is conserved only in the 20%. As mention before, in the 43% of the fHbp variants reported, Aspartic 191 is replaced by a glutamic residue, therefore it is logical to hypnotize that this atomic interaction could be maintained between almost 64% of the isolates

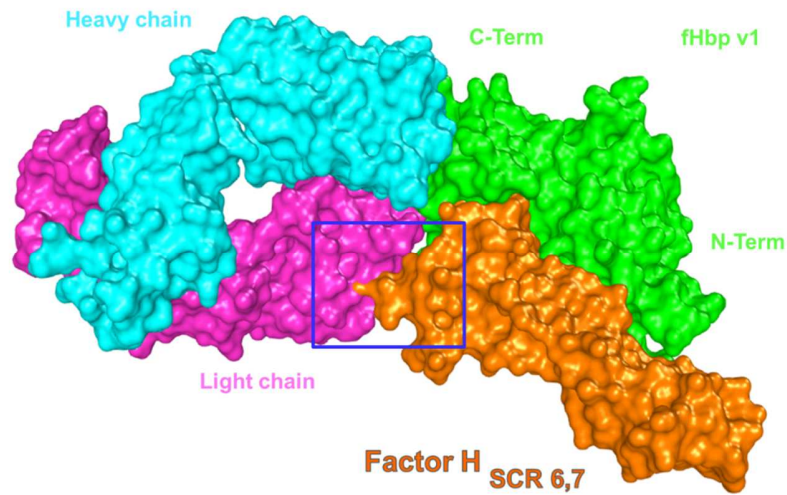


Figure 13. Competition between human Fab4B3 and human factor H for fHbp binding. Superimposition of the crystal structures of huFab 4B3 and the domains 6 and 7 of the human factor H (PDB 4AYI) in complex with the fHbp v1 represented as cartoons (a) or as solid surface (b), with the heavy chain, the light chain, the fHbp v1 and the human factor H colored in cyan, light pink, green and orange respectively. The blue box indicates a slight overlapping between the light chain of the huFab 4B3 and the domain 6 of the human factor H.

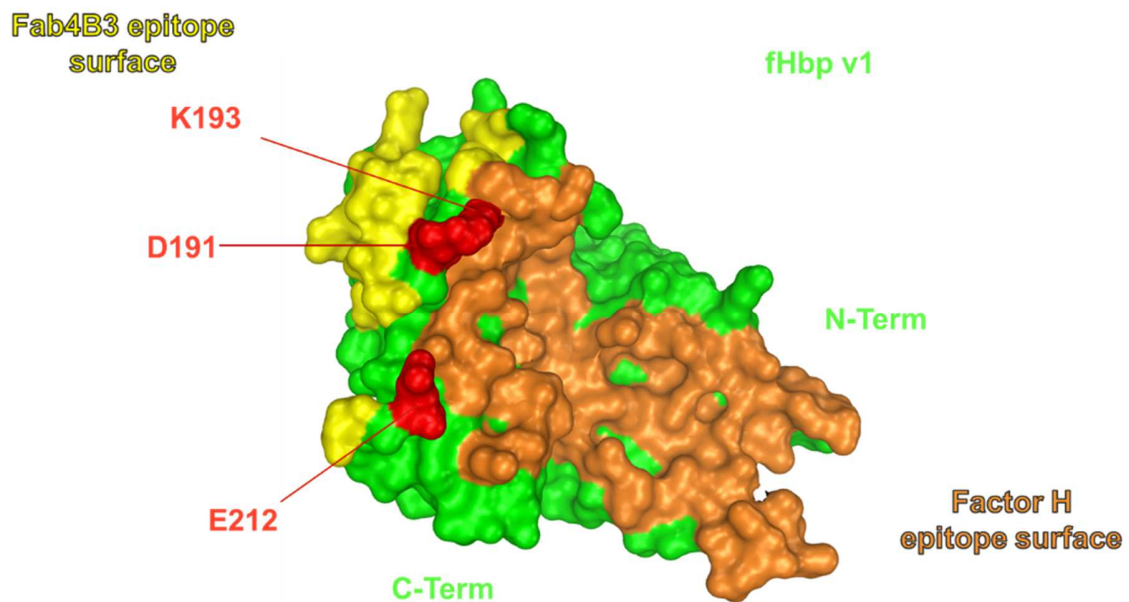


Figure 14. Surface plot of the competition of huFab4B3 with human factor H for fHbp binding site. The epitope of the huFab 4B3 is represented in yellow instead the epitope of human factor H in orange. In red are highlighted the residues in common between the two complexes.

3.13 Overall crystal structure of Fab 1E6 in complex with fHbp v3

From the co-crystallization trials set up with different antibodies and different fHbp variants, (table 3) the crystal structure of the fHbp v3 in complex with the cross-reactive human Fab 1E6 was obtained. The crystal structure of huFab 1E6 in complex with fHbp v3 was determined at 2.7 Å resolution. X-ray data collection, processing and refinement statistics are shown in Table 7. The structure was solved by molecular replacement and the resulting electron density maps allowed unambiguous model building.

X-ray data collection, processing and refinement statistics are show in the table 7 below.

resolution range (Å)	63.56 - 2.646 (2.741 - 2.646)
Space group	P 2 21 21
Unit cell dimensions	
<i>a, b, c</i> (Å)	42.9789 65.2795 278.828
<i>α, β, γ</i> (°)	90 90 90
Total reflections	1142421 (114785)
Unique reflections	23438 (2302)
Completeness (%)	96.79 (97.92)
Mean <i>I</i> / <i>σ</i> (<i>I</i>)	7.58 (2.12)
Wilson <i>B</i> -factor	39.14
Rmerge	0.952 (2.24)
Rmeas	0.9618 (2.263)
CC1/2	0.898 (0.44)
R-work	0.2340 (0.3021)
R-free	0.2695 (0.3621)
Number of atoms	
Macromolecules	5003
Protein residues	665
RMS bonds (Å)	0.004
RMS angles (°)	0.97
Ramachandran favored (%)	93.09
Ramachandran allowed (%)	6.30
Ramachandran outliers (%)	0.61
Rotamer outliers (%)	0.00
Average <i>B</i> -factor	47.90
Macromolecules	48.10
Solvent	38.49

Considered alone, the two proteins maintained their typical structural characteristics (Fig.15); the fHbp assumed the canonical 3D structure of two β -barrels connected by a short linker and the Fab exhibits the standard Ig domain fold. The structure of the 1E6 immunoglobulin domains consists of anti-parallel β -sheets arranged in a “sandwich” fashion with the heavy chain folding into VH and CH domains, and the light chain folding into VL and CL domains. The two sides of the sandwich motif are covalently linked by disulfide bonds. The elbow angle, defined by the relative displacement of the variable domains and the constant domains, is 138.2 degrees [53].

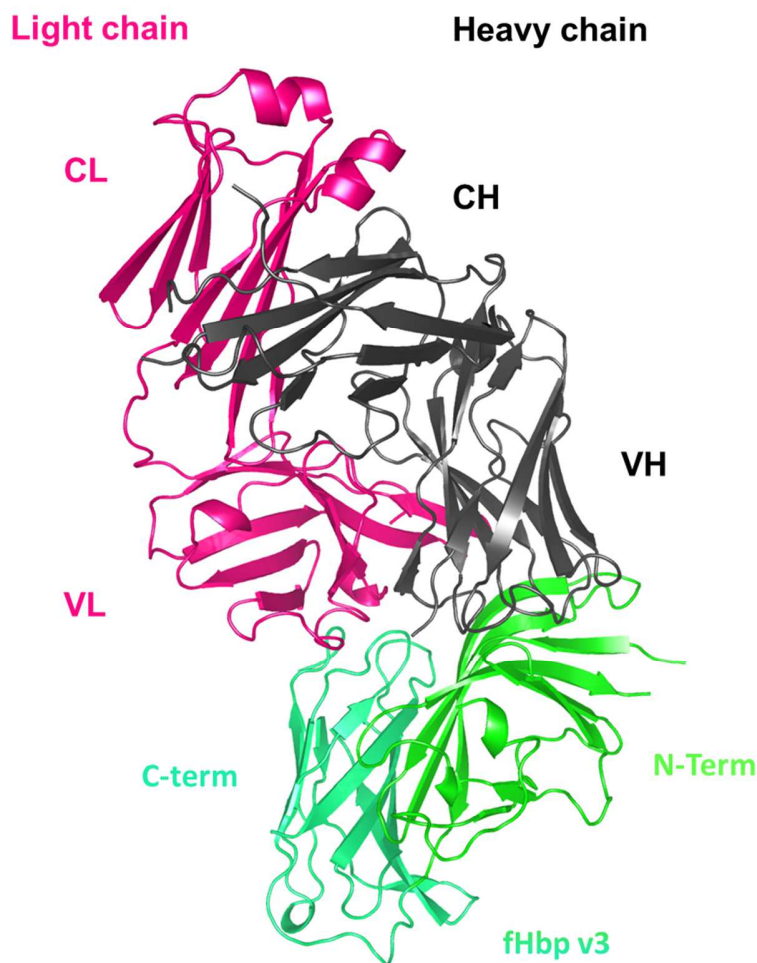


Figure 15. Crystal structure of Fab 1E6 in complex with the fHbp v3.

The structure of Fab 1E6 and fHbp v3 are shown as cartoons, with the heavy chain and the light chain colored in black and hot pink respectively. Meanwhile C-term β -barrel of the fHbp v3 is in greencyan and the N-terminus in green.

Antibody topology can be further divided into two parts, the framework and antigen binding regions. The sequence variability in the VL and VH are limited to hypervariable regions loop, which forms the antigen binding site of the molecule, also called complementarity determining region (CDR). CDR of mab 1E6 are mapped as L1:N26-V32, L2: Y49-S55, L3:Q88-W97, H1: G26- P33, H2: F51-S57, A97-102 is a loop connecting two β -strands, which points to the antigens Fig 16(a) (b). The 1E6’s CDR L1, L2, H1 H2 assumed canonical structure similar to Chothia class 2, 1, 1,2 [54]. The CDR-L3 shows no canonical conformation of the same loop length known [54]. Fab 1E6 forms a broad network of

interactions with N-term region of the fHbp v3 instead only three residues of the C-term are involved in the binding. The calculated interface buries a total area of 1058 \AA^2 , which is in the typical range of the interaction surface between antibodies and Fab:antigens [56], [57] and the N-term resulted mainly affected (Figure 15 c) . Both chains of huFab 1E6 contribute to binding of the fHbp v3 with the heavy chain that contacts only the N-terminal defining an interface area of 551 \AA^2 , whereas the light chain contacts both domains of fHbp (Fig. 16 a,b) on a surface of 507 \AA^2 .

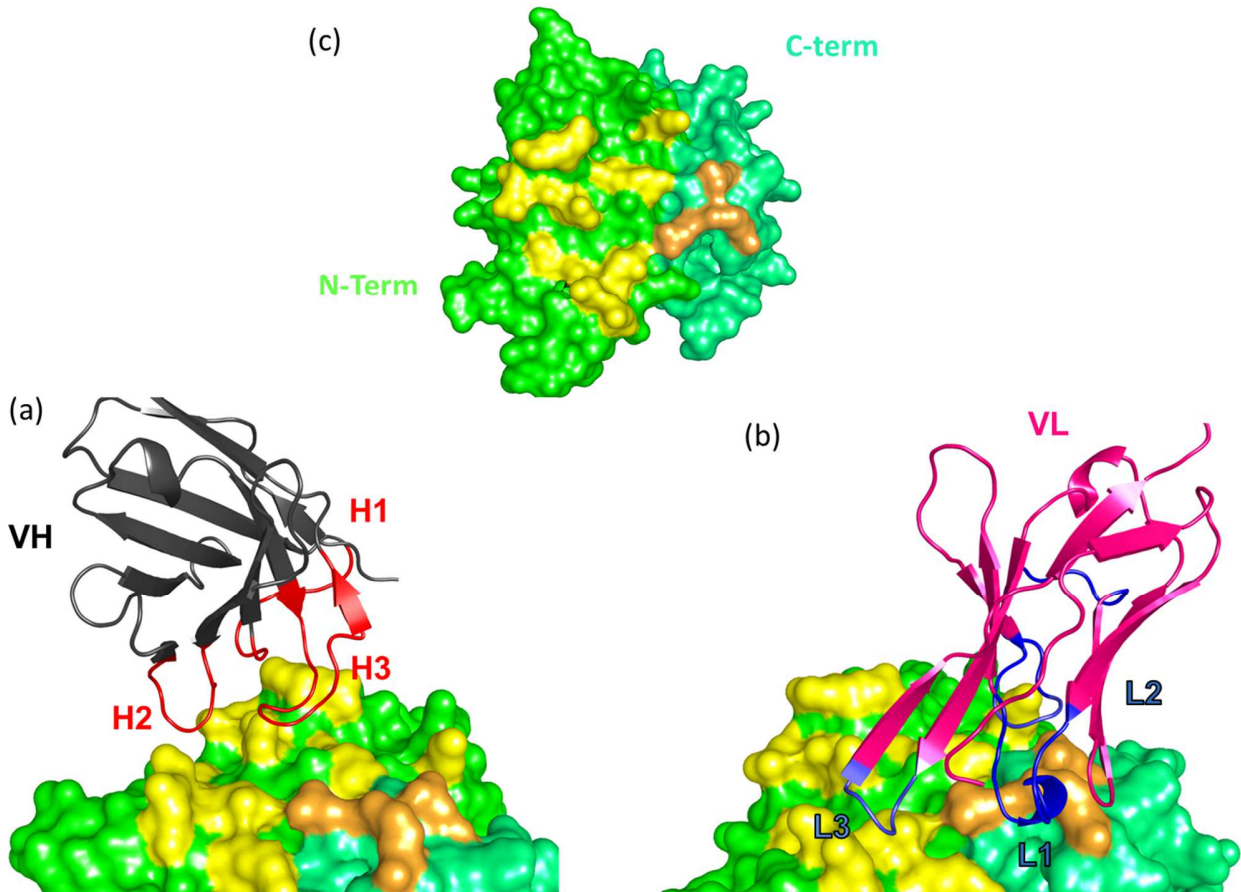


Figure 16. huFab 1E6 interaction with fHbp v3. The plot shows the fHbp v3 surface where the N-term is colored in green and the C-term in greencyan. The buried surface on the N-term is labeled in yellow whereas the area on the C-term in orange. (c) fHbp v3 is rotated of 90° upward. Variable region of heavy (in black) and light chain (in pink) are shown as cartoons. Finally the H-CDR are highlighted in red and the L-CDR in blue.

The binding did not followed the classical “lock and key or induced fit model” [58] indeed the epitope appears localized on a essentially flat area. (Fig. 15 (c)) Nevertheless, several polar and electrostatic interactions are formed, mediated by side chain atoms from the huFab heavy chain H1, H2, and H3 and light chain L1, L2 and L3 as reported in table 8.

Table 8. Molecular interactions between key residues constituent the Fab1E6/fHbp v3 epitope

fHbp v3	huFab 1E6	CDR	Bond type
S53	L54	H2	VdW
Q55	Y32, D100	H1, H3	Hydrogen bond
G56	D31, Y32	H1, H1	VdW, VdW
E58	R56	H2	Salt bridge
K79	D52	L2	Salt bridge, VdW
R82	T101	H3	Hydrogen bond
D84	T101, A102	H3	Salt bridge, Salt bridge
V86	L54	H2	VdW
S100	F55	H2	VdW
E119	R92	L3	Salt bridge
K120	D95	L3	Salt bridge
N132	D95	L3	Hydrogen bond
D166	T31, G29, R92,	L1, L1, L3	VdW, Hydrogen bond , Salt bridge
N169	S51, D50	L2, L2	Salt bridge, Hydrogen bond
K191	D50 , A28, K30	L2, L1, L1	Salt bridge , Hydrogen bond, Hydrogen bond

X-ray structures of the complexes between antigens and antibodies are essential to exploit the details of the epitope-paratope interaction. The closer examination of the key residues reveals the polar nature of the binding as hydrogen bonds and salt bridges contribute to the high affinity of this mAb for the meningococcal fHbp. Notably some residues engaged a complex and strong network of molecular interactions that connect more than two amino-acids, such as the interconnection established between fHbp v3 E119, D166, K191 and the light chain A28, K30, D50, R92 (Figure17a) and fHbp v3 residues E58, S53 and heavy chain L54, R56 (Figure17 b).

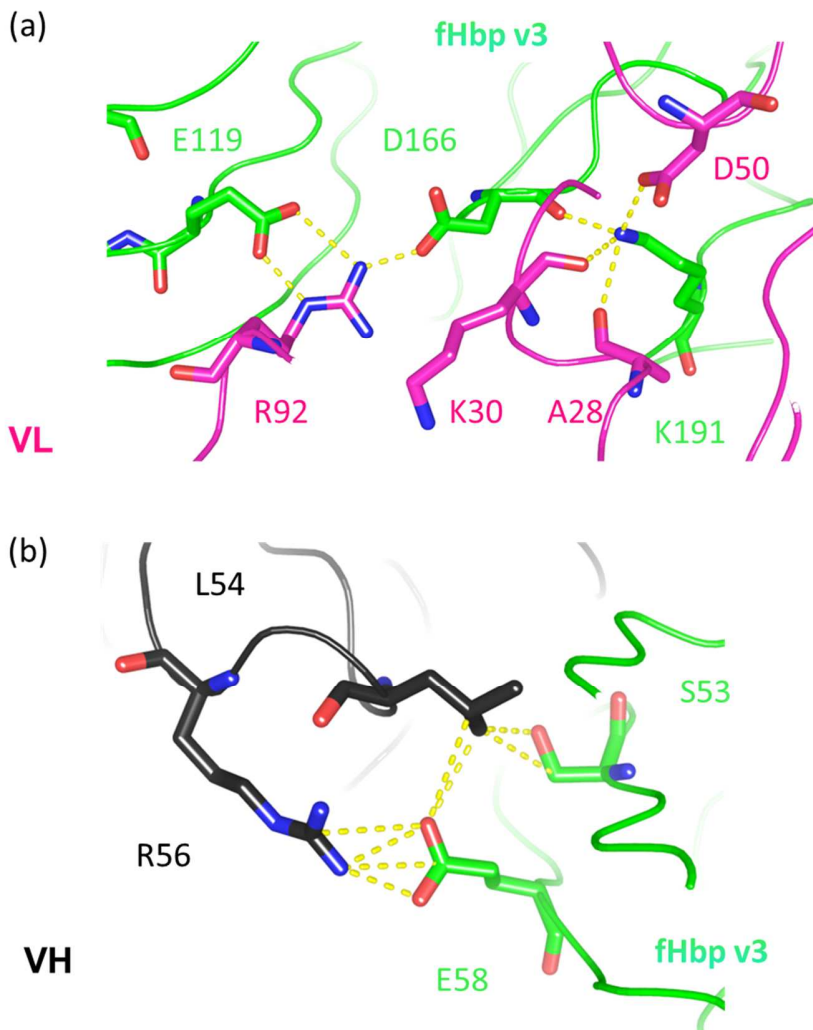


Figure 17. Multiple network between fHbp v3 and huFab1E6.

Closer view of key residues (shown as sticks) between N-terminal of fHbp v3 in green and the light chain in pink (a) and the heavy chain in black (b). In both panels yellow dashed lines indicate intermolecular H bonds or salt bridges $< 4 \text{ \AA}$

3.14 High conservation of the epitope indicates broadly coverage of mAbs 1E6

Antigenic drift is the continuous process of genetic and antigenic changes that occur through point mutations. The antigenic distance between meningococcal strains is increasing within the time by the drift increasing the grade of variability to escape that immune system of the hosts. Several studies of the diversity of the fHbp gene and the encoded protein in a representative sample of meningococcal isolates confirmed the high variability in this protein, with sequence identities falling as low as approximately 62% for some pairwise comparisons [58]. Therefore, to estimate qualitatively the coverage of the mAbs 1E6 we calculated the percentage of conservation of the residues constituent the epitope. A total of 1119 allele were retrieved from the public database *Neisseria meningitidis* multilocus sequence typing (MLST) [59] and the grade of conservation of each residue is shown in figure 18 and the variability is listed in table 9. Interestingly 10 out of 15 residues constituting the epitope are conserved more than 99% between all currently known fHbp amino acid sequences examined. Remarkable instances are represented by Q55, K79, D166 present in the 100% of known meningococcal fHbp sequences. These three epitope residues

play a key role in the binding of mAb 1E6. Of the remaining 5 residues comprising the epitope, the K120 and, N132 are conserved in the 40% of the isolates while the S53, V86 and N169 are represented only in less of than 30% of meningococcal strains (Fig.18 and Table 9). Collectively, these observations suggest that mAb 1E6, shows to bind representatives of all the three fHbp variant groups and might indeed display broad cross-reactivity across the entire repertoire of fHbps.

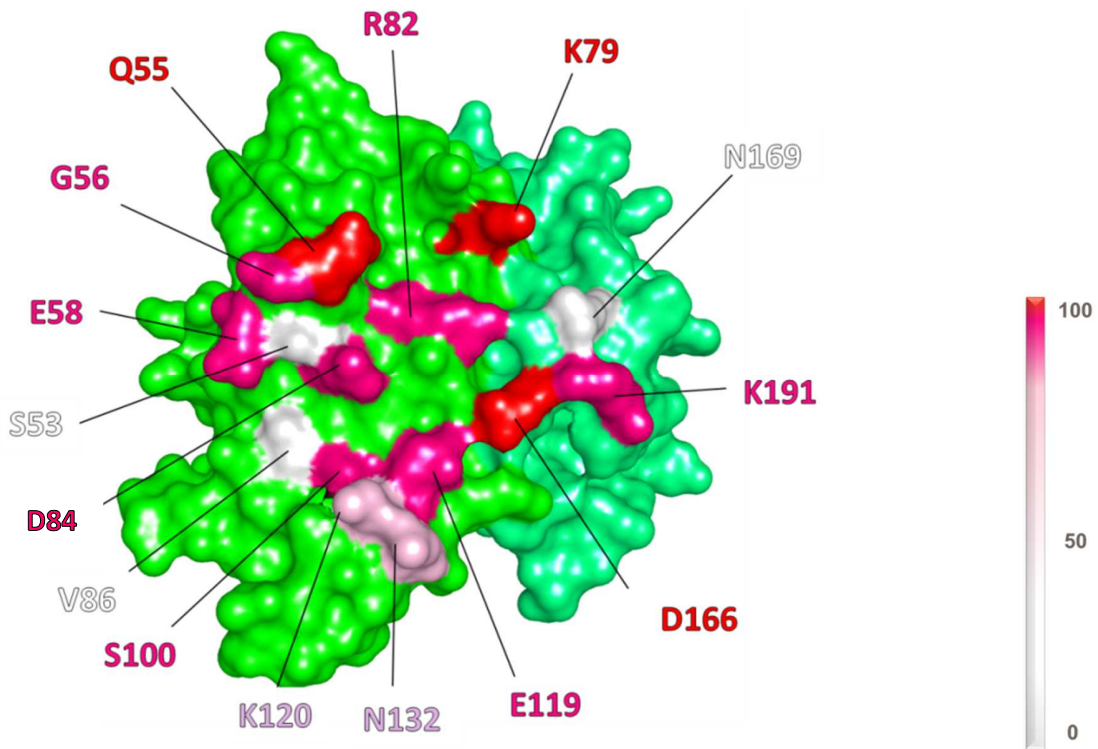


Figure 18. Allelic conservation of the key residues of fHbp v3 involved in the interaction with huFab 1E6. The figure shows fHbp v3 as solid surface. Each residue of the epitope is colored based on its conservation among the fHbp gene repertoire which includes 1119 allelic sequences.

Table 9. Degree of conservation of the key residues involve in fHbp v3 and Ab 1E6

	%G	%A	%L	%M	%F	%W	%K	%Q	%E	%S	%P	%V	%I	%C	%Y	%H	%R	%N	%D	%T	%K
S53	70.42								29.31			0.27									
Q55								100													
G56	99.82								0.09								0.09				
E58							0.09		99.91												
K79																					100
R82																0.18	99.73		0.09		
D84																		0.18	99.82		
V86												21.09	78.91								
S100									99.02			0.18					0.27	0.54			
E119	0.18								99.73												0.09
K120							43.16	56.84													
N132	56.57											0.09					0.09	43.07	0.09		
D166																					100
N169	77.12	0.27							3.66								0.09	18.59	0.27		
K191							99.91		0.09												

3.15 Cross-reactive anti-fHbp antibodies exhibit different binding model

To date, several human anti-fHbp antibodies have been described in functional assays [37], [40], [36]. Data about high resolution epitope mapping at atomic level of antibodies elicited in humans are relatively rare up to now: (REFERENCES). to our knowledge only Giuliani *et al.* [36] restricted the epitope localization of one cross-reactive anti-fHbp mAb 1G3 to short fragments of fHbp v1 by HDX-MS, whereas López-Sagaseta *et al* [35] were able to fully characterize at high resolution the first human antibody, the1A12 identifying the epitope on fHbp v1, By X-ray crystallography. Fab 1A12 targets exclusively the C-terminal β -barrel, whereas the Fab 1E6 binds mainly the N-terminal region on the opposite side compared to the binding site for hfH (Fig. 19). The latter suggests that Fab 1E6 would not inhibit the binding of fHbp to hfH. This hypothesis was confirmed using a competition assay performed by flow cytometry (section 3.6). Three residues of the C-terminal β -barrel fHbp v3 are involved in 1E6 binding but only residue K191, which engaged a strong network of interactions results to be a crucial residue in both fHbp v1:Fab 1A12 and fHbp v3:Fab 1E6 complexes, further underling the important antigenic role of this specific amino acid.

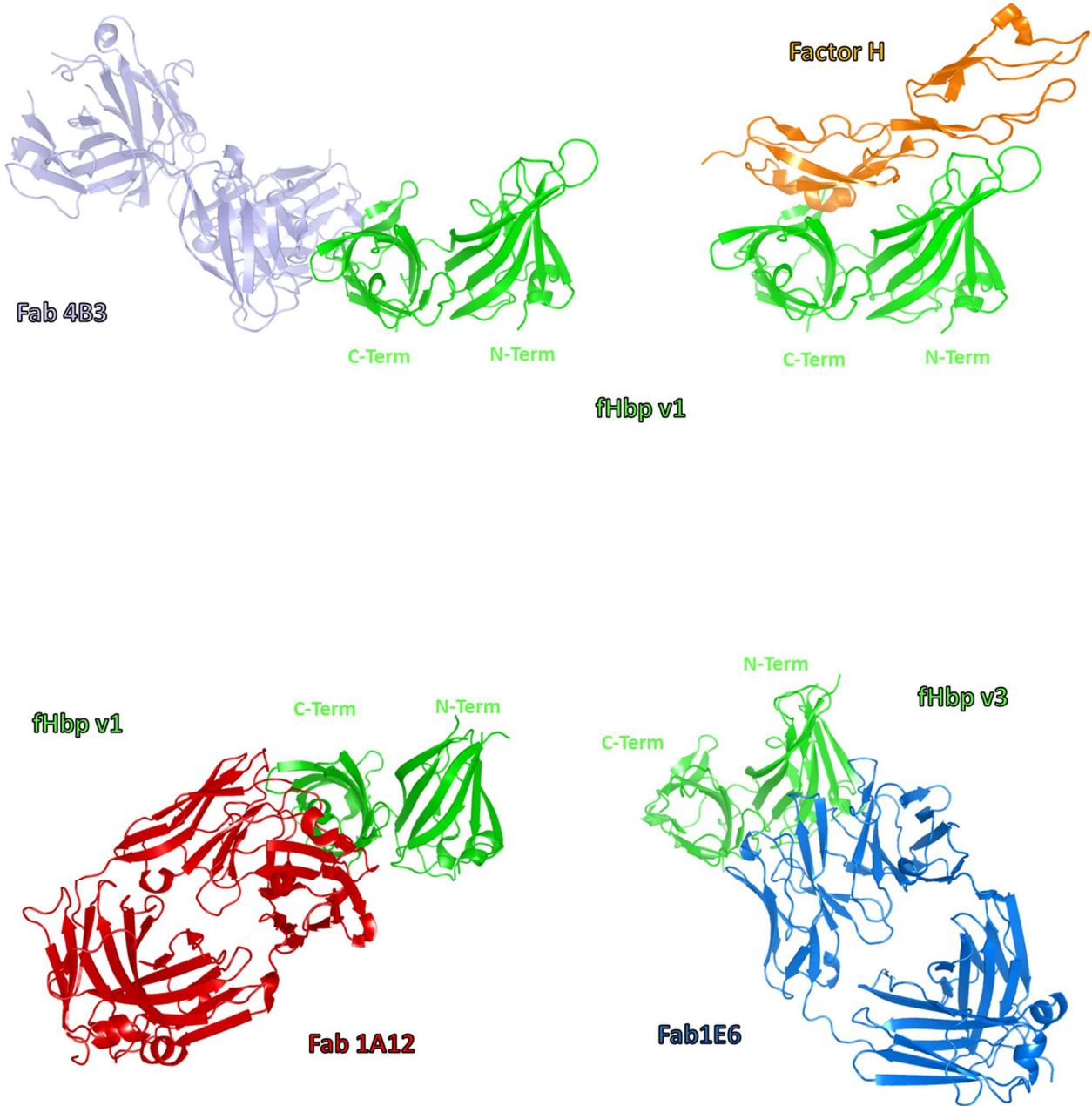


Figure 19. Cartoon representations of fHbp (green), bound to huFab 1A12 (red) pdb 5UR8, huFab1E6 (blue) huFab 4B3 (light violet) and human factor H (orange).

4. Discussion

Neisseria meningitidis remains the most common cause of bacterial meningitis, often leading to permanent disabilities or even death [60]. After many years of research and development, two vaccines to protect against MenB are now licensed, and both contain fHbp, a key meningococcal virulence factor. Recent data from the United Kingdom infant immunization campaign against MenB reported >80% 4CMenB vaccine-mediated protection [61]. Here, we report detailed molecular studies that describe important elements of the human immune response to 4CMenB.

As an extension of previous smaller scale investigations [36] the study presented here probes the repertoire of human mAbs isolated from three additional vaccine recipients following vaccine administration. From this study, a new library of huFab expression constructs was obtained. The library encodes over 100 distinct huFabs that recognize fHbp. This library is a vast reservoir of immunologically relevant data and potentially contains a wealth of information about the humoral immune response, and thus represents an unprecedented, unique resource for the scientific community. Most notably, even if the 4CMenB vaccine contains specifically the fHbp variant 1, subjects immunized with 4CMenB produced at least some cross-reactive antibodies, as we identified 13 (of 110 total) huFabs that were able to recognize all three fHbp variants (Fig.2). Protein microarray epitope mapping experiments suggested that these 13 cross-reactive huFabs bind diverse regions of fHbp, mostly involving conformational epitopes requiring the full-length fHbp, although three huFabs bind to the isolated C-terminal beta-barrel domain and, remarkably, just one huFab bound to the isolated N-terminal domain (Table 2).

The 13 cross-reactive antibodies and the additional mAb called 1B1 were further functionally characterized for complement-mediated bactericidal activity with both rabbit and human complement sources and for their ability to inhibit binding of hfH to live bacteria.

Several murine anti-fHbp mAbs have been described in literature [26], [27] and some of them have been reported to be able to inhibit the binding of the hfH to the bacterial surface [27], [62]. In a recently published paper, Beernink and coworkers [37] focused their analysis on a small panel of ten anti-fHbp Fabs and found that none of the Fabs was able to inhibit hfH binding. Based on this finding, it has been hypothesized that mice immunized with recombinant fHbp develop serum α -fHbp antibodies that block the binding of hfH because the injected recombinant fHbp does not bind the murine fh [37] [31], [13], [38], [32, 63]. On the contrary, as the meningococcal fHbp specifically binds the human fh [26], [37] after human immunization, the fHbp present in the vaccine could form a complex with hfH hiding the binding site .

One of the most outstanding results of this work is that for the first time, we identified cross-protective human mAbs, which are able to compete with the hfH for fHbp binding, suggesting that the hfH binding site in the recombinant fHbp present in the 4CMenB vaccine can be accessible to the immune system upon immunization. Moreover, the analysis of the sequence diversity of fHbp mapped onto the three dimensional structure shows that hfH binding site is the most variable face of the protein, and thus could explain why the identification of cross-reactive mAbs able to inhibit hfH binding has been unsuccessful so far [33].

In this work, we found four mAbs able to inhibit the hfH binding on live meningococci. mAbs 4F9, 4B3 and 3G7 resulted to be able to reduce the signal of hfH binding on meningococcal strains expressing the

three main variants of fHbp. Interesting, one of them, the mAbs 1B1 competed with human hfH binding on meningococcal strain expressing v2 and v3 but not v1. Although 1B1 resulted to have high affinity for v1 in SPR assays, mAb 1B1 shows a low recognition signal of naive fHbp v1 on carrier strain, and that could explain why it is not able to block the human factor H binding on strains carrying variant 1. Antibodies have two distinct functions: one is to bind specifically to their target antigens and the other is to elicit an immune response recruiting other cells and molecules. We found that although all mAbs gave positive titers in rabbit SBA (a standardized method to evaluate the immune response against *Neisseria meningitidis* which correlates with vaccine efficacy [40] [64] [52] with at least one variant, seven antibodies (1D1,3F1,1E6, 2C8, 4F9, 4B3 and 3G7) were bactericidal against all strains carrying the three different fHbp variants. Remarkably, these antibodies are not only cross-reactive but also cross-protective. Previous studies demonstrated that the quantity of fHbp present on the bacterial surface varies between isolates and in the strains used, MC58, M08-0240104 and UK320 the concentration of fHbp was determined to be 2900 (fHbp v1), 9390 (fHbp v2), 1111(fHbp v3) molecules for cell respectively [49]. The antigen density displayed on the surface, can differ even of 9-fold therefore explaining why the binding and the killing on strains carrying v2 is higher than on v1 and v3 (Fig. 7b).

When tested in human SBA, four human mAbs gave positive titers tested individually, the same antibodies that were also able to compete with human factor H binding. The titers obtained are higher compared with those reported for the human anti-fhbp mAbs 1G3 and 1A12 previously reported [36].

Based on antigen binding affinities, epitope mapping performed by Protein microarray and performance in serum bactericidal assays, six antibodies have been selected for expression as high quality Fabs in mammalian cells and co-crystallization studies.

To date, the 3D structure of only one huFab (1A12) in complex with fHbp (v 1) has been reported [35]. In this thesis work, we present the crystal structure of two human antibodies, the 4B3 and 1E6, in complex with fHbp. The crystal structure of fHbp variant 3 (only 62% sequence identify with variant 1 [20]) has been obtained in complex with huFab, 1E6. The structure of Fab 1E6:fHbp v3 is quite different from the previously reported complex of Fab 1A12:fHbpv1, deepening our understanding of the molecular bases determining the cross-reactive antibody response in humans (Fig.19). The structure revealed a large conformational epitope, featuring a dense network of salt bridges and hydrogen bonds, mainly localized at the N-terminus of fHbp variant 3 that was not previously seen in other crystal structures of fHbp complexed with murine Fabs, nor with huFab 1A12 which targets a very different region on the C-terminal domain of fHbp (Fig16,17,19). The crystal structure of fHbp v3 in complex with the complement control protein (CCP) domain 6 and 7 of hfH was determined previously [23]. Comparing the binding site of hfH and Fab 1E6, we observe that 1E6 binds fHbp v3 on the opposite side thus explaining the data obtained by flow cytometry analyses which show that this antibody is not able to inhibit the hfH binding to fHbp.

To understand and better elucidate the nature of the hfH competition, many attempts were done to obtain the crystals of the 4B3 in complex with fHbp. The efforts leadas the 3D structure of the Fab fragment of the antibody 4B3 has been obtained in complex with fHbp v1.

Differently by the human mAb 1A12 already published and the human mAb 1E6 crystallized in this work, the mAb 4B3 is not only cross-reactive and cross-protective in hSBA, but it represents the first human antibody crystallized able to inhibit the human factor H recruitment on the surface of the *Neisseria Meningitidis*.

The crystal structure of fHbp in complex with the complement control protein (CCP) domain 6 and 7 of the hfH is available in the PDB, revealing crucial residues located either in the C-terminal beta-barrel either in the N-terminal [23]. Superimposing the crystal structures of the complexes of fHbp v1:Fab4B3 and fHbp v1: hfH we observed that the binding region partially overlap as they have in common three conserved key residues (K193, E212, D191). To investigate whether two partners compete for the interaction with the same protein target, the key is to know whether they share an interaction interface. However, in this competition model is present an important simplification; as only the domain 6 and 7 of the hfH, representing only 1/10 of entire protein are present in the structure of the complex, as well as the Fab fragment is only 1/3 of the full length antibody.

Some additional steric encumbrance could occur when the two entire macro proteins of 150 kDa (the hfH and the antibody) try to bind the same protein in the same region simultaneously.

Both complexes Fab4B3:fHbp v1 and Fab1E6:fHbp v3 shares common features as the molecular surfaces in contact upon complex formation are of comparable size, and involve a similar number of contact residues. Overall, numerous H-bonds, salt bridges and VdW interactions are widely distributed across the binding interface and contribute collectively to the very strong affinity to the fHbp and to the stability of complex, according with the SPR data. In total fifteen residues are involved in the binding and the sequences alignment indicate that more than the an half of the key residues are well conserved between the variants tested. Biochemical assays shown the capability of the mAb 4B3 and mAb 1E6 to bind three representative variant of fHbp therefore we assumed that residues which contribute to variants recognition to be more strongly conserved. We were also interested in extend the application of the concept on the vast number of fHbp sequence variants identified from clinical isolates and carrier strains. In biochemical SPR studies, huFab 1E6 was found to bind tightly to fHbp variants 1, 2 and 3, with highest affinity for variant 2 (Fig. 7a). Similarly, huFab 1E6 binds to live meningococcal cells expressing fHbp variant 1, 2 and 3 when examined by flow cytometry (Fig. 7b). The crystal structure enabled a clear understanding of this cross-reactivity. Of fifteen total fHbp variant 3 residues involved in binding to huFab 1E6 (Fig. 5), ten are fully conserved in the variants 1 and 2 tested herein. Further, we calculated the degree of conservation of epitope residues considering the 1119 fHbp alleles (from clinical isolates and carrier strains) deposited in the Bacterial Isolate Genome Sequence Database (BIGSDB) [59]. Again, we found out that 10 of the 15 epitope residues are conserved more than 99% in the entire known fHbp sequence database, suggesting that mAb 1E6 could have a very broad recognition of most circulating meningococcal strains.

In addition to its antigenic cross-reactivity, the functional characterization of mAb 1E6 and 4B3 showed that it is cross-protective in rSBA.

Although they have some features in common, these mAbs have unique differences; first they show completely different binding model and interact with a divers set of fHbp residues. Moreover mAbs 1E6 targets the fHbp on an essentially flat area on the N-terminus region instead during the interaction between mAb 4B3 and fHbp seems that the epitope and the paratope contact area undergoes some

conformational adjustment assuming a reciprocal complementary shape which might contribute to reinforce the strength of the binding. Although the fHbp C-terminal β -barrel is usually a highly folded and stable domain of the fHbp protein, the loops which connect the antiparallel strands confer some flexibility to the structure and long-range forces, like ionic interactions or directed hydrogen bonds could lead shape-induced-conformational-changes [58]. Overall, these findings although not predictable of the vaccine coverage, reinforce the finding that vaccination with 4CMenB induce the production of at least low abundance cross-protective antibodies.

In conclusion, we have obtained the first detailed characterization of cross-protective huMabs elicited by 4CMenB and, in particular, we gained structural data on huFab 4B3, which is able to compete for hfH binding to fHbp. These structural and functional data suggest that the hfH binding site on fHbp can be accessible to the human immune system upon immunization, enabling the generation of a highly potent antibody response.

Moreover, improving the knowledge of the epitope profiles identified by human antibodies could potentiate antigen engineering aiming to induce the immune system to continuously generate novel antibodies able to recognize multiple sites for a broadly protective response. Epitope mapping is a crucial step in the development of therapeutic mAbs allowing improvements of the affinity, recognition breadth, and bactericidal efficacy potentially for treatment of meningococcal infections. The results presented are an important proof-of-concept for the use of memory B-cell derived huFab sequences in the structural and functional analysis of the human immune response after 4CMenB vaccination. This information will be useful for future vaccine

5. RESULTS EXPECTED VS RESULTS OBTAINED

During this PhD program, we planned to select a subset of 10-20 of cross-reactive huFabs targeting fHbp from a library of 110 antibodies, and to characterize them in terms of affinity, recognition profile and activity in SBA assays against different meningococcal strains. The aim of the study was to use these anti-fHbp huFabs to perform structural studies in complexes with different variants of recombinant fHbp proteins to reveal the molecular insight of the recognition profiles of the most interesting huFabs identified.

110 α -fHbp huFabs were successfully produced and screened for binding specificity and between these a sub set of 13 cross-reactive α -fHbp huFabs were identified, according to what we predicted.

The most interesting huFabs were successfully produced in mammalian cells with high purity, and further characterized for their antigen binding affinities, ability to recognize native fHbp naturally expose on the surface of the bacterium, bactericidal activity and capacity to inhibit the hfH binding.

In total 10 huFab:fHbp complexes were produced and screened in hundreds of crystallization conditions. The bottleneck of the work was to obtain high quality diffracting crystals; indeed only for four complexes we obtained diffraction data suitable for 3D structural characterization of the complex.

The most important result of this work is that for the first time we identified cross-protective human mAbs which are bactericidal with human complement and which are able to compete for the hfH binding. These results were highly desired but not granted as so far such antibodies were never been identified.

Moreover solving the crystal structure of these cross-reactive α -fHbp antibodies bound to fHbp has allowed us to identify the structural bases of cross-variant epitopes, revealing a unique set of residues constituent conformational epitopes which were not previously seen in other crystal structures. Unfortunately, we were unable to complete the structure of the complexes involving the fHbp v2 raising several questions which will be addressed in future studies.

In conclusion, we achieved our purpose to generate new structural data, combined with the biochemical and functional data, allowing to define at high-resolution the most broad and cross-protective epitopes generated by vaccination with 4CMenB.

Transparency statement

This work was undertaken at the request of and sponsored by GlaxoSmithKline Biologicals SA. Federica Bianchi is a student of the University of Florence (Università degli studi di Firenze), and participated in a PhD postgraduate studentship program at GSK. Bexsero is a trademark owned by or licensed to the GSK group of companies.

1. Stephens, D.S., B. Greenwood, and P. Brandtzaeg, *Epidemic meningitis, meningococcaemia, and Neisseria meningitidis*. Lancet, 2007. **369**(9580): p. 2196-2210.
2. Sharip, A., et al., *Population-based analysis of meningococcal disease mortality in the United States: 1990-2002*. Pediatr Infect Dis J, 2006. **25**(3): p. 191-4.
3. Borrow, R., et al., *Serological basis for use of meningococcal serogroup C conjugate vaccines in the United Kingdom: reevaluation of correlates of protection*. Infect Immun, 2001. **69**(3): p. 1568-73.
4. Snape, M.D., et al., *Immunogenicity of a tetravalent meningococcal glycoconjugate vaccine in infants: a randomized controlled trial*. JAMA, 2008. **299**(2): p. 173-84.
5. Shea, M.W., *The Long Road to an Effective Vaccine for Meningococcus Group B (MenB)*. Ann Med Surg (Lond), 2013. **2**(2): p. 53-6.
6. Finne, J., et al., *An IgG monoclonal antibody to group B meningococci cross-reacts with developmentally regulated polysialic acid units of glycoproteins in neural and extraneural tissues*. J Immunol, 1987. **138**(12): p. 4402-7.
7. Perkins, S.J., et al., *Complement factor H-ligand interactions: self-association, multivalency and dissociation constants*. Immunobiology, 2012. **217**(2): p. 281-97.
8. Blaum, B.S., et al., *Structural basis for sialic acid-mediated self-recognition by complement factor H*. Nat Chem Biol, 2015. **11**(1): p. 77-82.
9. Langford-Smith, A., et al., *Complementing the Sugar Code: Role of GAGs and Sialic Acid in Complement Regulation*. Front Immunol, 2015. **6**: p. 25.
10. Kajander, T., et al., *Dual interaction of factor H with C3d and glycosaminoglycans in host-nonhost discrimination by complement*. Proc Natl Acad Sci U S A, 2011. **108**(7): p. 2897-902.
11. Schmidt, C.Q., et al., *A new map of glycosaminoglycan and C3b binding sites on factor H*. J Immunol, 2008. **181**(4): p. 2610-9.
12. Pangburn, M.K., et al., *Molecular mechanisms of target recognition in an innate immune system: interactions among factor H, C3b, and target in the alternative pathway of human complement*. J Immunol, 2000. **164**(9): p. 4742-51.
13. Madico, G., et al., *The meningococcal vaccine candidate GNA1870 binds the complement regulatory protein factor H and enhances serum resistance*. J Immunol, 2006. **177**(1): p. 501-10.
14. Hallstrom, T., et al., *Haemophilus influenzae interacts with the human complement inhibitor factor H*. J Immunol, 2008. **181**(1): p. 537-45.
15. Amdahl, H., et al., *Interactions between Bordetella pertussis and the complement inhibitor factor H*. Mol Immunol, 2011. **48**(4): p. 697-705.
16. Kunert, A., et al., *Immune evasion of the human pathogen Pseudomonas aeruginosa: elongation factor Tuf is a factor H and plasminogen binding protein*. J Immunol, 2007. **179**(5): p. 2979-88.
17. Blackmore, T.K., et al., *M protein of the group A Streptococcus binds to the seventh short consensus repeat of human complement factor H*. Infect Immun, 1998. **66**(4): p. 1427-31.
18. Meri, T., et al., *The yeast Candida albicans binds complement regulators factor H and FHL-1*. Infect Immun, 2002. **70**(9): p. 5185-92.
19. McNeil, L.K., et al., *Detection of LP2086 on the cell surface of Neisseria meningitidis and its accessibility in the presence of serogroup B capsular polysaccharide*. Vaccine, 2009. **27**(25-26): p. 3417-21.
20. Maignani, V., et al., *Vaccination against Neisseria meningitidis using three variants of the lipoprotein GNA1870*. J Exp Med, 2003. **197**(6): p. 789-99.
21. Cantini, F., et al., *Solution structure of the factor H-binding protein, a survival factor and protective antigen of Neisseria meningitidis*. J Biol Chem, 2009. **284**(14): p. 9022-6.
22. Cendron, L., et al., *Structure of the uncomplexed Neisseria meningitidis factor H-binding protein fHbp (rLP2086)*. Acta Crystallogr Sect F Struct Biol Cryst Commun, 2011. **67**(Pt 5): p. 531-5.
23. Johnson, S., et al., *Design and evaluation of meningococcal vaccines through structure-based modification of host and pathogen molecules*. PLoS Pathog, 2012. **8**(10): p. e1002981.

24. Seib, K.L., et al., *Characterization of diverse subvariants of the meningococcal factor H (fH) binding protein for their ability to bind fH, to mediate serum resistance, and to induce bactericidal antibodies.* Infect Immun, 2011. **79**(2): p. 970-81.
25. Domina, M., et al., *Functional characterization of a monoclonal antibody epitope using a lambda phage display-deep sequencing platform.* Sci Rep, 2016. **6**: p. 31458.
26. Giuntini, S., et al., *Monoclonal antibodies to meningococcal factor H binding protein with overlapping epitopes and discordant functional activity.* PLoS One, 2012. **7**(3): p. e34272.
27. Giuntini, S., D.C. Reason, and D.M. Granoff, *Complement-mediated bactericidal activity of anti-factor H binding protein monoclonal antibodies against the meningococcus relies upon blocking factor H binding.* Infect Immun, 2011. **79**(9): p. 3751-9.
28. Giuntini, S., D.C. Reason, and D.M. Granoff, *Combined roles of human IgG subclass, alternative complement pathway activation, and epitope density in the bactericidal activity of antibodies to meningococcal factor h binding protein.* Infect Immun, 2012. **80**(1): p. 187-94.
29. Mascioni, A., et al., *NMR dynamics and antibody recognition of the meningococcal lipidated outer membrane protein LP2086 in micellar solution.* Biochim Biophys Acta, 2010. **1798**(2): p. 87-93.
30. Scarselli, M., et al., *Epitope mapping of a bactericidal monoclonal antibody against the factor H binding protein of Neisseria meningitidis.* J Mol Biol, 2009. **386**(1): p. 97-108.
31. Beernink, P.T., et al., *Fine antigenic specificity and cooperative bactericidal activity of monoclonal antibodies directed at the meningococcal vaccine candidate factor h-binding protein.* Infect Immun, 2008. **76**(9): p. 4232-40.
32. Welsch, J.A., et al., *Complement-dependent synergistic bactericidal activity of antibodies against factor H-binding protein, a sparsely distributed meningococcal vaccine antigen.* J Infect Dis, 2008. **197**(7): p. 1053-61.
33. Faleri, A., et al., *Two cross-reactive monoclonal antibodies recognize overlapping epitopes on Neisseria meningitidis factor H binding protein but have different functional properties.* FASEB J, 2014. **28**(4): p. 1644-53.
34. Vu, D.M., et al., *A broadly cross-reactive monoclonal antibody against an epitope on the n-terminus of meningococcal fHbp.* Sci Rep, 2012. **2**: p. 341.
35. Lopez-Sagaseta, J., et al., *Crystal structure reveals vaccine elicited bactericidal human antibody targeting a conserved epitope on meningococcal fHbp.* Nat Commun, 2018. **9**(1): p. 528.
36. Giuliani, M., et al., *Human protective response induced by meningococcus B vaccine is mediated by the synergy of multiple bactericidal epitopes.* Sci Rep, 2018. **8**(1): p. 3700.
37. Beernink, P.T., et al., *Functional Analysis of the Human Antibody Response to Meningococcal Factor H Binding Protein.* MBio, 2015. **6**(3): p. e00842.
38. Granoff, D.M., J.A. Welsch, and S. Ram, *Binding of complement factor H (fH) to Neisseria meningitidis is specific for human fH and inhibits complement activation by rat and rabbit sera.* Infect Immun, 2009. **77**(2): p. 764-9.
39. Granoff, D.M., S. Ram, and P.T. Beernink, *Does binding of complement factor H to the meningococcal vaccine antigen, factor H binding protein, decrease protective serum antibody responses?* Clin Vaccine Immunol, 2013. **20**(8): p. 1099-107.
40. Costa, I., R. Pajon, and D.M. Granoff, *Human factor H (FH) impairs protective meningococcal anti-FHbp antibody responses and the antibodies enhance FH binding.* MBio, 2014. **5**(5): p. e01625-14.
41. Feavers, I.M. and M.C.J. Maiden, *Recent Progress in the Prevention of Serogroup B Meningococcal Disease.* Clin Vaccine Immunol, 2017. **24**(5).
42. van den Berg, S., et al., *Improved solubility of TEV protease by directed evolution.* J Biotechnol, 2006. **121**(3): p. 291-8.
43. Giuliani, M.M., et al., *The region comprising amino acids 100 to 255 of Neisseria meningitidis lipoprotein GNA 1870 elicits bactericidal antibodies.* Infect Immun, 2005. **73**(2): p. 1151-60.

44. Battye, T.G., et al., *iMOSFLM: a new graphical interface for diffraction-image processing with MOSFLM*. Acta Crystallogr D Biol Crystallogr, 2011. **67**(Pt 4): p. 271-81.
45. McCoy, A.J., et al., *Phaser crystallographic software*. J Appl Crystallogr, 2007. **40**(Pt 4): p. 658-674.
46. Emsley, P., et al., *Features and development of Coot*. Acta Crystallogr D Biol Crystallogr, 2010. **66**(Pt 4): p. 486-501.
47. Rosano, G.L. and E.A. Ceccarelli, *Recombinant protein expression in Escherichia coli: advances and challenges*. Front Microbiol, 2014. **5**: p. 172.
48. Irani, V., et al., *Molecular properties of human IgG subclasses and their implications for designing therapeutic monoclonal antibodies against infectious diseases*. Mol Immunol, 2015. **67**(2 Pt A): p. 171-82.
49. Biagini, M., et al., *Expression of factor H binding protein in meningococcal strains can vary at least 15-fold and is genetically determined*. Proc Natl Acad Sci U S A, 2016. **113**(10): p. 2714-9.
50. Jodar, L., K. Cartwright, and I.M. Feavers, *Standardisation and validation of serological assays for the evaluation of immune responses to Neisseria meningitidis serogroup A and C vaccines*. Biologicals, 2000. **28**(3): p. 193-7.
51. Lucidarme, J., et al., *Molecular targets in meningococci: efficient routine characterization and optimal outbreak investigation in conjunction with routine surveillance of the meningococcal group B vaccine candidate, fHBP*. Clin Vaccine Immunol, 2011. **18**(2): p. 194-202.
52. Keyserling, H., et al., *Safety, immunogenicity, and immune memory of a novel meningococcal (groups A, C, Y, and W-135) polysaccharide diphtheria toxoid conjugate vaccine (MCV-4) in healthy adolescents*. Arch Pediatr Adolesc Med, 2005. **159**(10): p. 907-13.
53. Stanfield, R.L., et al., *Antibody elbow angles are influenced by their light chain class*. J Mol Biol, 2006. **357**(5): p. 1566-74.
54. Al-Lazikani, B., A.M. Lesk, and C. Chothia, *Standard conformations for the canonical structures of immunoglobulins*. J Mol Biol, 1997. **273**(4): p. 927-48.
55. Martin, A.C., *Accessing the Kabat antibody sequence database by computer*. Proteins, 1996. **25**(1): p. 130-3.
56. Rubinstein, N.D., et al., *Computational characterization of B-cell epitopes*. Mol Immunol, 2008. **45**(12): p. 3477-89.
57. MacRaid, C.A., et al., *Antibody Recognition of Disordered Antigens*. Structure, 2016. **24**(1): p. 148-157.
58. Csermely, P., R. Palotai, and R. Nussinov, *Induced fit, conformational selection and independent dynamic segments: an extended view of binding events*. Trends Biochem Sci, 2010. **35**(10): p. 539-46.
59. Jolley, K.A. and M.C. Maiden, *BIGSdb: Scalable analysis of bacterial genome variation at the population level*. BMC Bioinformatics, 2010. **11**: p. 595.
60. Sadarangani, M. and A.J. Pollard, *Can we control all-cause meningococcal disease in Europe?* Clin Microbiol Infect, 2016. **22 Suppl 5**: p. S103-S112.
61. Parikh, S.R., et al., *Effectiveness and impact of a reduced infant schedule of 4CMenB vaccine against group B meningococcal disease in England: a national observational cohort study*. Lancet, 2016. **388**(10061): p. 2775-2782.
62. Malito, E., et al., *Defining a protective epitope on factor H binding protein, a key meningococcal virulence factor and vaccine antigen*. Proc Natl Acad Sci U S A, 2013. **110**(9): p. 3304-9.
63. Malito, E., et al., *Neisseria meningitidis factor H-binding protein bound to monoclonal antibody JAR5: implications for antibody synergy*. Biochem J, 2016. **473**(24): p. 4699-4713.
64. Miller, E., et al., *Safety and immunogenicity of coadministering a combined meningococcal serogroup C and Haemophilus influenzae type b conjugate vaccine with 7-valent pneumococcal conjugate vaccine and measles, mumps, and rubella vaccine at 12 months of age*. Clin Vaccine Immunol, 2011. **18**(3): p. 367-72.

Acknowledgement

Undertaking this PhD has been a truly life-changing experience for me and it would not have been possible to do without the support and guidance that I received from many people.

Firstly, I would like to express my sincere gratitude to my mentor Roberta Cozzi for the continuous support of my PhD study and related research, for his patience, motivation, and immense knowledge. Her guidance helped me in all the time of research and writing of this thesis. I could not have imagined having a better advisor and mentor for my PhD study.

Besides my advisor, I would like to thank Dr Domenico Maione and Matthew Bottomley for provided me an opportunity to join their team as intern, and who gave access to the laboratory and research facilities and for their insightful comments and encouragement, but also for the hard question which incited me to widen my research from various perspectives.

I want express special thanks to my labmates especially Manuele Martinelli who still offering guidance and suggestions; not only for research aspects. I am also very grateful to Concetta De Santis, Adele Fantoni e Katia Sampieri, without they precious support it would not be possible to conduct my research during my time in GSK.

Thanks to all the teaching and research CERM staff which guided me through the meanders of Italian bureaucracy during this three years and give the possibility to constantly show, in oral presentation, the progress of my work. That represented a precious opportunity to critically discuss the data obtained to achive best results and improve my oral skills.



Last but not the least, I would like to thank my family: my parents and to my brothers for supporting me spiritually along the way anything not have been possible without their warm love, continued patience, and endless support.

ARTICLE

DOI: 10.1038/s41467-018-02827-7

OPEN

Crystal structure reveals vaccine elicited bactericidal human antibody targeting a conserved epitope on meningococcal fHbp

Jacinto López-Sagaseta¹, Peter T. Beernink ², Federica Bianchi¹, Laura Santini¹, Elisabetta Frigimelica ¹, Alexander H. Lucas², Mariagrazia Pizza¹ & Matthew J. Bottomley³

Data obtained recently in the United Kingdom following a nationwide infant immunization program against serogroup B *Neisseria meningitidis* (MenB) reported >80% 4CMenB vaccine-mediated protection. Factor H-binding protein (fHbp) is a meningococcal virulence factor and a component of two new MenB vaccines. Here, we investigated the structural bases underlying the fHbp-dependent protective antibody response in humans, which might inform future antigen design efforts. We present the co-crystal structure of a human antibody Fab targeting fHbp. The vaccine-elicited Fab 1A12 is cross-reactive and targets an epitope highly conserved across the repertoire of three naturally occurring fHbp variants. The free Fab structure highlights conformational rearrangements occurring upon antigen binding. Importantly, 1A12 is bactericidal against MenB strains expressing fHbp from all three variants. Our results reveal important immunological features potentially contributing to the broad protection conferred by fHbp vaccination. Our studies fuel the rationale of presenting conserved protein epitopes when developing broadly protective vaccines.

¹GSK Vaccines srl, Via Fiorentina 1, 53100 Siena, Italy. ²Immunobiology and Vaccine Development, UCSF Benioff Children's Hospital, 5700 Martin Luther King Jr. Way, Oakland, CA 94609, USA. ³GSK Vaccines, 14200 Shady Grove Road, Rockville, MD 20817, USA. Alexander H. Lucas is deceased. Correspondence and requests for materials should be addressed to J.L.-S. (email: jlopez.sagaseta@gmail.com) or to M.J.B. (email: matthew.j.bottomley@gsk.com)

Meningococci cause fatal cases of bacterial sepsis and meningitis, with serogroup B (MenB) strains particularly prevalent in Europe^{1,2}. Two vaccines based on protein antigens were developed for the prevention of MenB disease. One of these antigens is factor H-binding protein (fHbp), which was identified independently by reverse vaccinology using genomic sequences³ and by traditional methods using biochemical fractionation⁴. fHbp elicits protective antibody responses in mice, rabbits, rhesus macaques^{3,5,6}, and humans^{7–9}. The vaccines are referred to as 4CMenB (Bexsero; GSK) and Bivalent rLP2086 (Trumenba; Pfizer) and both are licensed for use in adolescents in the United States. Only 4CMenB is licensed for infants starting 2 months of age in Europe, Canada, Australia, and several countries in South America. Of note, following a nationwide implementation of 4CMenB, a recent study showed >80% vaccine-mediated protection against all current MenB strains in the United Kingdom^{10,11}.

Antibodies to fHbp elicit protection through complement-mediated bactericidal activity^{3,4}. Some antibodies also inhibit the binding of human complement factor H (fH) to the bacteria, rendering them more susceptible to complement¹². While some antibodies to fHbp elicited in mice inhibited the binding of fH to the bacterial surface^{12,13}, the antibodies elicited in rhesus macaques^{14,15} or humans¹⁶ generally did not inhibit binding of fH. This difference may result from the inability of murine fH to bind fHbp¹⁶, in contrast to human fH that binds fHbp, such that the dynamics of epitope exposure, dependent on fH binding, are likely different when immunizing mice and humans.

Bactericidal polyclonal antibodies raised in mice were reported to be mainly directed against the carboxyl (C)-terminal domain of fHbp¹⁷. Epitope mapping of murine anti-fHbp monoclonal antibodies (mAbs) has confirmed that many of the amino-acid residues involved in antibody binding are located in the C-terminal domain^{17–19}. There are several examples, however, of epitopes involving residues in the amino (N)-terminal domain^{20–23}. Detailed epitope-mapping studies of anti-fHbp mAbs have been performed using nuclear magnetic resonance spectroscopy^{18,22}, hydrogen-deuterium exchange followed by mass spectrometry^{21,24}, and by X-ray crystallography^{24,25}. The latter studies recently defined a mechanism by which two murine anti-fHbp antibodies (mAbs JAR5 and 12C1) may synergize to elicit complement-mediated bactericidal activity^{25,26}. Moreover, both mAbs target epitopes that overlap with the fH-binding site^{24,25}, thus revealing the structural basis for their inhibition of fH binding. Structural epitope-mapping studies with murine Fabs have also been performed for another protective antigen present in 4CMenB, namely the outer membrane protein PorA^{27–29}.

In an important recent study, the human antibody repertoire to fHbp was investigated for the first time, by characterization of a panel of 10 human anti-fHbp antibody fragments (Fabs) cloned from three subjects vaccinated with 4CMenB¹⁶. Therein, two of the three subjects raised broadly reactive antibodies (termed 9B and 10C). Fab 9B (hereafter termed Fab 1A12) was of particular interest since it bound with extremely high affinity ($K_D = 19$ pM)

to fHbp variant 1.1 (var1.1) and, moreover, cross-reacted with all eight fHbp sequence variants tested, including representatives from all three phylogenetic variant groups. This Fab was particularly unusual because most known antibodies against fHbp are “variant group-specific”, i.e., most mAbs efficiently bind fHbp from one variant group, but not from both the other two variant groups. Indeed, despite previous analyses of hundreds of mAbs raised against fHbp by animal immunizations, only a few have been reported to exhibit some cross-reactivity, including MN86-994-11³⁰, JAR41²³, 17C1²¹, and 30G4²¹. Within the fHbp variant groups, amino-acid sequence identity is usually above 87%; whereas, between variant groups the sequence identity can fall to as little as 62%, and this high antigenic variability presumably underlies the rarity of eliciting cross-reactive mAbs^{3,23,30}.

The observations summarized above raise the question: “What is the structural basis of the broad antigen-recognition properties of the vaccine-elicited human antibody 1A12?” Since meningococci display enormous antigenic diversity (~1000 sequence variants of fHbp have been reported³¹), it is important to understand how current MenB vaccine antigens interact with the human immune system. Such details are expected to provide insights into vaccine efficacy and may enable the design of next-generation vaccines.

In this study, we present the crystal structures of the broadly reactive Fab 1A12 alone and in a complex with fHbp, thereby elucidating the structural basis for the antigen-recognition properties of this human antibody. We also show that Fab 1A12 as an intact IgG antibody has high affinity for different fHbp variants, and for point mutants, revealing the contribution of specific amino acids in the epitope recognized by the human antibody. Finally, in functional assays, IgG 1A12 has bactericidal activity. These data provide the crystallographic and functional characterization of a functional vaccine-elicited human antibody targeting a bacterial pathogen.

Results

Human mAb 1A12 shows affinity and broad reactivity for fHbp. Fab 1A12 derives from an adult human subject immunized with a MenB vaccine formulation that contained fHbp var1.1 (see Methods). The cross-reactivity of recombinant Fab 1A12 in enzyme-linked immunosorbent assay (ELISA) experiments using the three different variant groups of fHbp was reported previously¹⁶. To extend those investigations, here we used mammalian cells to produce 1A12 as an intact full-length mAb of the IgG1 subclass (the subclass most abundant in human sera), and *Escherichia coli* to produce recombinant fHbp antigens. Surface plasmon resonance (SPR) was used to determine the kinetics for immobilized mAb 1A12 binding to solution phase fHbp antigens representative of the three different variant groups: fHbp var1.1; fHbp var2.16; and fHbp var3.45. All three variants were recognized by mAb 1A12, as indicated by the sub-nanomolar equilibrium dissociation constant (K_D) values of 87, 384, and 138 pM for fHbp var1.1, var2.16, and var3.45, respectively (Fig. 1 and Table 1).

Table 1 Binding kinetic values determined for mAb 1A12 by surface plasmon resonance

	Var1.1	Var2.16	Var3.45	Var1.1 A162P	Var1.1 G163A	Var1.1 G163N	Var1.1 K180A	Var1.1 K185A	Var1.1 N190A	Var1.1 N215G
k_{on} ($M^{-1} s^{-1}$) $\times 10^5$	6.2 \pm 0.1	2.3 \pm 0.01	4.2 \pm 0.01	10.1 \pm 0.8	6.3 \pm 0.02	8.3 \pm 1.0	3.3 \pm 0.01	1.5 \pm 0.02	4.7 \pm 0.2	8.1 \pm 0.04
k_{off} (s^{-1}) $\times 10^{-5}$	5.4 \pm 0.7	8.7 \pm 0.5	5.7 \pm 0.3	2.4 \pm 0.9	2.7 \pm 0.2	4.6 \pm 0.7	0.9 \pm 0.2	32.1 \pm 1.8	175.8 \pm 7.9	50.2 \pm 0.7
K_D^a (pM)	87 \pm 10	384 \pm 24	138 \pm 7	24 \pm 11	44 \pm 3	55 \pm 2	28 \pm 6	2158 \pm 149	3713 \pm 11	620 \pm 12

^a $K_D = k_{off}/k_{on}$; mean and SD values were calculated from SPR experiments performed in duplicate for each fHbp variant and mutant

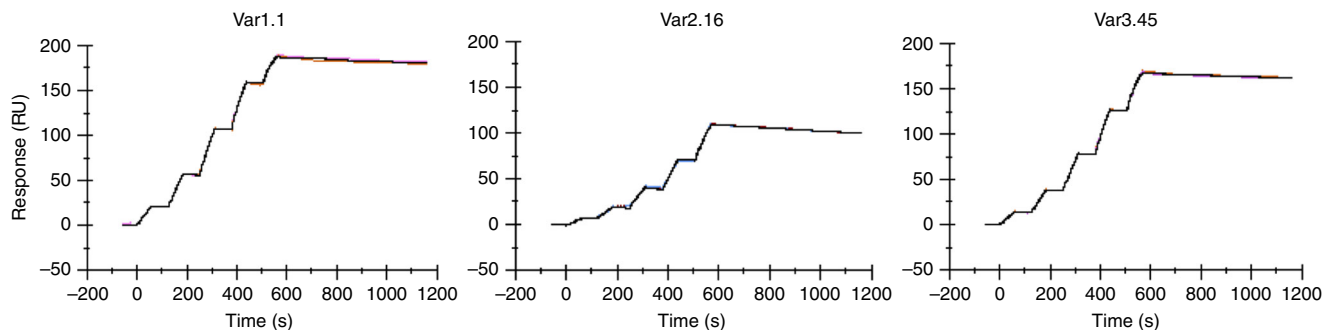


Fig. 1 mAb 1A12 shows high-affinity cross-reactive binding to fHbp in SPR studies. In each panel, sensorgrams show the experimental association and dissociation traces (colored) performed in duplicate for the binding of the different fHbp subvariants to captured mAb 1A12; the calculated fitting traces are shown in dark gray. Full kinetic analyses of each interaction are reported in Table 1

Structure determination of human Fab 1A12 bound to fHbp.

Since mAb 1A12 was raised by vaccination with fHbp var1.1, we sought structural information to explain its cross-reactivity and the precise recognition mode of its epitope. We obtained crystals of Fab 1A12 bound to fHbp var1.1 that initially diffracted to 3.5 Å resolution. By an iterative streak-seeding approach, we subsequently obtained better diffracting crystals (belonging to space group $P2_1$) and ultimately determined the structure via molecular replacement with a resolution of 2.2 Å ($I/\sigma I = 0.98$, $CC_{1/2} = 0.26$ in the highest resolution shell³², see Methods and Table 2). Two Fab/fHbp complexes were present in the asymmetric unit and were essentially identical, exhibiting a root mean square deviation (rmsd) of 0.5 Å across all alpha carbon atoms. The overall structure of the complex shows Fab 1A12 projecting all six complementarity-determining region (CDR) loops onto a surface-exposed region at one end of the C-terminal β barrel of fHbp, while the N-terminal region of fHbp does not contribute to the interaction (Fig. 2). Overall, 17 fHbp residues are involved in a curved interface. The buried surface area on fHbp is 800 Å², which is typical for Fab/antigen complexes^{33,34}. Fab 1A12 binds fHbp with a major contribution from the heavy chain, and a minor contribution from the light chain (590 Å² vs. 210 Å²). The binding interface comprises charged, polar, and van der Waals (VDW) interactions.

The Fab 1A12-binding site on fHbp is completely different from the two structurally characterized epitopes of the murine Fabs 12C1 and JAR5^{24,25}, which are both specific only for fHbp variant group 1 antigens. To compare the modes of binding to fHbp, we conceptually divided the fHbp molecule into quadrants by drawing “crosshairs” on its long and short axes, thus creating a reference frame (Fig. 3). While both JAR5 and 12C1 target the left half of fHbp, and in particular the upper (N-terminal) and lower (C-terminal) quadrants, respectively, 1A12 binds fHbp on its lower right quadrant, in a distinctly new region (Fig. 3). Similarly, the 1A12-binding site does not overlap that of human factor H, which binds on the two left quadrants of fHbp³⁵, thus providing the molecular explanation for previous observations that Fab 1A12 does not inhibit binding of fHbp to factor H¹⁶.

Details of a cross-reactive conformational epitope on fHbp. A

close inspection of the Fab 1A12/fHbp-binding interface reveals a predominant role in antigen recognition for the Fab heavy chain, and especially for the heavy chain variable (V_H) CDR3 loop which extends into a notable groove on the fHbp surface (Fig. 4a). In the V_H CDR3 loop, all residues from Q101 to P107 (except V102) act to secure an extensive network of backbone and side-chain polar and VDW contacts, and presumably all contribute to the extremely tight interaction with the antigen (Fig. 4a and

Table 2 X-ray data collection, processing, and refinement statistics

	Fab 1A12-fHbp complex	Fab 1A12 alone
Resolution range (Å)	48.91-2.20 (2.27-2.20)	70.88-1.76 (1.82-1.76)
Space group	$P 1 2_1 1$	$P 3_1 2 1$
Unit cell dimensions		
<i>a</i> , <i>b</i> , <i>c</i> (Å)	42.82 163.95 110.66	131.90 131.90 90.38
α , β , γ (°)	90.0 97.7 90.0	90.0 90.0 120
Total reflections	414 763 (25 038)	1 615 701 (132 068)
Unique reflections	74 237 (5623)	88 113 (8430)
Multiplicity	5.6 (4.5)	18.3 (15.6)
Completeness (%)	96.0 (73.0)	97.0 (93.0)
Mean $I/\sigma(I)$	6.98 (0.98)	33.18 (1.68)
Wilson <i>B</i> -factor	27.4	22.3
Rmerge	0.194 (1.193)	0.155 (2.534)
Rmeas	0.214 (1.353)	0.170 (2.827)
CC1/2	0.987 (0.263)	0.919 (0.185)
R-work	0.192 (0.307)	0.199 (0.347)
R-free	0.250 (0.355)	0.223 (0.355)
Number of atoms		
Macromolecules	9848	3497
Ligands	13	0
Protein residues	1318	444
RMS bonds (Å)	0.003	0.007
RMS angles (°)	0.58	0.91
Ramachandran favored (%)	97	96.8
Ramachandran allowed (%)	3.2	3.2
Ramachandran outliers (%)	0.077	0.0
Average <i>B</i> -factor	22.23	27.62
Macromolecules	22.01	27.03
Ligands	21.47	n/a
Solvent	24.55	34.30

Values in parentheses are for highest resolution shell. $R_{\text{merge}} = \frac{\sum_{hkl} \sum_{i=1}^n |I_i(hkl) - \bar{I}(hkl)|}{\sum_{hkl} \sum_{i=1}^n I_i(hkl)}$; $R_{\text{meas}} = \frac{\sum_{hkl} \sqrt{\frac{1}{n} \sum_{i=1}^n |I_i(hkl) - \bar{I}(hkl)|^2}}{\sum_{hkl} \sum_{i=1}^n I_i(hkl)}$

Supplementary Table 1). In addition, several other striking contacts are established via salt bridges between Asp161 on fHbp and Arg54 on the heavy chain (Fig. 4b, upper left), and Lys185 on fHbp and Asp55/Asp57 on the heavy chain (Fig. 4b, lower left), and, via hydrogen bonds between Asn190 on fHbp and Gln101 on V_H CDR3 (Fig. 4b, upper right). Further, a water-mediated hydrogen bond is formed between Thr91 in the light chain CDR3 and Tyr214 on fHbp (Fig. 4b, lower right). Importantly, Asn215 on fHbp simultaneously contacts both the heavy and light chains of Fab 1A12, by hydrogen bonding with the gamma oxygen

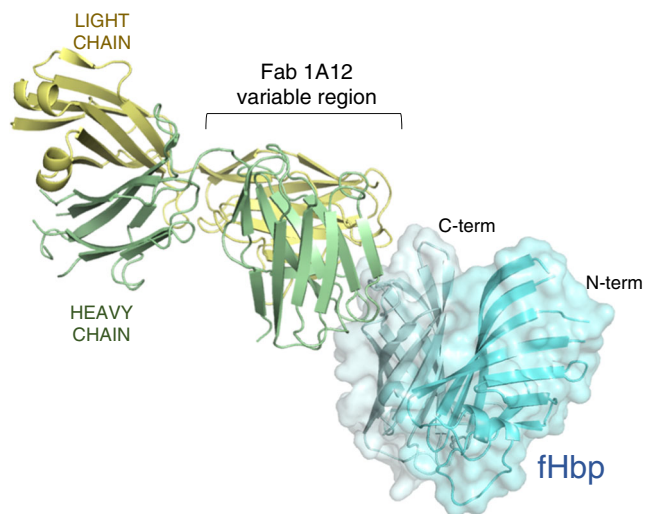


Fig. 2 The Fab 1A12-fHbp complex crystal structure. Ribbon diagram in which the heavy and light chains of Fab 1A12 are colored green and yellow, respectively; fHbp is represented in cyan with a transparent surface. Artwork was prepared using PyMOL

atoms of three serine residues (heavy chain Ser106 directly, and light chain Ser30 and Ser32 indirectly through water-mediated interactions) and with Val31 (backbone nitrogen) on the light chain (Fig. 4c).

A surface representation of all the fHbp residues that interact with 1A12 reveals the nature of the conformational epitope on fHbp, lying on a surface-exposed well-ordered region of the C-terminal β barrel. The epitope is concentrated in a cluster of residues targeted by the V_H CDR2 and CDR3 loops, and a more isolated area contacted by the light chain (Fig. 5a).

Basis of 1A12 cross-reactivity despite antigenic diversity. The elucidation of the present structure allows us to provide a detailed molecular explanation for the versatility of mAb 1A12 to recognize fHbp antigens from all three variant groups. Remarkably, many of the fHbp residues that participate in the interaction with the Fab (12 of the 17 residues in the 1A12 epitope) are conserved across the three different fHbp variants tested here by SPR, i.e., var1.1, var2.16, and var3.45 (Fig. 5b). Notably, residues Asp161 and Asn190 are completely conserved in fHbp variants 1.1, 2.16, and 3.45, and play key roles in the overall network of interactions with the Fab (Fig. 4b). Further, the motif $_{180}\text{KIEHLK}_{185}$, and residues Asn190, Val191, and Tyr214 are also conserved in the same three variants tested by SPR. Therefore, the degree of conservation assigns a leading role to these residues in the cross-recognition by the human mAb 1A12.

The *Neisseria* Multi Locus Sequence Typing database now contains ~1000 different polypeptide sequences for fHbp obtained from naturally occurring strains³¹. Therefore, we performed a deeper analysis in silico and calculated the degree of conservation associated with residues in the 1A12 epitope in 984 fHbp sequence variants available to date, which include sequences from serogroup B strains and from other serogroups³¹. Most notably, five residues (Ile181, Glu182, Leu184, Val191, and Tyr214) are 100% conserved throughout the whole fHbp sequence repertoire (Fig. 5b). Furthermore, five additional epitope residues show $\geq 99\%$ conservation (Asp161, His183, Lys185, Pro187, and Asn190). Together, these observations suggest that mAb 1A12 might display cross-reactivity with a vast breadth of recognition across almost the entire known polymorphic repertoire of fHbp.

Effects of polymorphisms in the 1A12-fHbp-binding interface.

To better define the contribution of individual residues and the effect of polymorphisms within the epitope, we made single-amino-acid substitutions in the fHbp var1.1 background: A162P; G163A; G163N; K180A; K185A; N190A; and N215G. The fHbp Asn215 residue makes contacts directly or indirectly with six different residues in the heavy and light chains of Fab 1A12 (Fig. 4c and Supplementary Table 1). Substitution of Asn215 with Gly (N215G), as found in var2.16 and var3.45, resulted in a notable decrease in binding to mAb 1A12 (Fig. 6a). However, given the extremely tight binding of mAb 1A12 to wild-type var1.1, the seven-fold decrease in affinity due to the N215G mutation nevertheless resulted in a very tight antigen/antibody interaction ($K_D = 620$ pM, compared to 87 pM for wild type).

The fHbp residue Gly163 is also found in the epitope/paratope interface, using its backbone carbonyl oxygen to contact the important heavy chain residue Arg54 (Fig. 4b). It was conceivable that this backbone-mediated interaction coupled with the small size of Gly163 (and of its neighbor Ala162) were key factors in the optimal accommodation of the Arg54 side chain from 1A12. However, the single mutations A162P and G163N (both polymorphisms naturally occurring at this position in some variant 2 and 3 proteins) actually resulted in mild increases in binding affinity toward mAb 1A12 (Fig. 6b, c). fHbp var1.1 G163A and K180A mutants also slightly increased the binding affinity (approximately two- to threefold), thus suggesting that the side-chain characteristics in these positions are not crucial determinants for cross-recognition by mAb 1A12 (Table 1 and Fig. 6d, e). These results contribute to a better understanding of the molecular basis of this interaction and the potential overall cross-reactivity of mAb 1A12, since G163 and K180 show lower prevalence throughout all strains (G163 is found in ~50% of subvariants; K180 in ~70% of subvariants), despite both being conserved in var1.1, var2.16, and var3.45. In summary, known polymorphisms occurring in fHbp at positions 163 and 180 are unlikely to preclude binding of mAb 1A12 to meningococcal strains expressing such antigens.

Finally, we studied the roles of Lys185 and Asn190. The former establishes salt bridges with two acidic residues on the Fab heavy chain, Asp55 and Asp57, and VDW contacts with His52 and Arg54 (Fig. 4b and Supplementary Table 1) while the latter is directly involved in hydrogen bonds with Gln101 and Gly104 and VDW contacts with Ser103. In SPR studies, mutant K185A reduced the binding affinity to 1A12 by ~25-fold (Fig. 6f and Table 1). Similarly, N190A notably impacted the binding to 1A12 with an ~50-fold reduction in the affinity (Fig. 6g and Table 1). While both the association and dissociation rates are affected in the case of K185A, it is predominantly the increased dissociation rate (k_{off}) that is responsible for the lower affinity of N190A. These results confirm the importance of these highly conserved positions on fHbp recognition by 1A12.

In conclusion, the very high affinity of mAb 1A12 for wild-type fHbp var1.1 appears to be the result of a cooperative and elaborate network of interactions. Despite the sequence diversity inherent to fHbp, we show here that mAb 1A12 recognizes a series of fHbp variants with very high affinities, suggesting a high breadth of coverage potentially conferred by this human mAb.

Structure of free Fab 1A12 reveals paratope flexibility. We also determined the crystal structure of the free Fab 1A12 at 1.76 Å resolution (Table 2). Comparison of the free and antigen-bound Fab structures shows that they are highly similar (rmsd 0.69 Å on alpha carbons). However, superposition reveals that while most of the CDR loops do not change their conformation (Fig. 7a), there

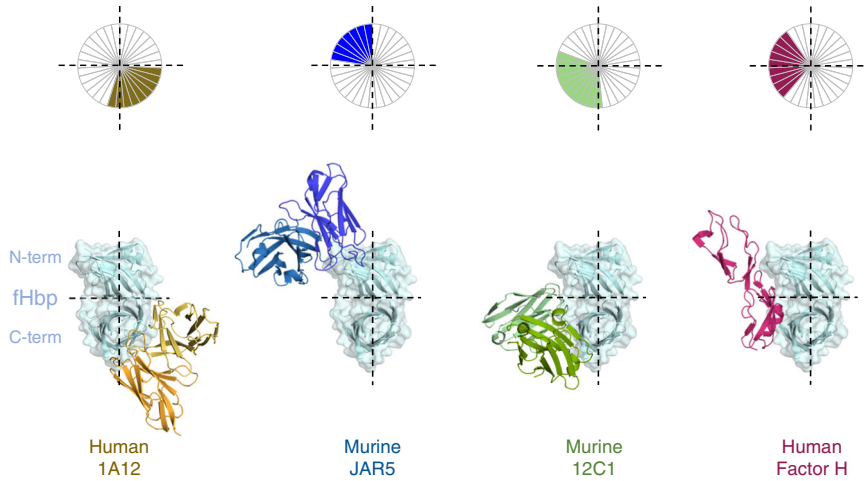


Fig. 3 Fab 1A12 shows a unique binding mode. Bottom: surface and ribbon representations of fHbp, bound to 1A12 (yellow), JAR5 (blue), 12C1 (green), and factor H (red). For clarity, only the Fab variable regions are shown. Top, schematic diagram of the different binding sites on fHbp

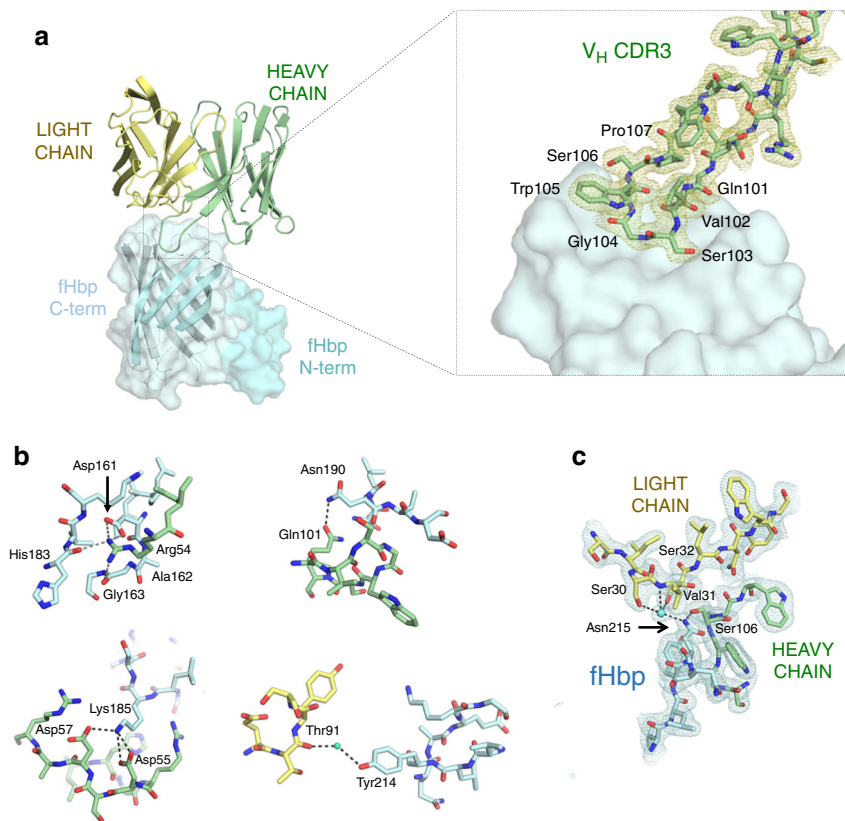


Fig. 4 Intermolecular interactions in the Fab 1A12/fHbp-binding interface. **a** Left: ribbon representation highlighting the region where the Fab V_H CDR3 loop contacts fHbp. The N- and C-terminal domains of fHbp are displayed in surface mode in different blue palette colors; the Fab is colored as in Fig. 2. For clarity, the constant regions of the Fab have been omitted. Right: the V_H CDR3 loop (stick bonds) and its 2Fo-Fc electron density map (yellow mesh) at 1 σ contour level. Fab constant regions are omitted for clarity. **b** Noteworthy salt bridges and other polar interactions at the binding interface, involving V_H CDR2 and 3. (fHbp: cyan; Fab light chain: yellow; Fab heavy chain: green). **c** The binding interface centered around fHbp residue Asn215 is shown as sticks. Polar interactions (≤ 3.3 Å) established with the heavy and light chains are represented by dashed lines. The cyan sphere represents a water molecule. The blue mesh depicts the 2Fo-Fc electron density map associated with the region displayed, plotted at 1 σ contour level

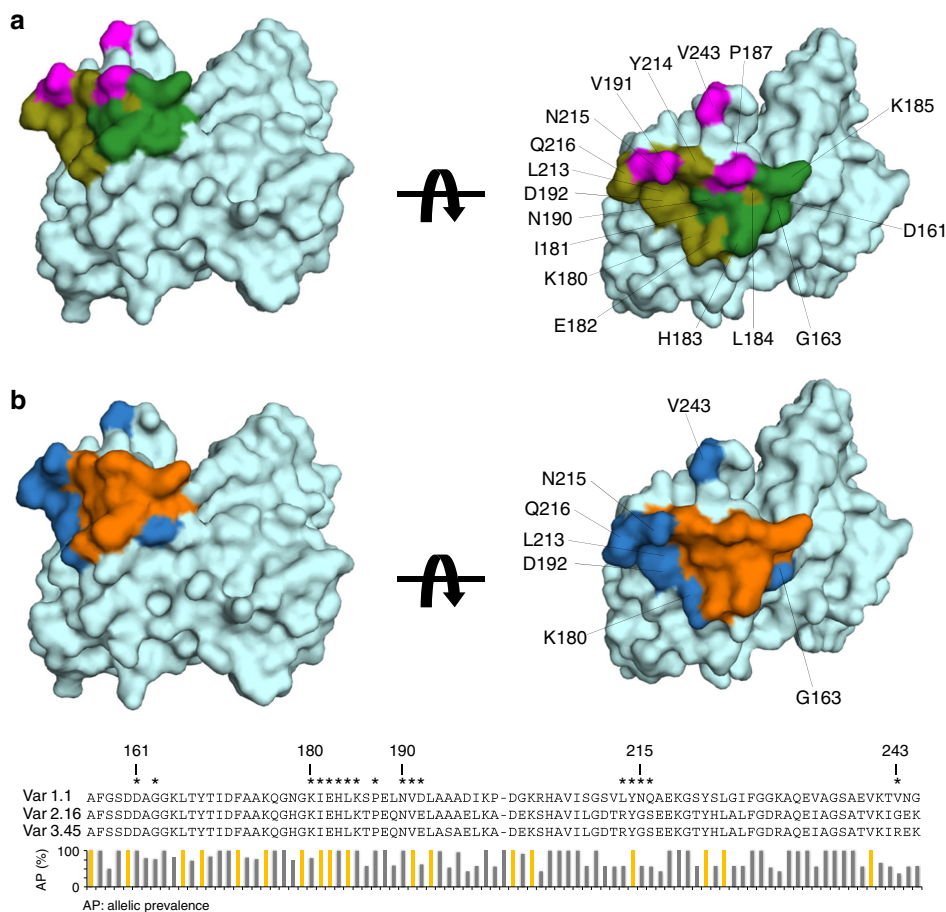


Fig. 5 The 1A12 epitope and its allelic diversity in the fHbp global gene repertoire. **a** Two views of the 1A12 epitope “footprint” on the surface of fHbp. Residues contacted by the heavy chain are highlighted in green and olive colors for polar and VDW interactions, respectively. The contacts made by the light chain are in magenta. Asn215 establishes polar contacts with both the heavy and light chains. **b** Allelic diversity in the 1A12 epitope. Upper panel: residues within the 1A12 epitope with a degree of conservation >99% in all fHbp gene repertoire are colored orange; residues with a prevalence lower than 99% are shown in dark blue and labeled with their position number. Bottom panel: sequence alignment of fHbp var1.1, 2.16, and 3.45. (The gap at position 200–201 reflects one subvariant of 984 that presents a single-residue insertion (Trp) at this position. Despite the gap, the numbering shown above the alignment corresponds to the numbering used in the main text). The allelic prevalence among 984 fHbp sequences is shown for each position in the 1A12 epitope³¹. Orange columns depict sites non-polymorphic in all 984 sequences known. The residues that form the 1A12 epitope are indicated with an asterisk

is a difference in the V_H CDR3 loop conformation upon complex formation. Most notably, Gly104 in V_H CDR3 shifts position by 4 Å, thus avoiding a steric clash with Tyr214 on fHbp (Fig. 7b).

In the complex, Gly104 establishes polar and water-mediated contacts with fHbp residues Asn215 and Gln216 (Fig. 7c). Similarly, the neighboring V_H CDR3 residues Ser103 and Trp105 also show changes of varying magnitude in their side-chain positions (Fig. 7d), enabling them to make favorable contacts with fHbp. On the other side of the interface, when compared with free fHbp³⁶, it emerges that upon binding most fHbp residues do not change conformation. One exception is a short loop (fHbp residues 241–246), wherein the alpha carbon of Val243 moves by 3 Å and its side chain undergoes a rotation of ~90° thereby optimizing contacts with Fab 1A12.

mAb 1A12 recognizes diverse fHbp variants on MenB surface.

We sought to understand how the broad cross-reactivity of 1A12 relates to the function of this antibody. We used 1A12 as an intact human IgG1 mAb and examined its binding to live bacteria by flow cytometry. We observed that mAb 1A12 binds to all three tested MenB strains expressing fHbp from different variant

groups: strains H44/76 (fHbp var1.1); M08-0240104 (fHbp var2.16); and M01-0240320 (fHbp var3.45). The var2.16-expressing strain showed the strongest binding, whereas slightly lower levels of binding were observed with the var1.1- and var3.45-expressing MenB strains (Fig. 8). The order of binding affinities found by SPR and the degree of binding observed via flow cytometry analysis were different. Assuming that technical differences (between SPR and flow cytometry) do not underlie these observations, we interpret the discrepancy as suggesting that factors other than affinity may affect the overall extent of mAb binding to the live bacterial cells; for example, the antigen density displayed on the bacterial surface. Indeed, the M08-0240104 strain was previously reported to have high expression of fHbp var2.16, whereas the var1.1 and var3.45 strains were reported to express approximately two- to fourfold lower amounts of fHbp antigen (Supplementary Table 2)³⁷. Nevertheless, these findings confirm the results of SPR analyses in a physiologically more relevant context (live bacterial cells), showing that there is broad cross-recognition by mAb 1A12 despite extensive fHbp sequence variability and likely numerous other phenotypic differences existing between diverse meningococcal strains.

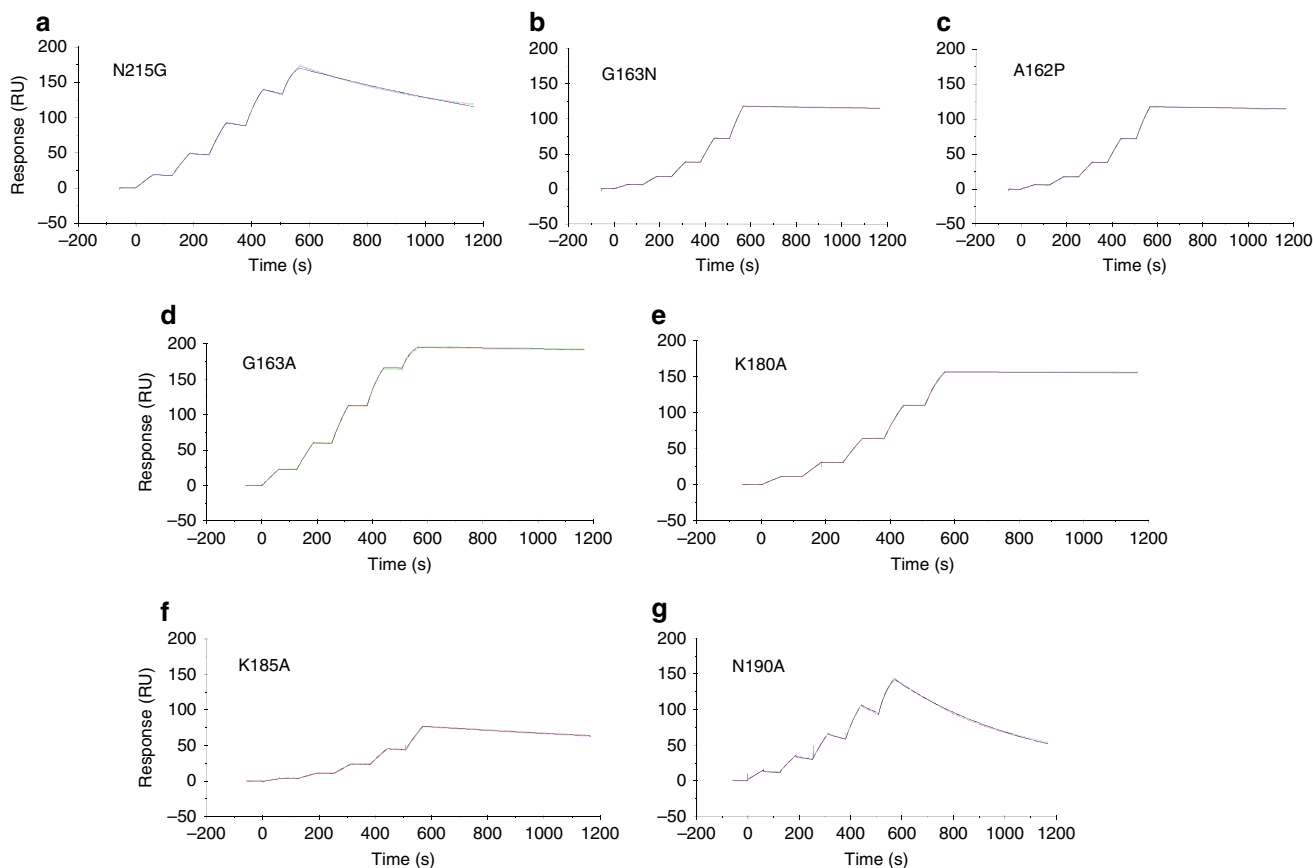


Fig. 6 Impact of fHbp var.1 site-specific mutations on the binding to mAb 1A12. The effect of the mutations was analyzed by SPR with mAb 1A12 captured on the surface, and the association and the dissociation of diverse mutants (panels **a–g**) were monitored in duplicate (colored traces). The single-cycle kinetics fitting (Langmuir 1:1 model) is represented as solid black lines in each sensorgram (full details of kinetic analyses are provided in Methods and Table 1)

Bactericidal activity of cross-reactive mAb 1A12. Finally, we investigated whether mAb 1A12 was bactericidal against MenB strains expressing different fHbp variants, in an assay measuring complement-dependent killing (using baby rabbit serum as the complement source). We selected this assay to assess the functional activity of the mAb because the serum bactericidal assay (SBA) is the widely accepted functional correlate of protection for *Neisseria meningitidis*^{38–40}. Meningococcal strains H44/76 (expressing fHbp var.1.1), M08-0240104 (expressing fHbp var.2.16), and M01-0240320 (expressing fHbp var.3.45) were incubated with different concentrations of mAb 1A12. Indeed, mAb 1A12 induced bactericidal activity against all three different strains. The concentrations of mAb 1A12 required for $\geq 50\%$ killing of bacteria when measured against strains expressing fHbp var.3.45, var.2.16, and var.1.1 were 0.06, 0.49, and 3.9 $\mu\text{g ml}^{-1}$, respectively. Consequently, 1A12 is not only immunologically cross-reactive, but most importantly, it is cross-protective, being able to elicit rabbit complement-dependent bactericidal activity against meningococci in all three of the fHbp variant groups tested herein.

Discussion

Vaccines against infectious diseases save an estimated 2–3 million lives each year⁴¹. Research now targets the development of new vaccines against diseases not yet preventable by current vaccines, and also aims to enhance the breadth of coverage of some current vaccines against highly mutable pathogens. Upon vaccination, protein antigens are recognized by host immune factors (surface-

bound B-cell receptors, or soluble antibodies) and elicit protection usually via an antibody-mediated regulatory, or killing, immune response. Therefore, high-resolution structural data of antibody–antigen complexes facilitate an understanding of the molecular bases of immunoprotection, and may consequently aid the development of optimal vaccine immunogens^{42–44}. Here we sought structural insights into the human immune recognition of fHbp, a key antigen in the two licensed MenB vaccines.

We determined the crystal structure of fHbp var.1.1 bound to the Fab fragment of a vaccine-elicited human mAb, 1A12. Despite having been generated in a human subject immunized with the fHbp sequence variant 1.1, the mAb 1A12 binds with remarkably high affinity (sub-nanomolar K_D) to representatives from each of the three distinct variant groups of fHbp, and is therefore an antibody of great interest. Our structural and biochemical insights reveal the molecular basis of this cross-reactivity. Previous reports of cross-reactive anti-fHbp mAbs were limited to those raised in mice, and mapped their epitopes to N-terminal regions^{21,23}, or did not provide any epitope-mapping information³⁰. An important implication of our findings is that human immunization with fHbp var.1.1 in the 4CMenB vaccine may contribute to confer an unexpectedly broad coverage against meningococci expressing fHbp from any of the three known variant groups.

To our knowledge, this is the first report of a vaccine-elicited human Fab bound to a bacterial antigen. One recent report described crystal structures of two human Fabs obtained from memory B cells of healthy donors, and described an unusual mode of recognition of a staphylococcal antigen predominantly

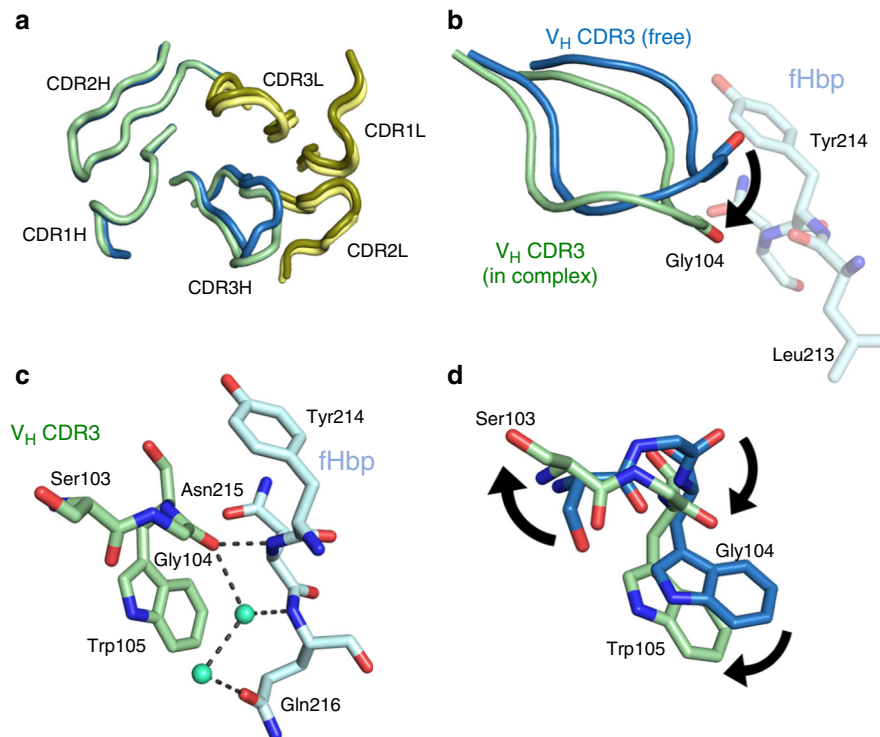


Fig. 7 Conformational changes between bound and free Fab 1A12. **a** Ribbon diagram showing the light (dark and light yellow) and heavy chains (green and blue) of Fab 1A12 both in the liganded (pale colors) and unliganded (dark colors) states. Only CDR3H shows a notable difference. **b** V_H CDR3 loop conformations are represented as cartoons with colors distributed in a similar manner to **a**; fHbp residue is colored cyan. The movement of Gly104 is indicated. **c** Detail of the Gly104 region in the bound state. **d** Side chains of Ser103 and Trp105 show notably different positions in bound and free forms

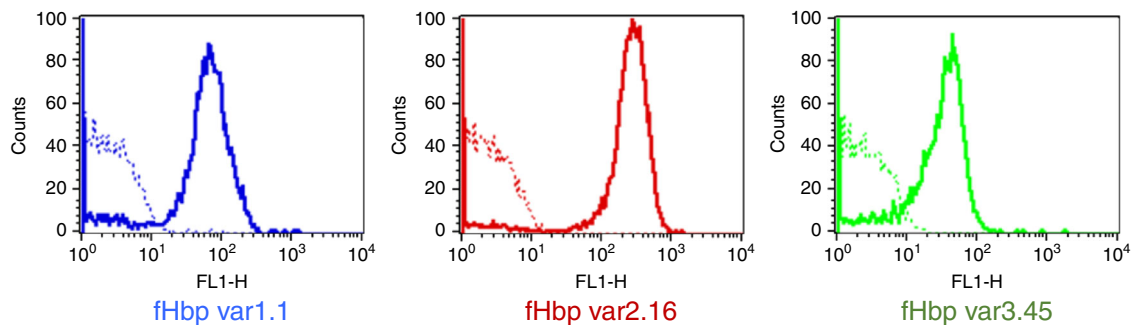


Fig. 8 mAb 1A12 binds meningococci expressing all three fHbp variant groups. Flow cytometry histograms showing the binding of mAb 1A12 to live serogroup B meningococci H44/76, M08-0240104, and M01-0240320 strains (blue, red and green lines, respectively) when incubated with $10 \mu\text{g ml}^{-1}$ of anti-fHbp mAb. Dotted-line histograms represent negative control, bacteria incubated with PBS and anti-human IgG FITC-conjugated

mediated by V_H CDR2⁴⁵. Here the structure of the 1A12/fHbp var1.1 complex shows how the hypervariable V_H CDR3 loop interacts with a groove containing several discontinuous residues clustered on a highly solvent-exposed region of the fHbp C-terminal β barrel domain. Overall, the recognition of the antigen by Fab 1A12 is governed by polar interactions. Numerous H-bonds, salt bridges, water-dependent contacts, and VDW interactions are widely distributed across the binding interface and contribute collectively to the very strong recognition of fHbp. This cross-reactive conformational epitope presents a unique binding mode that was not previously seen in other crystal structures of fHbp complexed with mAbs raised in mice^{24,25}, nor in additional murine mAbs reported to target epitopes on the N-terminal domain of fHbp^{21,23}. Further, comparison of the 1A12 epitope and the fH-binding site on fHbp³⁵ reveals two quite

distinct interaction areas, and thus provides the structural basis for the lack of inhibition of factor H binding to fHbp by human mAb 1A12, and also confirms that fHbp does not undergo notable conformational changes upon binding to either partner.

Recognition of fHbp by 1A12 does not follow the classical “lock and key” concept of antigen–antibody interactions. Rather, although fHbp var1.1 appears relatively rigid, the flexible V_H CDR3 loop of Fab 1A12 undergoes a notable conformational change, which allows the formation of several favorable interactions with fHbp. The V_H CDR3 sequence composition features small residues (Gly and Ser) and a large aromatic residue (Trp), which in itself is not unusual for a V_H CDR3⁴⁶. The availability of both free and antigen-bound states of a Fab^{47,48} allows inspection at high resolution of the functionality in the paratope. In 1A12, the presence of Gly and Ser may promote flexibility and allow the

versatile aromatic residues to mediate numerous interactions with epitope atoms, thus enabling antigen recognition⁴⁹. In short, it appears that the distinct sequence composition of Fab 1A12 enables a structural transition in V_H CDR3, which translates into an energetically favorable antigen-binding region ideally suited to bind fHbp.

A detailed analysis of the antibody/antigen interface reveals how mAb 1A12 can be vastly cross-reactive. In short, of the total 17 fHbp epitope residues that make contact with the Fab, 12 are absolutely conserved, and a further 4 are conserved moderately ($\geq 66\%$), in fHbp var1.1, var2.16, and var3.45. The high conservation of key epitope residues explains the ability of mAb 1A12 to cross-react with the different fHbp variants (either as purified fHbp proteins or when expressed on the surface of live meningococci). Moreover, even when a key fHbp epitope residue was mutated to remove its side-chain functionality (N215G), tight binding to mAb 1A12 was still observed (sub-nanomolar K_D value). Furthermore, other naturally occurring fHbp substitutions (A162P and G163N) actually increased the strength of mAb binding. These observations suggest that the epitope/paratope interface defined by 1A12 can also accommodate at least some known sequence polymorphisms without losing binding functionality.

A vast number of fHbp sequence variants identified from clinical isolates and carrier strains are now known³¹. Therefore, we also analyzed the conservation of the 1A12 epitope residues in the 984 subvariants reported to date. We found that several epitope residues are absolutely conserved (5 of 17 residues) throughout the entire fHbp antigenic repertoire, and an additional 5 residues have extremely high ($\geq 99\%$) prevalence. Therefore, 10 of 17 epitope residues are at least 99% conserved in the known antigenic repertoire. Although additional investigations would be needed to demonstrate the full cross-reactivity of mAb 1A12 toward the many known subvariants, we envisage a wide recognition of the great majority of fHbp antigens, with potential to induce bacterial killing either alone or cooperatively with other mAbs against fHbp or in synergy with antibodies against alternative MenB surface antigens. The observation that antibodies recognizing ordered conformational epitopes are less sensitive to antigen sequence diversity than those antibodies targeting disordered epitopes³³ further underscores the likelihood that mAb 1A12 may react with most fHbp variants.

We found that mAb 1A12 bound tightly to all three variants of fHbp when tested in biochemical assays (SPR), and live cell-based binding assays (flow cytometry). Interestingly however, we found that the binding affinities determined with the soluble recombinant proteins did not correlate closely with the amount of binding to whole bacteria as measured by flow cytometry (Table 2). Using the selected reaction monitoring mass spectrometry approach, the surface concentration of fHbp in these strains was previously determined to be ~ 4000 , 9000 , and 1000 molecules per cell for variants var1.1, var2.16, and var3.45, respectively³⁷. Given that mAb 1A12 showed very high affinity for each fHbp subvariant, it is likely that the higher antigen density on var2.16 underlies the higher fluorescence response measured here for the var2.16 strain.

Importantly, mAb 1A12 not only recognized the three fHbp variants on the surface of live meningococci, it was also able to activate the complement cascade and induce bacterial killing against MenB strains expressing fHbp var1, var2, or var3 antigens, as demonstrated in bactericidal assays, here using baby rabbit serum as the complement source. That is, mAb 1A12 is cross-protective as well as being cross-reactive. Some anti-meningococcal mAbs have bactericidal activity only when combined with other mAbs targeting different epitopes or even different antigens on the same bacterial cell. In contrast, mAb 1A12 is able to induce the killing alone (with higher efficiencies for var2

and var3 strains), presumably through highly efficient activation of the classical pathway of the complement system, which highlights the benefit of immunologically targeting this epitope on fHbp. Somewhat counter-intuitively, we observed that the killing activity was strongest against the M01-0240320 (fHbp var3.45) strain, where the surface density of fHbp is the lowest. It is possible either that the M01-0240320 strain is inherently more susceptible to killing, or that the particular fHbp var3.45 antigen density on this strain was sterically or geometrically more efficient for mAb 1A12-dependent activation of the complement pathway, or both. While the susceptibility to complement-mediated killing (using polyclonal anti-fHbp sera in the SBA assay) has been shown to correlate with the absolute amount of fHbp protein expressed by each meningococcal strain³⁷, some additional strain-specific differences in the intrinsic susceptibility to killing by unique mAbs are likely determined by other factors, such as the expression of virulence molecules that bind host complement regulators⁵⁰.

The most efficient complement-dependent immune response against a specific surface antigen may result from the activity of two or more different mAbs engaging the same antigen simultaneously²⁵. In general, it is not the action of only one mAb but the combination of different mAbs in a polyclonal response that are directed against alternative non-competing epitopes that will act cooperatively to maximize the efficiency of the immune response⁵¹. Therefore, the cross-protective human mAb 1A12 characterized here appears to be a potentially key player in such a multivalent bactericidal response. The extent to which such a cross-reactive mAb could contribute to meningococcal killing in vivo in a vaccinated individual may depend on its IgG subclass and will of course also depend on the absolute quantity in which the mAb is present⁵². While it was beyond the scope of this study to determine the serum concentrations of individual mAbs, recently published proteomic approaches combined with next-generation sequencing have demonstrated that a molecular deconvolution of the immune response can be performed⁵³, and this might form the basis of future studies to further explore the response to meningococcal vaccines such as 4CMenB.

In summary, we present here the crystal structures of an fHbp-specific human Fab in free and antigen-bound states, elicited by vaccination. We define a molecular signature that allows a vaccine-elicited human mAb to cross-react with the three different variants of fHbp and importantly, to induce complement-dependent killing responses against MenB strains harboring fHbp antigens from variants 1, 2, or 3. The existence of this cross-protective epitope on fHbp var1.1 suggests that the broad efficacy demonstrated by the 4CMenB vaccination in the United Kingdom^{10,11} could result from a multi-factorial effect, where antigens carrying cross-protective epitopes play key synergistic roles. Moreover, such detailed structural studies could be exploited for the design of vaccines with an immunofocusing approach toward cross-protective epitopes, aiming to further enhance the existing breadth of protection. More broadly, it is noteworthy that several current vaccines against bacterial pathogens are essentially based on surface-exposed polysaccharides that make up the outermost layer of the bacterial surface. However, when capsular polysaccharides are unsuitable vaccine candidates, or when polysaccharide serotypes are too numerous and variable, alternative reverse and structural vaccinology approaches may permit the identification and design of protein-based epitope-focused vaccine candidates. In this light, our studies provide an exploratory human vaccination model enabling the identification of broadly protective epitopes that could be expanded to the design of ideal saccharide-independent cross-protective bacterial targets.

Methods

Human samples. Human peripheral blood mononuclear cells were collected from three vaccinated subjects 8 days after the second dose of a multicomponent serogroup B meningococcal vaccine containing recombinant fHbp variant 1.1. Plasmablasts were processed individually (not pooled), were isolated as single cells, and were used as the source from which genes of heavy and light chain variable regions were amplified separately and then combined by overlap extension PCR, in order to obtain Fab region sequences. Recombinant Fabs were then produced in *E. coli* (see Protein expression description below) and were screened for antigen specificity through ELISA assays involving detection of fHbp-bound Fabs by Fab-specific goat anti-human IgG conjugated to alkaline phosphatase (Sigma; 1:5000 in phosphate-buffered saline (PBS)-Tween 20-bovine serum albumin (BSA)¹⁶. The samples were obtained from a clinical trial conducted in Krakow, Poland, in a study sponsored by Novartis Vaccines & Diagnostics, now part of the GSK group of companies. The clinical trial protocol was approved by the Bioethics Committee of the District Medical Doctors' Chamber in Krakow and the study was conducted in accordance with the Declaration of Helsinki. Written informed consent was obtained from each of the subjects.

Protein expression. All genes for the preparation of the fHbp subvariants and point mutants used in this study were cloned and amplified using DH5 α and MultiShot™ StripWell Mach1™ T1 Phage-Resistant Chemically Competent *E. coli* cells (Invitrogen), expressed from pET vectors (Novagen) induced by Isopropyl- β -D-thiogalactoside in *E. coli* strain BL21 (DE3) (New England Biolabs) and purified via C-terminal 6-His tags using Ni²⁺-affinity chromatography columns (His-Trap HP, 1 ml, GE Healthcare) and buffer solutions recommended by the manufacturer, controlled by an ÄKTA Purifier liquid chromatography system (GE Healthcare). PCR primers used to generate fHbp point mutants are listed (Supplementary Table 3). Full-length factor H was purchased from Calbiochem. For the expression of mAb 1A12, the variable regions of the heavy and light chains of 1A12 were codon-optimized (Supplementary Table 4) for expression in mammalian cells and synthesized by GeneArt (Thermo Fisher). Synthetic DNA sequences were digested with *EcoRI* (New England Biolabs) and cloned into the human pRS5a expression vectors encoding the Igy1 and Igk backbone, under the control of the cytomegalovirus promoter and in frame with a leader sequence for secretion derived from human immunoglobulins (Novartis-NIBR). The recombinant antibody was transiently expressed in Expi293 cells by transfecting the cells with equivalent amounts of both plasmids with the use of the Expi293 expression system (Thermo Fisher). Three and six days after transfection, cells were harvested, centrifuged for 10 min at 350 \times g, and filtered through a 0.2 μ m filter to remove cellular debris. Recombinant antibody was purified from the tissue culture expression medium with Protein G Sepharose 4 Fast Flow (GE Healthcare), following the manufacturer's protocol. A PD-10 Desalting Column (GE Healthcare) was used for buffer exchange and the antibody was eluted in PBS pH 7.4. 1A12 IgG concentration was determined in a NanoDrop spectrophotometer (Thermo Scientific) and its purity was assessed by SDS-PAGE on a 4–12% Bis-Tris Gel and Problue Safe Stain (Giotto Biotech).

The recombinant plasmid for human Fab 1A12 and the expression in *E. coli* (New England Biolabs) have been previously described¹⁶. The bacteria were suspended in 50 mM NaH₂PO₄, 500 mM NaCl, 20 mM imidazole, pH 7.0, and lysed using chicken egg white lysozyme, DNase, and RNase (Sigma; 0.1 mg ml⁻¹ each), and three freeze/thaw cycles. The clarified lysate was applied to a HiTrap Chelating HP (5 ml; GE Healthcare) column and the bound protein was eluted with an imidazole gradient from 20 to 250 mM. The Fab was further purified by cation exchange chromatography (HiTrap SP HP 5 ml; GE Healthcare) using 20 mM sodium acetate buffer, pH 5.5, and elution with a NaCl gradient from 0.02 to 1.0 M. Fractions containing the Fab were dialyzed against 20 mM Tris-HCl, 20 mM NaCl, pH 7.0 for crystallization trials.

For formation of the complex, fHbp var1.1 was expressed and purified as described above. Fab-expressing *E. coli* cells were first sonicated in ice-cold 10 mM HEPES (pH 7.4) and 150 mM NaCl, and centrifuged at 9500 \times g for 30 min. The supernatant was then filtered and loaded on a Ni²⁺ Sepharose 6 Fast Flow column (GE Healthcare) pre-saturated with recombinant fHbp var1.1. The bound protein was eluted with 10 mM HEPES (pH 7.4), 150 mM NaCl, and 300 mM imidazole. Next, the protein was subjected to three cycles of concentration and dilution with 10 mM HEPES (pH 7.4) and 150 mM NaCl using an Amicon concentrator (Millipore) with a 30 kDa cutoff. The complex was then recovered for crystallization assays.

Surface plasmon resonance. All interaction experiments were performed using a BIAcore T200 instrument (GE Healthcare), equilibrated at 25 °C. First, the mAb 1A12 was captured to a density of ~540 resonance units on the surface of a CM5 sensor chip previously coated with covalently immobilized monoclonal mouse anti-human IgG (Fc) antibody (GE Healthcare). In order to subtract the background signal for kinetic analysis, we prepared a control reference channel in a similar way but in the absence of the mAb. A series of concentrations of the different fHbp variants (wild type or mutants) were then injected in 0.01 M HEPES (pH 7.4), 0.15 M NaCl and 3 mM EDTA. To minimize nonspecific interactions, the running buffer was also supplemented with 0.005% v/v surfactant P20 and 0.1 %

(w/v) BSA. All kinetic parameters were calculated using standard single-cycle kinetics fitting and a Langmuir 1:1 binding model (BIAcore T200 evaluation software).

Crystallization and diffraction data. The purified Fab (7.1 mg ml⁻¹) was screened against 96 crystallization reagents (Index Screen, Hampton Research). Crystals were observed in multiple conditions; after 4 days, the largest crystals were found in 60% Tacsimate, pH 7.0. Optimization of the crystallization conditions was achieved in 57.5% Tacsimate (Hampton Research) at pH 6.0. Crystals were soaked in 15% PEG 3350 and 12% Tacsimate as cryoprotectant and cryo-cooled in liquid nitrogen. The crystals were tested for diffraction at beamline 5.0.1 at the Advanced Light Source, Lawrence Berkeley National Laboratory and several data sets were collected on an ADSC Q315R detector (Table 2). Data were integrated and scaled with iMosflm⁵⁴. The structure of the Fab was solved using Phaser⁵⁵ with a homology model constructed from the 1A12 sequence and the coordinates of the human anti HIV 21c Fab (PDB ID 3LMJ) using Swiss-Model⁵⁶.

The Fab 1A12-fHbp complex at 10 mg ml⁻¹ was screened with a matrix of ~800 crystallization conditions using a Crystal Gryphon robot (Art Robbins Instruments). Long plate-needle-looking crystals were found at days 7–10 with 17% PEG 3350 and 0.2 M sodium malonate (pH 4.0). Optimization of the original conditions was performed by changing the concentrations of the different components in the initial crystallization mixture. Changes in the pH did not yield any improvement. Crystals were soaked in the original mother liquor supplemented with 10 % ethylene glycol as cryoprotectant and prior to cryo-cooling in liquid nitrogen. Diffraction of the crystals was tested at beamline ID29 of the European Synchrotron Radiation Facility and several full data sets were collected on a Pilatus 6M detector. Diffraction data sets were indexed, integrated, and scaled with XDS⁵⁷ and Aimless⁵⁸, via the CCP4 suite⁵⁹. The structure of the complex was solved by molecular replacement with Phaser⁵⁵ using as model templates for fHbp, light chain, and heavy chains the coordinates deposited in the protein data bank under the codes 2YPV, 4YPG, and 4JQI, respectively. The CDR3 loop of the heavy chain was omitted in the template.

Structure refinement. Initial molecular replacement solutions were subjected to subsequent cycles of manual building in Cool⁶⁰ and refinement with Phenix.refine⁶¹. The buried surface areas and atomic interactions/contacts, and the root mean square displacements, were calculated with PISA⁶² and Superpose⁶³, respectively. All the structural figures were created with PyMOL⁶⁴.

Flow cytometry analysis. The ability of mAb 1A12 to bind the antigen exposed on the surface of *N. meningitidis* bacteria, expressing different fHbp variants, was determined using a FACScan flow cytometer. Bacteria grown until early log phase (OD600 of ~0.25) were incubated with mAb at the concentration of 10 μ g ml⁻¹. Antibody binding was detected using a goat anti-human IgG conjugated to fluorescein isothiocyanate (Jackson Immuno Research, catalog number 109-096-088) at a 1:100 dilution. Bacteria plus PBS-1% BSA and secondary antibody were used as negative control.

Bactericidal assay. Bacteria grown in Mueller Hinton broth supplemented with 0.25% glucose until early log phase (OD600 of ~0.25) were diluted in Dulbecco's PBS containing 1% BSA and 0.1% glucose at the working dilution of 10⁴–10⁵ colony forming units (CFU) per ml and incubated with serial twofold dilutions of test mAb starting from a concentration of 31.25 μ g ml⁻¹ (corresponding to 1/16 dilution in the reaction mixture in the well). Bactericidal titers were defined as the reciprocal mAb dilution resulting in 50% decrease in CFU per ml after a 60-min incubation of bacteria with the reaction mixture compared to the control CFU per ml at time zero. Pooled baby rabbit serum (Cedarlane) was used as a complement source.

Data availability. Structure factors and atomic coordinates have been deposited in the Protein Data Bank for the Fab 1A12 (ID 5UR8) and Fab 1A12-fHbp var1.1 complex (ID 5O14). Other data are available from the corresponding authors upon reasonable request.

Received: 22 June 2017 Accepted: 3 January 2018

Published online: 06 February 2018

References

- European Centre for Disease Prevention and Control. Annual Epidemiological Report on Communicable Diseases in Europe 2010. (Stockholm, ECDC, 2010).
- Sadarangani, M. & Pollard, A. J. Can we control all-cause meningococcal disease in Europe? *Clin. Microbiol. Infect.* **22** Suppl 5, S103–S112 (2016).

3. Maignani, V. et al. Vaccination against *Neisseria meningitidis* using three variants of the lipoprotein GNA1870. *J. Exp. Med.* **197**, 789–799 (2003).
4. Fletcher, L. D. et al. Vaccine potential of the *Neisseria meningitidis* 2086 lipoprotein. *Infect. Immun.* **72**, 2088–2100 (2004).
5. Jiang, H. Q. et al. Broad vaccine coverage predicted for a bivalent recombinant factor H binding protein based vaccine to prevent serogroup B meningococcal disease. *Vaccine* **28**, 6086–6093 (2010).
6. Koerberling, O. et al. Immunogenicity of a meningococcal native outer membrane vesicle vaccine with attenuated endotoxin and over-expressed factor H binding protein in infant rhesus monkeys. *Vaccine* **29**, 4728–4734 (2011).
7. Findlow, J. et al. Multicenter, open-label, randomized phase II controlled trial of an investigational recombinant Meningococcal serogroup B vaccine with and without outer membrane vesicles, administered in infancy. *Clin. Infect. Dis.* **51**, 1127–1137 (2010).
8. Marshall, H. S. et al. Safety and immunogenicity of a meningococcal B bivalent rLP2086 vaccine in healthy toddlers aged 18–36 months: a phase 1 randomized-controlled clinical trial. *Pediatr. Infect. Dis. J.* **31**, 1061–1068 (2012).
9. Marshall, H. S. et al. A phase 2 open-label safety and immunogenicity study of a meningococcal B bivalent rLP2086 vaccine in healthy adults. *Vaccine* **31**, 1569–1575 (2013).
10. Basta, N. E. & Christensen, H. 4CMenB vaccine effectiveness: reasons for optimism. *Lancet* **388**, 2719–2721 (2016).
11. Parikh, S. R. et al. Effectiveness and impact of a reduced infant schedule of 4CMenB vaccine against group B meningococcal disease in England: a national observational cohort study. *Lancet* **388**, 2775–2782 (2016).
12. Madico, G. et al. The meningococcal vaccine candidate GNA1870 binds the complement regulatory protein factor H and enhances serum resistance. *J. Immunol.* **177**, 501–510 (2006).
13. Costa, I., Pajon, R. & Granoff, D. M. Human factor H (FH) impairs protective meningococcal anti-FHbp antibody responses and the antibodies enhance FH binding. *MBio* **5**, e01625–14 (2014).
14. Granoff, D. M. et al. Enhanced protective antibody to a mutant meningococcal factor H-binding protein with low-factor H binding. *JCI Insight* **1**, e88907 (2016).
15. Granoff, D. M. et al. Binding of complement factor H (FH) decreases protective anti-FH binding protein antibody responses of infant rhesus macaques immunized with a meningococcal serogroup B vaccine. *J. Infect. Dis.* **212**, 784–792 (2015).
16. Beernink, P. T., Giuntini, S., Costa, I., Lucas, A. H. & Granoff, D. M. Functional analysis of the human antibody response to meningococcal factor H binding protein. *MBio* **6**, e00842 (2015).
17. Giuliani, M. M. et al. The region comprising amino acids 100 to 255 of *Neisseria meningitidis* lipoprotein GNA 1870 elicits bactericidal antibodies. *Infect. Immun.* **73**, 1151–1160 (2005).
18. Scarselli, M. et al. Epitope mapping of a bactericidal monoclonal antibody against the factor H binding protein of *Neisseria meningitidis*. *J. Mol. Biol.* **386**, 97–108 (2009).
19. Beernink, P. T. et al. Fine antigenic specificity and cooperative bactericidal activity of monoclonal antibodies directed at the meningococcal vaccine candidate factor h-binding protein. *Infect. Immun.* **76**, 4232–4240 (2008).
20. Beernink, P. T., LoPasso, C., Angiolillo, A., Felici, F. & Granoff, D. A region of the N-terminal domain of meningococcal factor H-binding protein that elicits bactericidal antibody across antigenic variant groups. *Mol. Immunol.* **46**, 1647–1653 (2009).
21. Faleri, A. et al. Two cross-reactive monoclonal antibodies recognize overlapping epitopes on *Neisseria meningitidis* factor H binding protein but have different functional properties. *FASEB J.* **28**, 1644–1653 (2014).
22. Mascioni, A. et al. Structural basis for the immunogenic properties of the meningococcal vaccine candidate LP2086. *J. Biol. Chem.* **284**, 8738–8746 (2009).
23. Vu, D. M., Pajon, R., Reason, D. C. & Granoff, D. M. A broadly cross-reactive monoclonal antibody against an epitope on the N-terminus of meningococcal fHbp. *Sci. Rep.* **2**, 341 (2012).
24. Malito, E. et al. Defining a protective epitope on factor H binding protein, a key meningococcal virulence factor and vaccine antigen. *Proc. Natl Acad. Sci. USA* **110**, 3304–3309 (2013).
25. Malito, E. et al. *Neisseria meningitidis* factor H-binding protein bound to monoclonal antibody JAR5: implications for antibody synergy. *Biochem. J.* **473**, 4699–4713 (2016).
26. Klontz, E. H. & Sundberg, E. J. Getting oriented with antibodies. *Biochem. J.* **474**, 517–519 (2017).
27. Derrick, J. P., Maiden, M. C. & Feavers, I. M. Crystal structure of an Fab fragment in complex with a meningococcal serosubtype antigen and a protein G domain. *J. Mol. Biol.* **293**, 81–91 (1999).
28. Oomen, C. J. et al. Crystal structure of an anti-meningococcal subtype P1.4 PorA antibody provides basis for peptide-vaccine design. *J. Mol. Biol.* **351**, 1070–1080 (2005).
29. van den Elsen, J. M. et al. Bactericidal antibody recognition of a PorA epitope of *Neisseria meningitidis*: crystal structure of a Fab fragment in complex with a fluorescein-conjugated peptide. *Proteins* **29**, 113–125 (1997).
30. McNeil, L. K. et al. Detection of LP2086 on the cell surface of *Neisseria meningitidis* and its accessibility in the presence of serogroup B capsular polysaccharide. *Vaccine* **27**, 3417–3421 (2009).
31. Jolley, K. A. & Maiden, M. C. BIGSdb: scalable analysis of bacterial genome variation at the population level. *BMC Bioinformatics* **11**, 595 (2010).
32. Diederichs, K. Crystallographic data and model quality. *Methods Mol. Biol.* **1320**, 147–173 (2016).
33. MacRaid, C. A., Richards, J. S., Anders, R. F. & Norton, R. S. Antibody recognition of disordered antigens. *Structure* **24**, 148–157 (2016).
34. Rubinstein, N. D. et al. Computational characterization of B-cell epitopes. *Mol. Immunol.* **45**, 3477–3489 (2008).
35. Schneider, M. C. et al. *Neisseria meningitidis* recruits factor H using protein mimicry of host carbohydrates. *Nature* **458**, 890–893 (2009).
36. Cendron, L., Veggi, D., Girardi, E. & Zanotti, G. Structure of the uncomplexed *Neisseria meningitidis* factor H-binding protein fHbp (rLP2086). *Acta Crystallogr. F Struct. Biol. Cryst. Commun.* **67**, 531–535 (2011).
37. Biagini, M. et al. Expression of factor H binding protein in meningococcal strains can vary at least 15-fold and is genetically determined. *Proc. Natl Acad. Sci. USA* **113**, 2714–2719 (2016).
38. Borrow, R., Andrews, N., Goldblatt, D. & Miller, E. Serological basis for use of meningococcal serogroup C conjugate vaccines in the United Kingdom: reevaluation of correlates of protection. *Infect. Immun.* **69**, 1568–1573 (2001).
39. Frasc, C. E., Borrow, R. & Donnelly, J. Bactericidal antibody is the immunologic surrogate of protection against meningococcal disease. *Vaccine* **27** Suppl 2, B112–B116 (2009).
40. Poolman, J. T. & Richmond, P. Multivalent meningococcal serogroup B vaccines: challenges in predicting protection and measuring effectiveness. *Expert Rev. Vaccines* **14**, 1277–1287 (2015).
41. Delany, I., Rappuoli, R. & De Gregorio, E. Vaccines for the 21st century. *EMBO Mol. Med.* **6**, 708–720 (2014).
42. Liljeroos, L., Malito, E., Ferlenghi, I. & Bottomley, M. J. Structural and computational biology in the design of immunogenic vaccine antigens. *J. Immunol. Res.* **2015**, 156241 (2015).
43. Malito, E., Carfi, A. & Bottomley, M. J. Protein crystallography in vaccine research and development. *Int J. Mol. Sci.* **16**, 13106–13140 (2015).
44. Rappuoli, R., Bottomley, M. J., D’Oro, U., Finco, O. & De Gregorio, E. Reverse vaccinology 2.0: human immunology instructs vaccine antigen design. *J. Exp. Med.* **213**, 469–481 (2016).
45. Yeung, Y. A. et al. Germline-encoded neutralization of a *Staphylococcus aureus* virulence factor by the human antibody repertoire. *Nat. Commun.* **7**, 13376 (2016).
46. Ramaraj, T., Angel, T., Dratz, E. A., Jesaitis, A. J. & Mument, B. Antigen-antibody interface properties: composition, residue interactions, and features of 53 non-redundant structures. *Biochim. Biophys. Acta* **1824**, 520–532 (2012).
47. Li, Y., Li, H., Smith-Gill, S. J. & Mariuzza, R. A. Three-dimensional structures of the free and antigen-bound Fab from monoclonal antilysozyme antibody HyHEL-63(.). *Biochemistry* **39**, 6296–6309 (2000).
48. Rini, J. M., Schulze-Gahmen, U. & Wilson, I. A. Structural evidence for induced fit as a mechanism for antibody-antigen recognition. *Science* **255**, 959–965 (1992).
49. Birtalan, S. et al. The intrinsic contributions of tyrosine, serine, glycine and arginine to the affinity and specificity of antibodies. *J. Mol. Biol.* **377**, 1518–1528 (2008).
50. Rossi, R., Beernink, P. T., Giuntini, S. & Granoff, D. M. Susceptibility of meningococcal strains responsible for two serogroup B outbreaks on U.S. University Campuses to serum bactericidal activity elicited by the MenB-4C vaccine. *Clin. Vaccine Immunol.* **22**, 1227–1234 (2015).
51. Sorman, A., Zhang, L., Ding, Z. & Heyman, B. How antibodies use complement to regulate antibody responses. *Mol. Immunol.* **61**, 79–88 (2014).
52. Giuntini, S. et al. Human IgG1, IgG3, and IgG3 hinge-truncated mutants show different protection capabilities against meningococci depending on the target antigen and epitope specificity. *Clin. Vaccine Immunol.* **23**, 698–706 (2016).
53. Wine, Y. et al. Molecular deconvolution of the monoclonal antibodies that comprise the polyclonal serum response. *Proc. Natl Acad. Sci. USA* **110**, 2993–2998 (2013).
54. Battye, T. G., Kontogiannis, L., Johnson, O., Powell, H. R. & Leslie, A. G. iMOSFLM: a new graphical interface for diffraction-image processing with MOSFLM. *Acta Crystallogr. D. Biol. Crystallogr.* **67**, 271–281 (2011).
55. McCoy, A. J. et al. Phaser crystallographic software. *J. Appl. Crystallogr.* **40**, 658–674 (2007).

56. Biasini, M. et al. SWISS-MODEL: modelling protein tertiary and quaternary structure using evolutionary information. *Nucleic Acids Res.* **42**, W252–W258 (2014).
57. Kabsch, W. Xds. *Acta Crystallogr. D. Biol. Crystallogr.* **66**, 125–132 (2010).
58. Evans, P. R. & Murshudov, G. N. How good are my data and what is the resolution? *Acta Crystallogr. D. Biol. Crystallogr.* **69**, 1204–1214 (2013).
59. Collaborative Computational Project, N. The CCP4 suite: programs for protein crystallography. *Acta Crystallogr. D. Biol. Crystallogr.* **50**, 760–763 (1994).
60. Emsley, P., Lohkamp, B., Scott, W. G. & Cowtan, K. Features and development of Coot. *Acta Crystallogr. D. Biol. Crystallogr.* **66**, 486–501 (2010).
61. Adams, P. D. et al. PHENIX: a comprehensive Python-based system for macromolecular structure solution. *Acta Crystallogr. D. Biol. Crystallogr.* **66**, 213–221 (2010).
62. Krissinel, E. & Henrick, K. Inference of macromolecular assemblies from crystalline state. *J. Mol. Biol.* **372**, 774–797 (2007).
63. Krissinel E. and Henrick K. Secondary-structure matching (SSM), a new tool for fast protein structure alignment in three dimension. *Acta Crystallogr. D. Biol. Crystallogr.* **D60**, 2256–2268 (2004).
64. The PyMOL Molecular Graphics System, Version 1.8. (Schrodinger, LLC, 2015)

Acknowledgements

We wish to thank the clinical study participants. We thank Drs Sumana Chandramouli, Oretta Finco, Paola Lo Surdo, Domenico Maione, Enrico Malito, and Vega Masignani at GSK, Siena, for useful discussions during this project. We thank Cecilia Brettoni for provision of fHbp var1.1 mutant clones, and Sara Marchi for fHbp proteins. We thank Elias Tsadik, Heather Stefek, and Emily Arnold (UCSF Benioff Children's Hospital Oakland) for technical assistance and staff at beam lines ID29 of the European Synchrotron Radiation Facility (ESRF, France) and 5.0.1 at the Advanced Light Source, Lawrence Berkeley National Laboratory for their assistance in collecting X-ray diffraction data. *N. meningitidis* strains used in this work were kindly provided: H44/76 by Dominique A. Caugant (Norwegian Institute of Public Health, Oslo, Norway); M08-0240104 and M01-0240320 by Ray Borrow (Health Protection Agency, Manchester, UK). This study was sponsored by GSK Vaccines srl (Siena, Italy). J.L.-S. was funded by a Marie Skłodowska-Curie Actions IF grant via the European Commission Horizon 2020 program (grant 659615). During this project, F.B. held a PhD Fellowship registered at the University of Florence, Italy. The work was supported in part by extramural research grants (R01 AI099125 and R01 AI114701) from the National Institute of Allergy and Infectious Diseases, National Institutes of Health, to P.T.B. The Advanced Light Source is supported by the Director, Office of Science, Office of Basic Energy Sciences, of the U.S.

Department of Energy under Contract No. DE-AC02-05CH11231. Bexsero is a trademark of the GSK group of companies. Trumenba is a trademark of Pfizer.

Author contributions

Conceived and designed the experiments: J.L.-S.; P.T.B.; A.H.L.; and M.J.B. Performed the experiments: J.L.-S.; P.T.B.; F.B.; L.S.; and E.F. Analyzed the data: J.L.-S.; P.T.B.; M.J.B.; and M.P. Wrote the paper: J.L.-S.; P.T.B., and M.J.B. All authors reviewed and approved the manuscript.

Additional information

Supplementary Information accompanies this paper at <https://doi.org/10.1038/s41467-018-02827-7>.

Competing interests: J.L.-S., L.S., E.F., M.P., and M.J.B. were employees of the GSK group of companies at the time of the study. M.J.B. and M.P. report ownership of GSK shares and/or restricted GSK shares. M.J.B., P.T.B., and M.P. are inventors named on patents and patent applications relating to meningococcal group B vaccines. The remaining authors declare no competing financial interests.

Reprints and permission information is available online at <http://npg.nature.com/reprintsandpermissions/>

Publisher's note: Springer Nature remains neutral with regard to jurisdictional claims in published maps and institutional affiliations.



Open Access This article is licensed under a Creative Commons Attribution 4.0 International License, which permits use, sharing, adaptation, distribution and reproduction in any medium or format, as long as you give appropriate credit to the original author(s) and the source, provide a link to the Creative Commons license, and indicate if changes were made. The images or other third party material in this article are included in the article's Creative Commons license, unless indicated otherwise in a credit line to the material. If material is not included in the article's Creative Commons license and your intended use is not permitted by statutory regulation or exceeds the permitted use, you will need to obtain permission directly from the copyright holder. To view a copy of this license, visit <http://creativecommons.org/licenses/by/4.0/>.

© The Author(s) 2018